AD-783 623

ELECTROMAGNETIC PULSE ENVIRONMENT STUDIES. VOLUME I. TWO-DIMENSIONAL GROUND-BURST ELECTROMAGNETIC PULSE CALCULATIONAL METHODS

Stephen J. Dalich, et al

Science Applications, Incorporated

Prepared for:

Defense Nuclear Agency
Air Force Weapons Laboratory

June 1974

This report was prepared by Science Applications, Inc., for Dikewood Corporation, Albuquerque, New Mexico, under Contract F29601-72-C-0117. The research was performed under Program Element 60707H, Project WDNE, and was funded by the Defense Nuclear Agency (DNA).

Inclusive dates of research were 5 May 1972 through 31 December 1973. The report was submitted 12 April 1974 by the Air Force Weapons Laboratory Project Officer, Captain John F. Morgan (ELP).

This technical report has been reviewed and is approved.

JOHN F. MORGAN
Captain, USAF
Project Officer

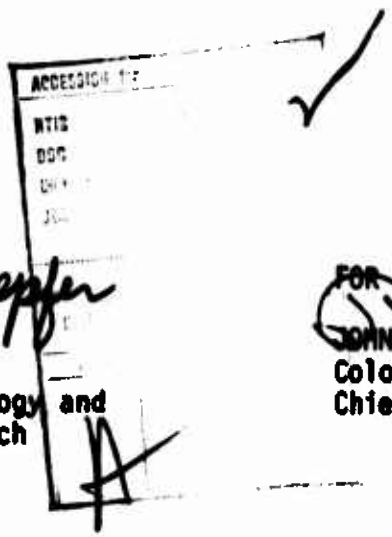

GORDON G. WEPFER
Lt Colonel, USAF
Chief, Phenomenology and
Technology Branch

FOR THE COMMANDER
JOHN W. SWAN
Colonel, USAF
Chief, Electronics Division

Field Command Printing Division

UNCLASSIFIED

SECURITY CLASSIFICATION OF THIS PAGE (When Data Entered)

AD 783 623

REPORT DOCUMENTATION PAGE

READ INSTRUCTIONS BEFORE COMPLETING FORM

1. REPORT NUMBER: AFWL-TR-73-286, Vol I
2. GOVT ACCESSION NO.
3. RECIPIENT'S CATALOG NUMBER

4. TITLE (and Subtitle): ELECTROMAGNETIC PULSE ENVIRONMENT STUDIES, Volume I
Two-Dimensional Ground-Burst Electromagnetic Pulse Calculational Methods

5. TYPE OF REPORT & PERIOD COVERED: Final Report for Period 5 May 72-31 Dec 73

6. PERFORMING ORG. REPORT NUMBER: SAI-73-514-AQ

7. AUTHOR(s): Stephen J. Dalich, Kenneth D. Granzow

8. CONTRACT OR GRANT NUMBER(s): F29601-72-C-0117

9. PERFORMING ORGANIZATION NAME AND ADDRESS: Science Applications, Inc., for Dikewood Corp., Albuquerque, New Mexico 87108

10. PROGRAM ELEMENT, PROJECT, TASK AREA & WORK UNIT NUMBERS: 60707H; WDNE0705 DC XED; DNA Sub. R99QAXEA094-41

11. CONTROLLING OFFICE NAME AND ADDRESS: Director, Defense Nuclear Agency, Washington, D.C. 20305

12. REPORT DATE: June 1974

13. NUMBER OF PAGES: ~~150~~ 147

14. MONITORING AGENCY NAME & ADDRESS(if different from Controlling Office): Air Force Weapons Laboratory (ELP), Kirtland Air Force Base, New Mexico 87117

15. SECURITY CLASS. (of this report): UNCLASSIFIED

15a. DECLASSIFICATION/DOWNGRADING SCHEDULE

16. DISTRIBUTION STATEMENT (of this Report): Approved for public release; distribution unlimited.

17. DISTRIBUTION STATEMENT (of the abstract entered in Block 20, if different from Report)

18. SUPPLEMENTARY NOTES

19. KEY WORDS (Continue on reverse side if necessary and identify by block number)
Electromagnetic pulse (EMP)
Low-altitude EMP
EMP code development
EMP prediction techniques

20. ABSTRACT (Continue on reverse side if necessary and identify by block number)

A description of the physics and numerical methods used in two-dimensional ground burst electromagnetic pulse calculations is given. In particular the SCX code, one of two computer codes which performs such calculations, is described. The source terms, air chemistry, and boundary conditions are also discussed. Multipole expansion techniques for outer boundary conditions are described in detail. Comparisons between the SCX code and the LEMP1 code are presented. Instructions for running SCX are contained in Appendix III.

147

DD FORM 1 JAN 73 1473 EDITION OF 1 NOV 65 IS OBSOLETE

1.

UNCLASSIFIED

SECURITY CLASSIFICATION OF THIS PAGE (When Data Entered)

TABLE OF CONTENTS

LIST OF ILLUSTRATIONS

LIST OF ILLUSTRATIONS (Continued)

SECTION I

INTRODUCTION

SCX is a two-dimensional computer code designed to solve Maxwell's equations in the environment of a ground nuclear burst. The calculational regime includes both the air and ground regions. It is well-known that the detonation of a nuclear device results in the generation of large electric and magnetic fields. This phenomenon is commonly referred to as the EMP (electromagnetic pulse). Information concerning the EMP is of vital interest in the design of both offensive and defensive weapons systems. For this reason the SCX code was developed at the Air Force Weapons Laboratory (AFWL) and is presently used at AFWL in the prediction of EMP environments.

The numerical methods employed in the SCX code are similar to methods used in other EMP codes; however, the code is essentially an extension of the original British RAG codes. Methods used in these codes were expanded by AFWL in the writing of B, a two-dimensional medium altitude code. The B code was then modified and, using the combination spherical-cylindrical grid suggested by Longmire, converted to a ground burst code. The original version of SCX, called SC, was developed by G. K. Schlegel and G. Waller. The production version of the code now in use at AFWL is a similar, but expanded, version of the original code. S. J. Dalich was not involved in the development of the original code but, along with J. N. Wood, is responsible for certain portions of the present production code.

This document is meant to be as up to date as possible. All areas of the calculation, including source and air chemistry,

are included. The main text and Appendices II and III were written by S. J. Dalich of Science Applications, Inc. Appendix I was written by K. D. Granzow of The Dikewood Corporation. Assistance in compiling the variable list in Appendix III was obtained from A. A. Henden, also from The Dikewood Corporation.

The SCX code is not generally available for distribution. While the majority of the code is written in standard FORTRAN IV, it is not generally compatible with computer systems other than the AFWL system. This is the result of the extensive use made of extended core storage on the CDC 6600 at AFWL. A typical SCX run requires 250_8K of central memory and 760_8K of extended core storage. Also, several of the subroutines are written in assembler language.

SECTION II

FIELD CALCULATION

Obviously the primary calculation in the SCX code involves the field algorithm. The field calculation is, however, coupled to the conductivity calculation through the field dependence of the electron mobility and electron attachment rate. The conductivity calculation is discussed in Section III, and in the following it will be assumed that the appropriate conductivity has already been obtained.

1. FIELD EQUATIONS

Two coordinate systems are used in the field calculation in the SCX code. These are a spherical system in the air portion and cylindrical coordinates in the ground. The use of these two systems allows for the application of the inner boundary conditions due to Longmire. Specifically, an infinitely conducting hemisphere is assumed to surround the burst point in the air portion of the grid. In the ground an infinitely conducting cylinder with radius equal to the radius of the air-hemisphere is assumed to extend down to several skin depths.

The Maxwell equations of interest, in MKS units, are

$$\vec{\nabla} \times \vec{E} = - \frac{\partial \vec{B}}{\partial t} \tag{1}$$

$$\vec{\nabla} \times \vec{H} = \vec{J} + \sigma \vec{E} + \frac{\partial \vec{D}}{\partial t} \tag{2}$$

The two divergence equations are not included as they are only initial conditions on the problem. In the air the free space values of the permitivity, ϵ, and permeability, μ, are assumed. These are input parameters in the ground equations. Using the constitutive relations, Eqs. (1) and (2) are written

$$\vec{\nabla} \times \vec{E} = - \frac{\partial \vec{B}}{\partial t} \tag{3}$$

$$\vec{\nabla} \times \vec{B} = \mu \vec{J} + \mu\sigma \vec{E} + \mu\epsilon \frac{\partial \vec{E}}{\partial t} \tag{4}$$

Carrying out the operations indicated in Eqs. (3) and (4) generally results in two sets of three equations. These sets represent the transverse electric and transverse magnetic fields. In the SCX code azimuthal symmetry is assumed and the transverse electric equations are eliminated. The remaining three equations are

(Air-spherical)

$$\frac{1}{r \sin\theta} \frac{\partial}{\partial\theta} (B_\varphi \sin\theta) = \mu J_r + \mu\sigma E_r + \mu\epsilon \frac{\partial E_r}{\partial t} \tag{5}$$

$$- \frac{1}{r} \frac{\partial}{\partial r} (rB_\varphi) = \mu J_\theta + \mu\sigma E_\theta + \mu\epsilon \frac{\partial E_\theta}{\partial t} \tag{6}$$

$$\frac{\partial}{\partial r} (rE_\theta) - \frac{\partial E_r}{\partial \theta} = - \frac{\partial}{\partial t} (rB_\varphi) \tag{7}$$

(Ground-cylindrical)

$$-\frac{\partial B_\varphi}{\partial z} = \mu J_\rho + \mu\sigma E_\rho + \mu\epsilon \frac{\partial E_\rho}{\partial t} \tag{8}$$

$$\frac{1}{\rho}\frac{\partial}{\partial \rho}(\rho B_\varphi) = \mu J_z + \mu\sigma E_z + \mu\epsilon \frac{\partial E_z}{\partial t} \tag{9}$$

$$\frac{\partial}{\partial z} E_\rho - \frac{\partial E_z}{\partial \rho} = -\frac{\partial B_\varphi}{\partial t} \tag{10}$$

Before attempting to solve Eqs. (5) through (7) (the air equations), a transformation to retarded time is made,

$$r' = r$$

$$\varphi' = \varphi$$

$$\theta' = \theta$$

$$\tau = t - r/c \tag{11}$$

In effect the transformation eliminates the steep gradients in the r direction. At a constant retarded time all points in space represent the same point on the wave front. Thus, no special gridding is required in the r direction. With the above transformation the partial differential operators in Eqs. (5) through (7) become

$$\frac{\partial}{\partial r} = \frac{\partial}{\partial r'} - \frac{1}{c}\frac{\partial}{\partial \tau} \tag{12}$$

$$\frac{\partial}{\partial \varphi} = \frac{\partial}{\partial \varphi'} \tag{13}$$

$$\frac{\partial}{\partial \theta} = \frac{\partial}{\partial \theta'} \tag{14}$$

$$\frac{\partial}{\partial t} = \frac{\partial}{\partial \tau} \tag{15}$$

The air equations in this system are (the primes on the transformed variables have been dropped)

$$\frac{1}{\mu r^2 \sin\theta}\frac{\partial}{\partial \theta}(rB_\varphi \sin\theta) = J_r + \sigma E_r + \epsilon \frac{\partial E_r}{\partial \tau} \tag{16}$$

$$-\frac{1}{\mu r}\left[\frac{\partial}{\partial r}(rB_\varphi) - \frac{1}{c}\frac{\partial}{\partial \tau}(rB_\varphi)\right] = J_\theta + \sigma E_\theta + \epsilon \frac{\partial E_\theta}{\partial \tau} \tag{17}$$

$$\frac{1}{r}\left[\frac{\partial}{\partial r}(rE_\theta) - \frac{1}{c}\frac{\partial}{\partial \tau}(rE_\theta) - \frac{\partial}{\partial \theta}E_r\right] = -\frac{\partial B_\varphi}{\partial \tau} \tag{18}$$

In the ground equation the retarded time is obtained by considering a refracted wave. In Fig. 1 the path of this wave is defined.

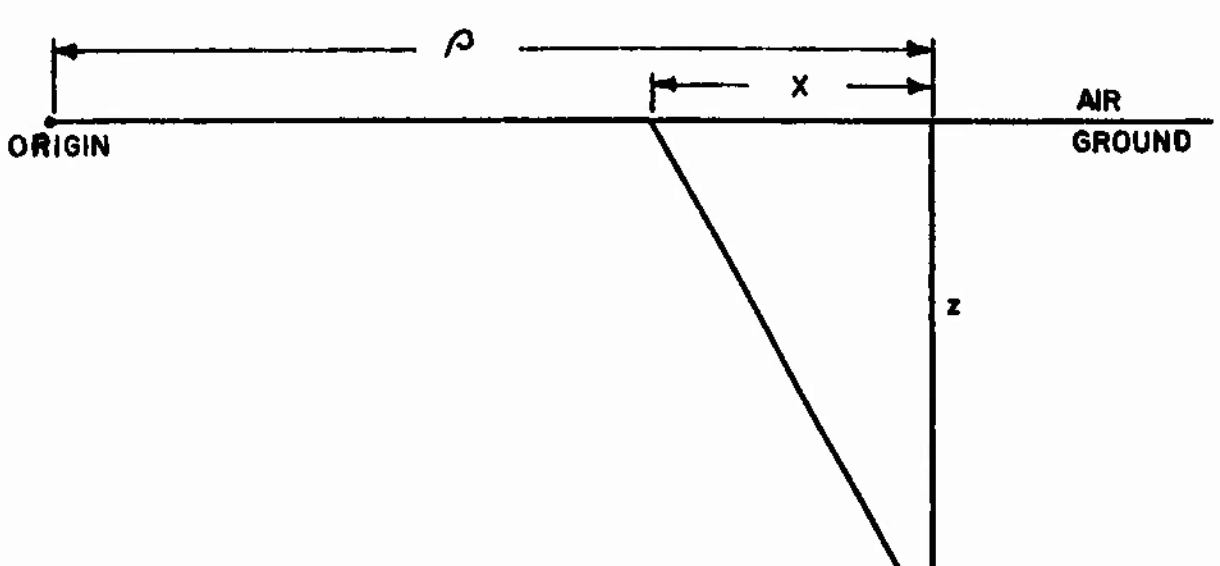

Figure 1. Path to (ρ,z) by a refracted wave.

Using variational methods, the minimum time for a wave to reach (ρ, z) by the above path is given by

$$t_{min} = \frac{\rho}{c} + \frac{|z|}{c_g}\sqrt{1 - \frac{c_g^2}{c^2}} \qquad (19)$$

where c is the speed of light in the air and c_g is the light speed in the ground. This minimum time is used to define the retarded time in the ground as

$$\tau = t - \frac{\rho}{c} + \frac{|z|}{c_g}\sqrt{1 - \frac{c_g^2}{c^2}} \qquad (20)$$

The space coordinates transform as

$$\rho' = \rho$$

$$z' = z$$

$$\varphi' = \varphi \qquad (21)$$

and the differential operators in the ground become

$$\frac{\partial}{\partial t} = \frac{\partial}{\partial \tau} \qquad (22)$$

$$\frac{\partial}{\partial \rho} = \frac{\partial}{\partial \rho'} - \frac{1}{c}\frac{\partial}{\partial \tau} \qquad (23)$$

$$\frac{\partial}{\partial z} = \frac{\partial}{\partial z'} + \frac{\sqrt{1 - c_g^2/c^2}}{c_g}\frac{\partial}{\partial \tau} \qquad (24)$$

$$\frac{\partial}{\partial \varphi} = \frac{\partial}{\partial \varphi'} \qquad (25)$$

(note that as presently used in the code z is negative)

In the transformed system the ground equations [(8)-(10)] are given by (primes have been dropped)

$$-\frac{1}{\mu}\left(\frac{\partial B_\varphi}{\partial z}+\frac{\sqrt{1-c_g^2/c^2}}{c_g^2}\frac{\partial B_\varphi}{\partial \tau}\right)=J_\rho+\sigma E_\rho+\epsilon\frac{\partial E_\rho}{\partial \tau} \tag{26}$$

$$\frac{1}{\mu\rho}\left[\frac{\partial}{\partial\rho}(\rho B_\varphi)-\frac{1}{c}\frac{\partial}{\partial\tau}(\rho B_\varphi)\right]=J_z+\sigma E_z+\epsilon\frac{\partial E_z}{\partial\tau} \tag{27}$$

$$\frac{\partial}{\partial z}E_\rho+\frac{\sqrt{1-c_g^2/c^2}}{c_g^2}\frac{\partial}{\partial\tau}E_\rho-\frac{\partial}{\partial\rho}E_z+\frac{1}{c}\frac{\partial}{\partial\tau}E_z=-\frac{\partial B_\varphi}{\partial\tau} \tag{28}$$

The ground equations are modified further by assuming that all currents are zero in the ground. These currents are available and could be implemented; however, studies at AFWL, using the one-dimensional code NEW1, have shown that for a burst on the ground the effect is negligible. If the height of burst is greater than zero, the ground currents should be included.

2. GRIDDING CONSIDERATIONS

Figure 2 illustrates the grid used in the SCX code. Examining Eqs. (16) through (18) indicates that centering derivatives in θ is simplified by defining $B\varphi$ and $E\theta$ on full angles and E_r on half angles. Thus, in Fig. 2 the crosses refer to positions where E_r is defined and the circles to $E\theta, B\varphi$ positions.

E_θ (E_z), B_ϕ Are calculated on lines marked by O.

E_r (E_ρ) Are calculated on lines marked by X.

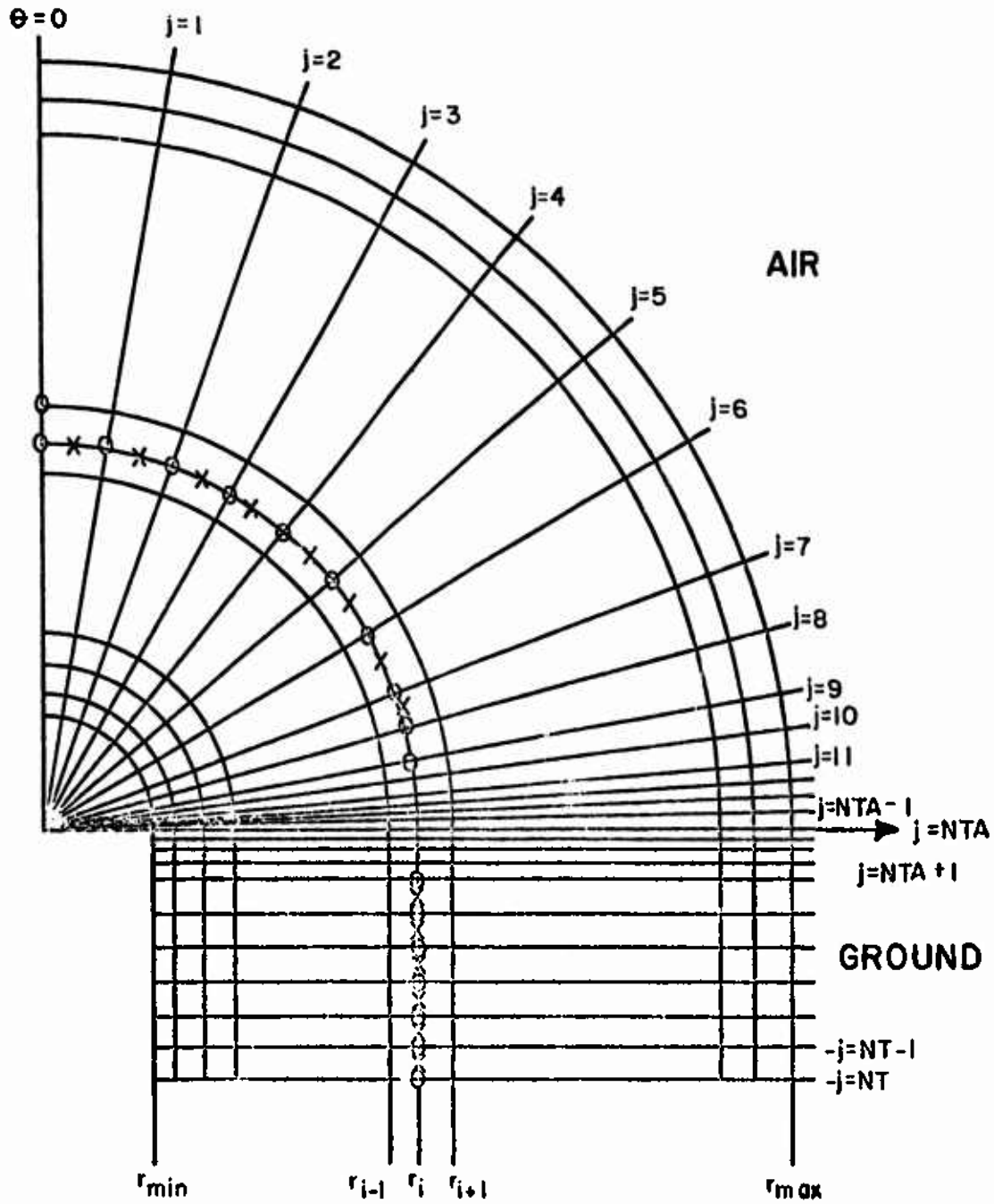

Figure 2. Sample grid as used in the SCX code.

Similarly in the ground, E_ρ is defined at half z positions while E_z and B_φ are defined on the full grid lines.

z_{max} in the ground grid is chosen by the code or is given as an input parameter. If chosen by the code (the usual running mode), z_{max} is obtained as several skin depths at a 8 MHz frequency. Generally, the entire 0^o to 90^o region is included in the air grid; however, the option does exist to begin the calculation off the vertical. This latter option is virtually never used in the normal running of SCX.

The asymmetry at the air-ground interface necessitates a further modification of the grid. At points far from the interface, where no asymmetry exists, fairly large grid steps can be taken. Near the interface the grid steps must be much smaller since variations in this region are expected to be highest. Thus, a variable grid spacing in both the air and ground region is desirable. In the code this is accomplished as follows: first, the air region is divided into N1 angle bins, the lower N2 of these bins are then halved. The process of halving the lower N2 bins is repeated N3 times. The total number of air angle bins is then given by

$$NTA = N1 + N2 \times N3$$

A similar process is also preformed in the ground portion of the grid. The net result is a uniform grid at points far from the air-ground interface but an increasingly finer grid in the region near the interface. In the normal running mode there are 7 bins of 10^o and 22 bins which decrease in size to a final bin of $9.766E\text{-}03^o$ next to the ground.

The regridding discussed above introduces certain problems in the centering of derivatives. These will be discussed in Section II-5.

3. BOUNDARY CONDITIONS

A few of the boundary conditions have already been mentioned while others have not been discussed at all. For completeness and at the risk of repetition, all of the boundary conditions used in the SCX code will be discussed in this section. Fig. 3 is a simplified grid for the code with the various boundaries labeled.

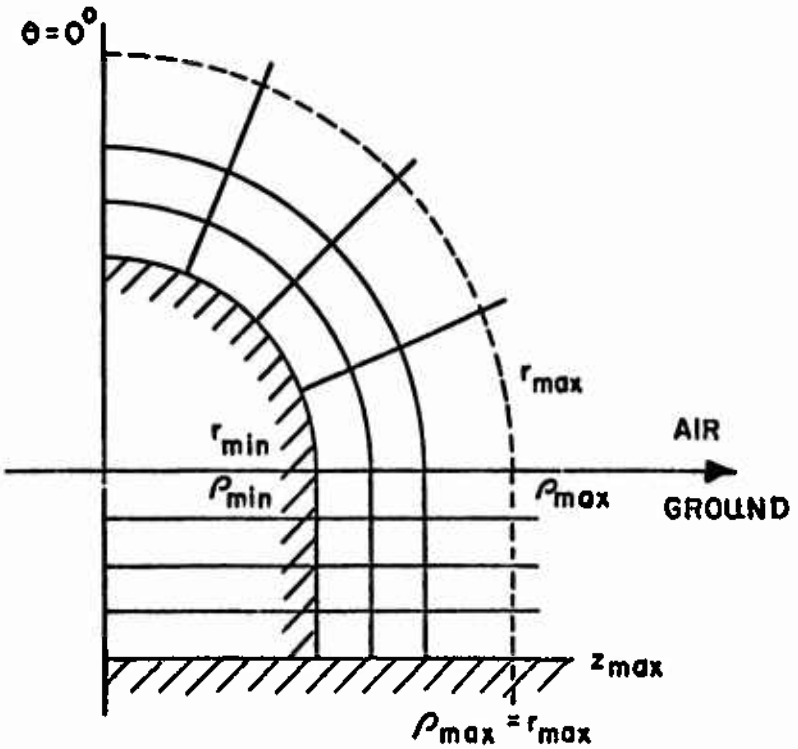

Figure 3. Sample SCX grid with labeled boundaries.

The inner boundary is defined as an infinitely conducting hemisphere in the air and an infinitely conducting cylinder in the ground. There are several reasons for choosing this type of inner boundary. First, it is reasonable since it is meant to represent the region in the immediate vicinity of the burst. In this region ionization is very high and the infinite conductivity approximation is fairly good. Second, it eliminates stability problems associated with quantities having a 1/r dependence. At the inner boundary, then,

$$E_\theta\Big|_{r=r_{min}} = 0$$

$$E_z\Big|_{\rho=\rho_{min}} = 0$$

In the general running mode r_{min} is chosen as 200 meters; however, any value can be input to the code.

Due to the assumption of azimuthal symmetry a boundary condition is obtained on the vertical axis at $\theta = 0^o$. Clearly, only radial vector components can have nonzero values here. Thus,

$$B_\varphi\Big|_{\theta=0^o} = 0$$

As discussed earlier, z_{max} is chosen automatically by the code as being equal to several skin depths. Thus, a reasonable assumption in this region is

$$E_z\Big|_{z=z_{max}} = 0$$

$$B_\varphi\Big|_{z=z_{max}} = 0$$

At the air ground interface both B_φ and E_r are continuous. Thus,

$$B_\varphi\Big|_{\theta=90^o} = B_\varphi\Big|_{z=0}$$

$$E_r\Big|_{\theta=90^o} = E_\rho\Big|_{z=0}$$

This condition becomes quite important in the actual fields algorithm. As will be seen in Section II-4, E_r and E_θ can be expressed in terms of B_φ; and, therefore, the continuity of B_φ at the interface provides a unique solution for B_φ.

Numerically the most difficult boundary occurs at $r = r_{max}$. Ideally one would like to choose r_{max} to be infinite and thus set the fields to zero at this boundary. Since a computer with infinite storage is not available, this is not possible. In SCECS two options are provided for handling the outer boundary. Both involve the assumption that r_{max} lies in the radiated region. Normally r_{max} will be between 5 and 7 km, and for most problems of interest the assumption is reasonable.

With the first option the fields at $r = r_{max}$ and $\rho = \rho_{max}$ are calculated by a first order Taylor expansion. In the air portion of the grid it is assumed that the fields go as 1/r and the expansion is on rB_{φ}. This essentially amounts to taking the first term of a multipole expansion. The second option does the actual multipole expansion. In this case it is assumed that beyond $r = r_{max}$ the air conductivity is zero and the ground conductivity infinite. The expansion methods were developed by K. Granzow and are documented in Appendix I and also in an independent paper (Ref. 1).

4. DIFFERENCING - THE FIELD ALGORITHM

The SCX code uses a combined explicit-implicit differencing scheme in the field algorithm. B_{φ} and E_{θ} (or E_z) are obtained implicitly while E_r (or E_{ρ}) is obtained explicitly. A step-by-step description of the differencing in both the air and the ground region will be given in this section. The equations have been described in an earlier Dikewood Corporation document which deals with the field algorithm only (Ref. 2). Also, AWRE Report No. 0-72/65 contains descriptions of the algorithms used in the various RAG codes, and these are quite similar to the techniques used in SCX. Both the above documents should serve as useful complements to the present paper.

The equations of concern were given in Section II-1 and will be repeated here for convenience in referencing.

$$\frac{1}{\mu r^2 \sin\theta} \frac{\partial}{\partial\theta} (rB_{\varphi} \sin\theta) = J_r + \sigma E_r + \epsilon \frac{\partial E_r}{\partial \tau} \qquad (16)$$

$$-\frac{1}{\mu r}\left[\frac{\partial}{\partial r}(rB_\varphi) - \frac{1}{c}\frac{\partial}{\partial \tau}(rB_\varphi)\right] = J_\theta + \sigma E_\theta + \epsilon \frac{\partial E_\theta}{\partial \tau} \qquad (17)$$

$$\frac{1}{r}\left[\frac{\partial}{\partial r}(rE_\theta) - \frac{1}{c}\frac{\partial}{\partial \tau}(rE_\theta) - \frac{\partial}{\partial \theta}E_r\right] = -\frac{\partial B_\varphi}{\partial \tau} \qquad (18)$$

Eq. (18) is multiplied by 1/2 and Eq. (17) by $c\mu r/2$; subtracting (17) from (18) then yields

$$c\frac{\partial}{\partial r}\left(rB_\varphi + \frac{rE_\theta}{c}\right) = \frac{\partial E_r}{\partial \theta} - c\sigma\mu(rE_\theta) - c\mu r J_\theta \qquad (29)$$

and by summing (17) and (18)

$$\frac{c}{2}\frac{\partial}{\partial r}\left(\frac{rE_\theta}{c} - rB_\varphi\right) - \frac{\partial}{\partial \tau}\left(\frac{rE_\theta}{c} - rB_\varphi\right) = \frac{1}{2}\frac{\partial E_r}{\partial \theta} + \frac{c\mu\sigma}{2}(rE_\theta) + \frac{c\mu r}{2}J_\theta \qquad (30)$$

These two equations, plus Eq. (16), are differenced in the air region of the SCX code.

Several comments concerning the above equations are in order. In the (r,θ,t) space the surfaces defined by $t - r/c$ = constant and $t + r/c$ = constant are the characteristic surfaces for the wave equation. It is well-known that a characteristic surface cannot serve as a boundary surface for hyperbolic differential equations. The retarded time

transformation, which is to a characteristic surface, thus eliminates the possibility of advancing certain of the variables exactly parallel to this direction. This is demonstrated by examining Eqs. (29) and (30), which contain the retarded time derivitives of E_θ and B_φ. It will be seen that these are not independent, and attempts to obtain two independent equations in $\partial B_\varphi/\partial\tau$ and $\partial E_\theta/\partial\tau$ will fail. Therefore, E_θ and B_φ cannot be advanced exactly parallel to the retarded time direction. As a result, a line of constant advanced time, $t + r/c$ = constant, is used to difference Eq. (30) and a line of constant retarded time to difference Eq. (29). Eq. (16) presents no such problem and is differenced along a line of constant radius. Fig. 4 is a (r, τ) grid showing the differencing lines for the three equations.

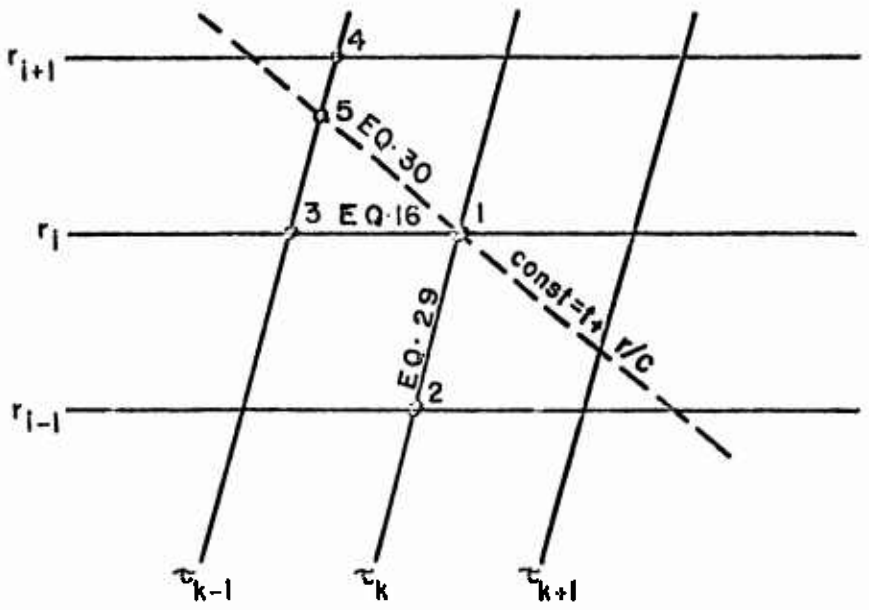

Figure 4. Differencing lines in the air grid.

Note that interpolation must be used to obtain values at point 5 in Fig. 4.

The steps used in differencing the field equations are described below. First, the following definitions are made.

$$r_i = r_0 + i \times \Delta r \qquad 1 \leq i \leq NDR$$

$$\rho_i = \rho_0 + i \times \Delta\rho \qquad 1 \leq i \leq NDR$$

$$\tau_k = k \times \Delta\tau \qquad 1 \leq k \leq NTY$$

$$\theta_j = \theta_{j-1} + \Delta\theta_j \qquad 1 \leq j \leq NTA$$

$$z_j = z_{j-1} + \Delta z_j \qquad NTA + 1 \leq j \leq NT$$

Note that because of the regridding in θ and z, no simple relation may be written for these coordinate positions. Further, E_r and E_ρ are defined at half angles and half z, respectively. In describing a half angle (or depth) variable, or coordinate, a superscript h will be used. Variables obtained through interpolation carry a subscript p.

a. Air Equations

The equations to be differenced in the air grid are

$$\frac{1}{\mu r^2 \sin\theta} \frac{\partial}{\partial\theta} (rB_\varphi \sin\theta) = J_r + \sigma E_r + \epsilon \frac{\partial E_r}{\partial\tau} \qquad (31)$$

$$c \frac{\partial}{\partial r} (rB_\varphi) + \frac{\partial}{\partial r} (rE_\theta) = \frac{\partial E_r}{\partial \theta} - c\mu\sigma(rE_\theta) - c\mu r J_\theta \tag{32}$$

$$\frac{\partial}{\partial \tau} \left(rB_\varphi\right) - \frac{c}{2} \frac{\partial}{\partial r} \left(rB_\varphi\right) - \frac{\partial}{\partial \tau} \left(\frac{rE_\theta}{c}\right) + \frac{c}{2} \frac{\partial}{\partial r} \left(\frac{rE_\theta}{c}\right)$$

$$= \frac{c\mu r J_\theta}{2} + \frac{c\mu\sigma(rE_\theta)}{2} + \frac{1}{2} \frac{\partial E_r}{\partial \theta} \tag{33}$$

Eq. (31) is differenced along a line of constant radius resulting in

$$\frac{1}{\delta\theta_j 2\mu r_i^2 \sin \theta_j^h} \left[\left((rB_\varphi)_{ij}^k + (rB_\varphi)_{ij}^{k-1}\right) \sin \theta_j - \left((rB_\varphi)_{ij-1}^k + (rB_\varphi)_{ij-1}^{k-1}\right)\right.$$

$$\left. \sin \theta_{j-1}\right] = \left(\frac{J_{rij}^{hk} + J_{rij}^{hk-1}}{2}\right) + \left(\frac{\sigma_{ij}^{hk} E_{rij}^{hk} + \sigma_{ij}^{hk-1} E_{rij}^{hk-1}}{2}\right)$$

$$+ \frac{\epsilon}{\delta\tau} \left(E_{rij}^{hk} - E_{rij}^{hk-1}\right) \tag{34}$$

Separating the variables in Eq. (34) according to the time superscript yields

$$\frac{\delta\tau c^2}{2r_i^2 \sin\theta_j^h \delta\theta_j}\left[\sin\theta_j\left(rB_\varphi\right)_{ij}^k - \sin\theta_{j-1}\left(rB_\varphi\right)_{ij-1}^k\right]$$

$$-\left(1+\frac{\delta\tau}{2\epsilon}\sigma_{ij}^{hk}\right)E_{rij}^{hk} = \frac{\delta\tau}{2\epsilon}\left(J_{rij}^{hk} - J_{rij}^{hk-1}\right) + \frac{\delta\tau c^2}{2r_i^2 \sin\theta_j^h \delta\theta_j}$$

$$\left[\sin\theta_{j-1}\left(rB_\varphi\right)_{ij-1}^{k-1} - \sin\theta_j\left(rB_\varphi\right)_{ij}^{k-1}\right]$$

$$-\left(1-\frac{\delta\tau}{2\epsilon}\sigma_{ij}^{hk-1}\right)E_{rij}^{hk-1} \qquad (35)$$

Eq. (32) is differenced on a line of constant retarded time and arranged similarly to Eq. (35). Thus,

$$\left(rB_\varphi\right)_{ij}^k + \left(\frac{1}{c}+\frac{\mu\delta r}{2}\sigma_{ij}^k\right)\left(rE_\theta\right)_{ij}^k + \frac{\delta r}{2c\delta\theta_j^h}\left(E_{rij}^{hk} - E_{rij+1}^{hk}\right)$$

$$= \left(rB_\varphi\right)_{i-1j}^k + \left(\frac{1}{c}-\frac{\mu\delta r}{2}\sigma_{i-1j}^k\right)\left(rE_\theta\right)_{i-1j}^k$$

$$+\frac{\delta r}{2c\delta\theta_j^h}\left(E_{ri-1j+1}^{hk} - E_{ri-1j}^{hk}\right) - \frac{\delta r\mu}{2}\left[\left(rJ_\theta\right)_{i-1j}^k + \left(rJ_\theta\right)_{ij}^k\right] \qquad (36)$$

Finally, Eq. (33) is differenced along a line of constant advanced time (note that on this line $\left.\frac{\partial}{\partial\tau}\right|_{\tau_a} = \frac{\partial}{\partial\tau} - \frac{c}{2}\frac{\partial}{\partial r}$

$$\left(rB_{\varphi}\right)_{ij}^{k} - \left(\frac{1}{c} + \frac{c\mu\delta\tau}{4}\sigma_{ij}^{k}\right)\left(rE_{\theta}\right)_{ij}^{k} + \frac{\delta\tau}{4\delta\theta_j^h}\left(E_{rij}^{hk} - E_{rij+1}^{hk}\right)$$

$$= \left(rB_{\varphi}\right)_{pj}^{k-1} - \left(\frac{1}{c} - \frac{c\mu\delta\tau}{4}\sigma_{pj}^{k-1}\right)\left(rE_{\theta}\right)_{pj}^{k-1} + \frac{\delta\tau}{4\delta\theta_j^h}\left(E_{rpj+1}^{hk-1} - E_{rpj}^{hk-1}\right)$$

$$+ \frac{\mu c\delta\tau}{4}\left[\left(rJ_{\theta}\right)_{ij}^{k-1} + \left(rJ_{\theta}\right)_{ij}^{k}\right] \qquad (37)$$

To simplify the above equations define the following

$$A1(j) = \left(1 + \frac{\delta\tau}{2\epsilon}\sigma_{ij}^{hk}\right) \qquad (38)$$

$$A21(j) = \frac{\delta\tau c^2}{2\delta\theta_j r_i^2}\frac{\sin\theta_j}{\sin\theta_j^h} \qquad (39)$$

$$A22(j) = \frac{\delta\tau c^2}{2\delta\theta_j r_i^2}\frac{\sin\theta_{j-1}}{\sin\theta_j^h} \qquad (40)$$

$$A3(j) = \frac{\delta\tau}{2\epsilon}\left(J_{rij}^{hk} + J_{rij}^{hk-1}\right) + \left(1 - \frac{\delta\tau}{2\epsilon}\sigma_{ij}^{hk-1}\right)E_{rij}^{hk-1}$$

$$+ \frac{\delta\tau c^2}{2\delta\theta_j r_i^2}\left[\frac{\sin\theta_j}{\sin\theta_j^h}\left(rB_{\varphi}\right)_{ij}^{k-1} - \frac{\sin\theta_{j-1}}{\sin\theta_j^h}\left(rB_{\varphi}\right)_{ij-1}^{k-1}\right] \qquad (41)$$

$$A4(j) = \frac{1}{c} + \frac{\mu \delta r}{2} \sigma_{ij}^{k} \tag{42}$$

$$A5(j) = \frac{\delta r}{2c\delta\theta_j^h} \tag{43}$$

$$A6(j) = \left(rB_{\varphi}\right)_{i-1j}^{k} + \left(\frac{1}{c} - \frac{\mu\delta r}{2}\sigma_{i-1j}^{k}\right)\left(rE_{\theta}\right)_{i-1j}^{k} + \frac{\delta r}{2c\delta\theta_j^h}\left(E_{ri-1j+1}^{hk} - E_{ri-1j}^{hk}\right) - \frac{\delta r\mu}{2}\left[\left(rJ_{\theta}\right)_{i-1j}^{k} + \left(rJ_{\theta}\right)_{ij}^{k}\right] \tag{44}$$

$$A7(j) = -\left(\frac{1}{c} + \frac{c\mu\delta\tau}{4}\sigma_{ij}^{k}\right) \tag{45}$$

$$A8(j) = \frac{\delta\tau}{4\delta\theta_j^h} \tag{46}$$

$$A9(j) = \left(rB_{\theta}\right)_{pj}^{k-1} - \left(\frac{1}{c} - \frac{c\mu\delta\tau}{4}\sigma_{pj}^{k-1}\right)\left(rE_{\theta}\right)_{pj}^{k-1} + \frac{\delta\tau}{4\delta\theta_j^h}\left(E_{rpj+1}^{hk-1} - E_{rpj}^{hk-1}\right) + \frac{\delta\tau\mu c}{4}\left[\left(rJ_{\theta}\right)_{ij}^{k-1} + \left(rJ_{\theta}\right)_{ij}^{k}\right] \tag{47}$$

With these definitions Eqs. (35), (36), and (37) may be written

$$A1(j)E^{hk}_{rij} - A21(j)(rB_{\varphi})^{k}_{ij} + A22(j)(rB_{\varphi})^{k}_{ij-1} = A3(j) \qquad (48)$$

$$(rB_{\varphi})^{k}_{ij} + A4(j)(rE_{\theta})^{k}_{ij} + A5(j)\left(E^{hk}_{rij} - E^{hk}_{rij+1}\right) = A6(j) \qquad (49)$$

$$(rB_{\varphi})^{k}_{ij} + A7(j)(rE_{\theta})^{k}_{ij} + A8(j)\left(E^{hk}_{rij} - E^{hk}_{rij+1}\right) = A9(j) \qquad (50)$$

Note that the A variables defined in Eqs. (38) through (47) involve values at k - 1 or i - 1. In the above, (49) and (50) are used to eliminate the $(rE_{\theta})^{k}_{ij}$ term; the result is then used in (48) to eliminate E^{hk}_{rij}. A three-term recursion relation in (rB_{φ}) is thus obtained

$$A10(j)(rB_{\varphi})^{k}_{ij-1} + A11(j)(rB_{\varphi})^{k}_{ij} + A12(j)(rB_{\varphi})^{k}_{ij+1} = A13(j) \qquad (51)$$

In Eq. (51) the following definitions have been used

$$A10(j) = \left(A8(j)A4(j) - A5(j)A7(j)\right)A22(j)/A1(j) \qquad (52)$$

$$A11(j) = A7(j) - A4(j) - \left(A8(j)A4(j) - A5(j)A7(j)\right) \times \left(A21(j)/A1(j) + A22(j+1)/A1(j+1)\right) \qquad (53)$$

$$A12(j) = \Big(A8(j)A4(j) - A5(j)A7(j)\Big)A21(j+1)/A1(j+1) \qquad (54)$$

$$A13(j) = A6(j)A7(j) - A4(j)A9(j) + \Big(A8(j)A4(j) - A5(j)A7(j)\Big) \times \Big(A3(j)/A1(j) - A3(j+1)/A1(j+1)\Big) \qquad (55)$$

Eq. (51) can be reduced to a two-term recursion relation by use of the boundary condition at $\theta = 0^{o}$. Here $rB_{\varphi} = 0$, so that choosing j = 1 in (51) yields

$$A11(1)(rB_{\varphi})^{k}_{i1} + A12(1)(rB_{\varphi})^{k}_{i2} = A13(1) \qquad (56)$$

Write the above in the form

$$(rB_{\varphi})^{k}_{i1} = E(1)(rB_{\varphi})^{k}_{i2} + F(1) \qquad (57)$$

where

$$E(1) = -\frac{A12(1)}{A11(1)}$$

$$F(1) = \frac{A13(1)}{A11(1)} \qquad (58)$$

Assuming that it is possible to write (57) for an arbitrary j, Eq. (51) for j + 1 becomes

$$(rB_{\varphi})^{k}_{ij+1} = -\frac{A12(j+1)}{A10(j+1)E(j) + A11(j+1)}(rB_{\varphi})^{k}_{ij+2} + \frac{A13(j+2) - F(j)A10(j+1)}{A10(j+1)E(j) + A11(j+1)} \quad (59)$$

Make the following definitions

$$E(j) = -\frac{A12(j)}{A10(j)E(j-1) + A11(j)}$$

$$F(j) = \frac{A13(j+1) - F(j-1)A10(j)}{A10(j)E(j-1) + A11(j)} \quad (60)$$

and Eq. (59) is of the same form as Eq. (57). Thus, by induction it is always possible to construct a two-term recursion relation in (rB_{φ}) (Ref. 3)

$$(rB_{\varphi})^{k}_{ij} = E(j)(rB_{\varphi})^{k}_{ij+1} + F(j) \quad (61)$$

b. Ground Equations

The equations to be differenced in the ground are

$$-\frac{\partial B_\varphi}{\partial z} - \frac{\sqrt{1 - c_g^2/c^2}}{c_g^2}\frac{\partial B_\varphi}{\partial \tau} = \mu\sigma E_\rho + \frac{1}{c_g^2}\frac{\partial E_\rho}{\partial \tau} \qquad (62)$$

$$\frac{1}{c}\frac{\partial B_\varphi}{\partial \tau} - \frac{1}{\rho}\frac{\partial}{\partial \rho}(\rho B_\varphi) + \mu\sigma E_z + \frac{1}{c_g^2}\frac{\partial E_z}{\partial \tau} = 0 \qquad (63)$$

$$\frac{\partial E_\rho}{\partial z} + \frac{\sqrt{1 - c_g^2/c^2}}{c_g^2}\frac{\partial E_\rho}{\partial \tau} - \frac{\partial E_z}{\partial \rho} + \frac{1}{c}\frac{\partial E_z}{\partial \tau} = -\frac{\partial B_\varphi}{\partial \tau} \qquad (64)$$

As discussed in the text, no currents are used in the ground. In the following let

$$Z = -\frac{\sqrt{1 - c_g^2/c^2}}{c_g^2}$$

Eq. (62) in differenced form is

$$\left(\frac{1}{c_g^2}+\frac{\sigma_g\mu_g\delta\tau}{2}\right)E^{hk}_{\rho ij}-\left(\frac{Z}{2}-\frac{\delta\tau}{2\delta z_j}\right)B^{k}_{\varphi ij}-\left(\frac{Z}{2}+\frac{\delta\tau}{2\delta z_j}\right)B^{k}_{\varphi ij-1}$$

$$=\left(\frac{1}{c_g^2}-\frac{\sigma_g\mu_g\delta\tau}{2}\right)E^{hk-1}_{\rho ij}-\left(\frac{Z}{2}+\frac{\delta\tau}{2\delta z_j}\right)B^{k-1}_{\varphi ij}$$

$$-\left(\frac{Z}{2}-\frac{\delta\tau}{2\delta z_j}\right)B^{k-1}_{\varphi ij-1} \qquad (65)$$

Similarly, Eqs. (63) and (64) become

$$\left(\frac{1}{c}-\frac{\rho_i}{\rho_i+\rho_{i-1}}\frac{\delta\tau}{\delta\rho}\right)B^{k}_{\varphi ij}+\left(\frac{1}{c_g^2}+\sigma_g\mu_g\frac{\delta\tau}{2}\right)E^{k}_{zij}$$

$$=\left(\frac{1}{c_g^2}-\sigma_g\mu_g\frac{\delta\tau}{2}\right)E^{k-1}_{zij}+\left(\frac{1}{c}-\frac{\rho_i}{\rho_i+\rho_{i+1}}\frac{\delta\tau}{\delta\rho}\right)B^{k-1}_{\varphi ij}$$

$$-\left(\frac{\rho_{i-1}}{\rho_i+\rho_{i-1}}\frac{\delta\tau}{\delta\rho}\right)B^{k}_{\varphi i-1j}+\left(\frac{\rho_{i+1}}{\rho_i+\rho_{i+1}}\frac{\delta\tau}{\delta\rho}\right)B^{k}_{\varphi i+1j} \qquad (66)$$

and

$$B^{k}_{\varphi ij} + \left(\frac{1}{c} - \frac{\delta\tau}{2\delta\rho}\right)E^{k}_{zij} + \left(-\frac{Z}{2} + \frac{\delta\tau}{2\delta z^{h}_{j+1}}\right)E^{hk}_{\rho ij+1} + \left(-\frac{Z}{2} - \frac{\delta\tau}{2\delta z^{h}_{j+1}}\right)E^{hk}_{\rho ij}$$

$$= B^{k-1}_{\varphi ij} + \left(\frac{1}{c} - \frac{\delta\tau}{2\delta\rho}\right)E^{k-1}_{zij} + \frac{\delta\tau}{2\delta\rho}\left(E^{k-1}_{zi+1j} - E^{k}_{zi-1j}\right)$$

$$+ \left(-\frac{Z}{2} - \frac{\delta\tau}{2\delta z^{h}_{j+1}}\right)E^{hk-1}_{\rho ij+1} + \left(-\frac{Z}{2} + \frac{\delta\tau}{2\delta z^{h}_{j+1}}\right)E^{hk-1}_{\rho ij} \qquad (67)$$

As in the air grid, the following definitions are made to simplify the above equations.

$$G1(j) = \frac{1}{c_g^2} + \sigma_g\mu_g\frac{\delta\tau}{2} \qquad (68)$$

$$G2(j) = \frac{Z}{2} - \frac{\delta\tau}{2\delta z_j} \qquad (69)$$

$$G22(j) = \frac{Z}{2} + \frac{\delta\tau}{2\delta z_j} \qquad (70)$$

$$G3(j) = \left(\frac{1}{c_g^2} - \sigma_g\mu_g\frac{\delta\tau}{2}\right)E^{hk-1}_{\rho ij} - \left(\frac{Z}{2} + \frac{\delta\tau}{2\delta z_j}\right)B^{k-1}_{\varphi ij}$$

$$- \left(\frac{Z}{2} - \frac{\delta\tau}{2\delta z_j}\right)B^{k-1}_{\varphi ij-1} \qquad (71)$$

$$G4(j) = \frac{1}{c}\frac{\rho_i}{\rho_i + \rho_{i-1}}\frac{\delta\tau}{\delta\rho} \tag{72}$$

$$G5(j) = \frac{1}{c_g^2} + \sigma_g\mu_g\frac{\delta\tau}{2} \tag{73}$$

$$G6(j) = \left(\frac{1}{c_g^2} - \sigma_g\mu_g\frac{\delta\tau}{2}\right)E_{zij}^{k-1} + \left(\frac{1}{c} - \frac{\rho_i}{\rho_i + \rho_{i+1}}\frac{\delta\tau}{\delta\rho}\right)B_{\varphi ij}^{k-1}$$

$$+ \left(\frac{\rho_{i+1}}{\rho_i + \rho_{i+1}}\frac{\delta\tau}{\delta\rho}\right)B_{\varphi\, i+1j}^{k-1} - \left(\frac{\rho_{i-1}}{\rho_i + \rho_{i+1}}\frac{\delta\tau}{\delta\rho}\right)B_{\varphi\, i-1j}^{k} \tag{74}$$

$$G7(j) = \frac{1}{c} - \frac{\delta\tau}{2\delta\rho} \tag{75}$$

$$G8(j) = -\frac{Z}{2} - \frac{\delta\tau}{2\delta z_{j+1}^h} \tag{76}$$

$$G81(j) = -\frac{Z}{2} + \frac{\delta\tau}{2\delta z_{j+1}^h} \tag{77}$$

$$G9(j) = B^{k-1}_{\varphi ij} + \left(\frac{1}{c} - \frac{\delta_\tau}{2\delta\rho}\right)E^{k-1}_{zij} + \frac{\delta_\tau}{2\delta\rho}\left(E^{k-1}_{zi+1j} - E^{k}_{zi-1j}\right)$$

$$+ \left(-\frac{Z}{2} + \frac{\delta_\tau}{2\delta z^h_{j+1}}\right)E^{hk-1}_{\rho ij} + \left(-\frac{Z}{2} + \frac{\delta_\tau}{2\delta z^h_{j+1}}\right)E^{hk-1}_{\rho ij} \qquad (78)$$

Eqs. (65), (66), and (67) may now be written

$$G1(j)E^{hk}_{\rho ij} - G21(j)B^{k}_{\varphi ij} - G22(j)B^{k}_{\varphi ij-1} = G3(j) \qquad (79)$$

$$G4(j)B^{k}_{\varphi ij} + G5(j)E^{k}_{zij} = G6(j) \qquad (80)$$

$$B^{k}_{\varphi ij} + G7(j)E^{k}_{zij} + G81(j)E^{hk}_{\rho ij+1} + G8(j)E^{hk}_{\rho ij} = G9(j) \qquad (81)$$

As in the air equations, the above equations may be used to obtain a three-term recursion relation in B_φ. Setting $B_\varphi = 0$ at the maximum depth further reduces this to a two-term recursion relation. The following definitions are made:

$$G10(j) = G8(j)G5(j)G22(j)/G1(j) \qquad (82)$$

$$G11(j) = G5(j)\left[1 + \left(G81(j)G22(j)/G1(j+1) + G8(j)G21(j)/G1(j)\right)\right]$$

$$- G4(j)G7(j) \qquad (83)$$

$$G12(j) = G5(j)G81(j)G21(j+1)/G1(j+1) \tag{84}$$

$$G13(j) = G5(j)\Big[G9(j) - \Big(G81(j)G3(j+1)/G1(j+1) + G8(j)G3(j)/G1(j)\Big)\Big] - G6(j)G7(j) \tag{85}$$

The recursion relation is given by

$$B^{k}_{\varphi ij} = GE(j)B^{k}_{\varphi ij-1} + GF(j) \tag{86}$$

where

$$GE(j) = -G10(j)/\Big(G11(j) + G12(j)E(j+1)\Big) \tag{87}$$

$$GF(j) = \Big(G13(j) - G12(j)F(j+1)\Big)/\Big(G11(j) + G12(j)E(j+1)\Big) \tag{88}$$

Starting values for GE and GF are

$$GE(NT-1) = G10(NT-1)/G11(NT-1) \tag{89}$$

$$GF(NT-1) = G13(NT-1)/G11(NT-1) \tag{90}$$

where NT - 1 represents the next to the last grid line.

Examination of the two recursion relations in B_φ [Eqs. (61) and (86)] indicates that the proper starting value is B_φ at the air-ground interface. The air recursion relation then provides B_φ values throughout the θ grid starting at $\theta = 0^o$. The ground relation starts at $z = 0$ and goes to $z = z_{max}$. The interface value of B_φ is obtained using the following boundary conditions:

$$B_\varphi\Big|^{air}_{\theta=90^o} = B_\varphi\Big|^{ground}_{z=0} \tag{91}$$

and

$$E_r\Big|^{air}_{\theta=90^o} = E_\rho\Big|^{ground}_{z=0}$$

Since E_r and E_ρ are defined on half grid lines, they must be extrapolated to the interface. Let j = NTA define the air-ground interface, then

$$E_r\Big|_{\theta=90^o} = \frac{3E^{hk}_{riNTA} - E^{hk}_{riNTA-1}}{2} \tag{92}$$

and

$$E_\rho\Big|_{z=0} = \frac{3E^{hk}_{\rho iNTA+1} - E^{hk}_{\rho iNTA+2}}{2}$$

Thus, the boundary condition on the E field at the interface may be written

$$3E^{hk}_{riNTA} - E^{hk}_{riNTA-1} = 3E^{hk}_{\rho iNTA+1} - E^{hk}_{\rho iNTA+2} \tag{93}$$

Eq. (48) can be used to express E_r in terms of B_φ

$$E^{hk}_{rij} = \frac{A3(j) + A21(j)(rB_\varphi)^k_{ij} - A22(j)(rB_\varphi)^k_{ij-1}}{A1(j)} \tag{94}$$

and Eq. (78) for E_ρ in terms of B_φ

$$E^{hk}_{\rho ij} = \frac{G3(j) + G21(j)B^k_{\varphi ij} + G22(j)B^k_{\varphi ij-1}}{G1(j)} \tag{95}$$

Using Eq. (94), the following is obtained

$$3E^{hk}_{riNTA} - E^{hk}_{riNTA-1} = \frac{3A21(NTA)}{A1(NTA)} (rB_{\varphi})^{k}_{iNTA}$$

$$- \left[\frac{3A22(NTA)}{A1(NTA)} + \frac{A21(NTA - 1)}{A1(NTA - 1)}\right](rB_{\varphi})^{k}_{iNTA-1}$$

$$+ \frac{A22(NTA - 1)}{A1(NTA - 1)} (rB_{\varphi})^{k}_{iNTA-2}$$

$$+ \left[\frac{3A3(NTA)}{A1(NTA)} - \frac{A3(NTA - 1)}{A1(NTA - 1)}\right] \qquad (96)$$

Note that B_{φ} values at three different j lines appear on the right side of Eq. (96). Since the interest is in the B_{φ} value at j = NTA only, the air recursion relation is used to obtain

$$(rB_{\varphi})^{k}_{iNTA-1} = E(NTA - 1)(rB_{\varphi})^{k}_{iNTA} + F(NTA - 1)$$

and

$$(rB_{\varphi})^{k}_{iNTA-2} = E(NTA - 2)\left[E(NTA - 1)(rB_{\varphi})^{k}_{iNTA} + F(NTA - 1)\right]$$

$$+ F(NTA - 2) \qquad (97)$$

Substituting the above equations into Eq. (96) results in an expression for E_r at the boundary which depends only on constants and B_φ at the boundary. After a great deal of messy algebra the following may be written

$$E_r\Big|^{air}_{\theta=90^o} = K1(rB_\varphi)^k_{iNTA} + K2 \tag{98}$$

where

$$K1 = \frac{3A21(NTA)}{A1(NTA)} - E(NTA-1)\left[\frac{3A22(NTA)}{A1(NTA)} + \frac{A21(NTA-1)}{A1(NTA-1)}\right]$$

$$+ \frac{E(NTA-1)E(NTA-2)A22(NTA-1)}{A1(NTA-1)} \tag{99}$$

and

$$K2 = \left[\frac{3A3(NTA)}{A1(NTA)} - \frac{A3(NTA-1)}{A1(NTA-1)}\right] - F(NTA-1)$$

$$\times \left[\frac{3A22(NTA)}{A1(NTA)} + \frac{A21(NTA-1)}{A1(NTA-1)}\right] + \frac{A22(NTA-1)}{A1(NTA-1)}$$

$$\times \left[E(NTA-2)F(NTA-1) + F(NTA-2)\right] \tag{100}$$

Using the same method, the following may be obtained for E_ρ at the interface

$$E_\rho\Big|_{z=0}^{\text{ground}} = K3B_{\varphi iNTA}^{k} + K4 \tag{101}$$

where K3 and K4 have forms similar to K1 and K2. Application of the boundary condition in Eq. (91) now yields

$$(B_\varphi)_{iNTA}^{k} = \frac{K2 - K4}{K3 - rK1} \tag{102}$$

Thus, having obtained B_φ at the interface, the recursion relations may be used to fill in the rest of the grid.

5. SPECIAL DERIVATIVES

Due to the regridding in the theta and z directions discussed in Section II-2, the code version of the difference equations are changed slightly from those presented above. The change involves centering derivatives at regrid points. Figure 5 isolates several grid lines in the ground portion of the code. From the figure it is obvious that using the normal form for a derivative of $E_{\rho j}^{h}$ with respect to z,

$$\frac{\partial E_{\rho j}^{h}}{\partial z_j} = \frac{E_{\rho j+1}^{h} - E_{\rho j}^{h}}{\delta z_j^{h}} \tag{103}$$

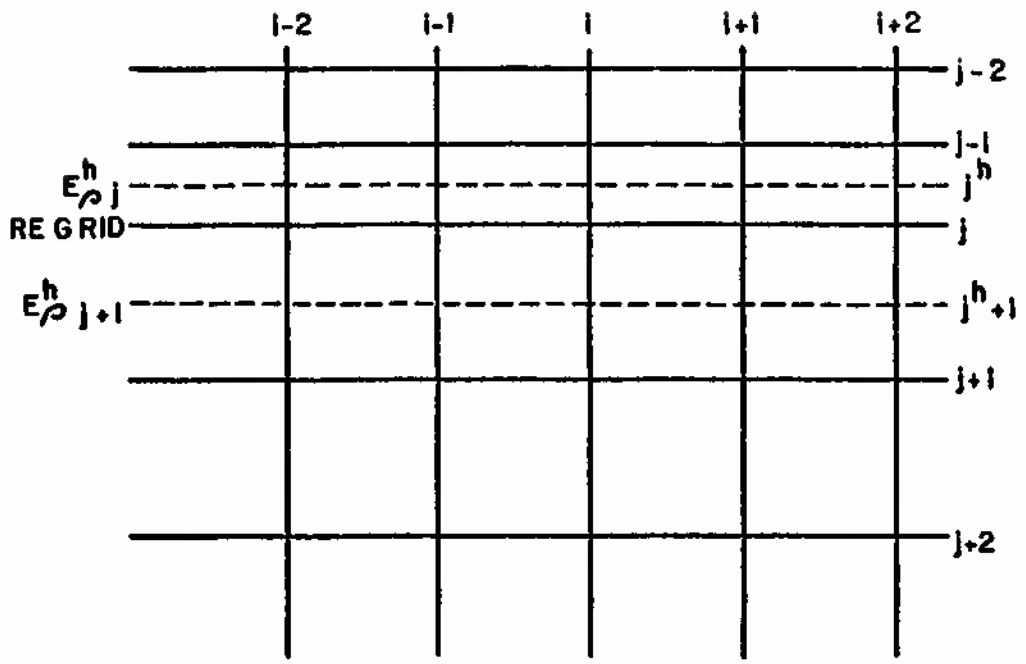

Figure 5. Isolation of z grid lines in a regrid portion of the grid. The dashed lines indicate half grid variables.

is incorrect. Thus, an adjustment must be made to center such derivatives. In the actual code such derivatives are calculated as

$$\frac{\partial E^h_{\rho j}}{\partial z^h_j} = \frac{E^h_{\rho j+1} - \frac{1}{2}\left(E^h_{\rho j} + E^h_{\rho j-1}\right)}{\partial z^h_{j+1}} \tag{104}$$

This averaging essentially centers the derivative by obtaining a value on the full grid line, j - 1. A similar situation occurs in the air portion of the grid when taking theta derivatives of E_r. The adjustment here is the same as in the ground.

In the code the differencing is carried out using the equations obtained in Section II-4. If the calculations are being performed on a regrid line, some of the quantities are then modified to properly center them as discussed above.

SECTION III

SOURCE AND AIR CHEMISTRY

In this section the driving currents and the air conductivity used in the SCX code will be discussed. As mentioned in the previous section, the ground conductivity is considered constant for the calculation; however, the air conductivity depends on the ionization rate and field values. Thus, the conductivity and field calculation are coupled. The methods used in handling this will be discussed below.

1. COMPTON CURRENT AND IONIZATION RATE

The source terms consist of currents and ionization rates resulting from the gamma and neutron output of the device. Prompt gammas undergo Compton collisions with the constituents of the atmosphere producing Compton electrons. Electrons so produced lose energy by ionizing the atmosphere and thus driving the conductivity. The neutrons interacting with the atmosphere produce additional gammas which also undergo interactions with the air. Two methods are currently used in EMP codes to obtain driving currents. In the first, analytic approximations are made and a functional form is obtained for the currents and ionization rates. These types of sources are by far the most convenient to use. It is not possible, however, to evaluate the effects of the approximation without performing a detailed transport calculation. In the second case the actual gamma and neutron transport is performed using Monte Carlo methods. These calculations yield delta function responses as a function of time, energy,

range, and angle for the currents and ionization rates. Results from Monte Carlo calculations are not generally in a form which can be directly implemented in EMP calculations. First, the results must be curve fit and the fits then implemented in a source program which calculates the currents and ionization rate for the final EMP program. Obviously, the second method is much more costly and time consuming that the first; however, it generally assures a greater accuracy in the final source terms used in EMP calculations. AFWL has chosen to use the second method in obtaining source terms for the SCX code to obtain the greater accuracy.

Sources due to prompt gammas are calculated using a separate code, GSOR, and serve as input to the SCX code. These input sources consist of the radial current, transverse current, and the ionization rate. The sources are based on monoenergetic, air-over-concrete gamma transport calculations using the TIG2 code. A complete documentation of this code and the results of the transport calculation are available (Ref. 4). Curve fits of the transport results were performed at AFWL (Ref. 5). The GSOR code uses the fitted delta function responses and convolution techniques to obtain the appropriate time history for the gamma sources. The fitted results are for eight monoenergetic gamma sources, and consequently GSOR also applies an appropriate energy spectrum to the sources.

Calculation of the neutron induced sources is performed within the SCX code. Neutron contributions are based on transport calculations for a neutron source at an air-ground

interface. Contributions from fast neutron collisions and secondary gamma ray collisions, arising from neutron inelastic scattering and capture of thermal neutrons, are included. The source energy spectrum is that of a typical thermonuclear device (Straker spectrum). Since the energy spectrum is folded into the transport, it cannot be altered; however, the neutron efficiency of the device can be input through SCX. The transport results, and the O5R-NIES code used to obtain them, are fully documented (Ref. 5). Curve fits to these results were performed by J. N. Wood (Ref. 7).

2. AIR CHEMISTRY AND CONDUCTIVITY

In Section III-1 the methods used to calculate the primary or Compton current were discussed. To obtain the total current density, the conduction currents must also be calculated. The creation of secondary electron-ion pairs by the Compton recoil electrons ionizes the atmosphere and renders it conducting. The resulting conduction currents which are set up must be accounted for in the EMP calculations. To do this the conductivity at the grid points must be obtained by keeping track of the formation and destruction of free electrons and ions and taking into account their mobility in the electric field.

The conduction current is defined by the generalized Ohms law as

$$j_s = \sigma E \tag{105}$$

and is generally obtained using the Lorentz model. Assume that plasma electrons are created at rest and that their motion is determined by collisions and the local electric field. The equation of motion for the electrons is then

$$\frac{d^2\vec{x}}{dt^2} + \nu_c \frac{d\vec{x}}{dt} = -\frac{e}{m}\vec{E} \tag{106}$$

where ν_c is the collision frequency. The creation of an electron at time t_0 results in the current

$$-e\frac{d\vec{x}}{dt} = \frac{e^2}{m}\int_{t_0}^{t} dt' \, e^{-\nu_c(t-t')}\vec{E}(t')$$

If $\dot{n}(t_0)$ is the rate of creation of secondary electrons, the total current density is given by

$$\vec{j}_s = \frac{e^2}{m}\int_{\infty}^{t} e^{-\nu_c (t-t')}\dot{\vec{E}}(t')\dot{n}(t')\, dt' \tag{107}$$

Eq. (107) is not generally soluble due to the spatial dependence of ν_c. However, for ν_c much larger or smaller than the frequencies of E and $\dot{n}$, approximate solutions may be easily obtained.

For a ground burst code such as SCX, the collision frequency will be on the order of 10^{12} sec^{-1} (Ref. 8). A solution to Eq. (107) can therefore be obtained using the high collision frequency approximation. The conduction current is then given by

$$\vec{j}_s = \frac{e^2 n}{m\nu_c} \vec{E} \tag{108}$$

Combining Eqs. (108) and (105), the following expression may be obtained for the conductivity

$$\sigma = \frac{e^2 n}{m\nu_c} \tag{109}$$

In a complete treatment of the conductivity, both the ionic density and the electron density must be considered. In actual calculations the collision frequency is replaced by a mobility defined as

$$\mu = \frac{q}{m\nu_c} \tag{110}$$

where q is the charge, m the mass, and ν_c the collision frequency of the particle in question. The conductivity is thus obtained from Eq. (109) as

$$\sigma = \sum_i q_i \mu_i n_i \qquad (111)$$

where the index i refers to the different species. The various number densities in the above equation are obtained by solving a set of rate equations.

An exact calculation of the number densities for Eq. (111) would require the consideration of all possible reactions between the constituents of the air and the weapon output. Fortunately, the EMP pulse length generally is small compared to the times required for most of the reactions and consequently only three possibilities need be considered. These are

1. Electron attachment.
2. Electron-Ion recombination.
3. Ion-Ion recombination.

The first concerns the attachment of free electrons to neutral oxygen molecules. This occurs through the two- and three-body processes,

$$e + O_2 \rightarrow O + O^- \qquad (112)$$

and

$$e + O_2 + M \rightarrow O_2^- + M$$

At field values less than 3×10^5 V/M the three-body process dominates while the two-body reaction is dominated at higher field values. Both processes are characterized by the attachment rate, β, which describes the rate of production of negative ions and disappearance rate of electrons. The rate equation for this process is then

$$\frac{dn_-}{dt} = - \frac{dn_e}{dt} \tag{113}$$

and

$$\frac{dn_e}{dt} = - \beta n_e \tag{114}$$

Since β is field dependent, it is coupled to the field calculation. In SCX a curve fit to experimental data is used for β. Fig. 6 shows the attachment rate as a function of total electric field as used in the SCX code.

Electron-ion recombination involves the dissociative recombination process

$$e + O_2^+ \rightarrow O + O \tag{115}$$

The rate coefficient for this process is α and the disappearance rate of O_2^+ and free electrons is given by

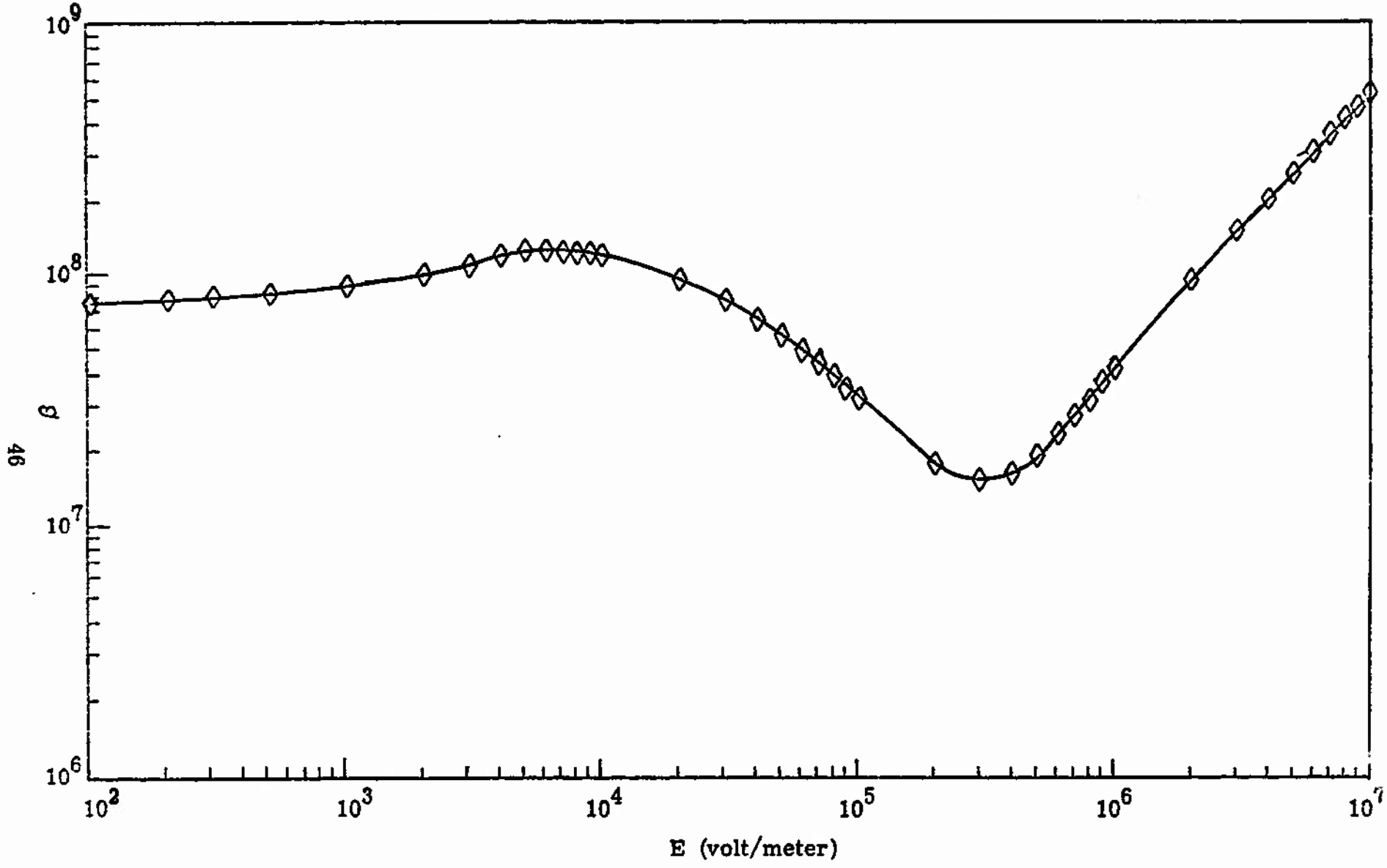

Figure 6. Electron attachment as a function of total electric field.

$$\frac{dn_e}{dt} = \frac{dn_+}{dt} \tag{116}$$

and

$$\frac{dn_e}{dt} = -\alpha n_e n_+ \tag{117}$$

The value for α used in SCX is taken from work by Van Lint and is

$$\alpha = 4.5 \times 10^{-12} \text{ meter}^3/\text{sec} \tag{118}$$

Ion-Ion recombination is a late time affect, becoming important when the electron density is low and the conductivity is dominated by ionic density. This is characterized by reactions such as

$$O^+ + O^- \rightarrow 2O \tag{119}$$

and

$$N_2^+ + O_2^- \rightarrow N_2 + O_2$$

The recombination rate is γ and the number density equations are

$$\frac{dn_+}{dt} = \frac{dn_-}{dt} \tag{120}$$

and

$$\frac{dn_+}{dt} = -\gamma n_+ n_- \tag{121}$$

Considering the above processes, the following rate equations can be written

$$\frac{dn_e}{dt} = Q - \beta n_e - \alpha n_e n_+ \tag{122}$$

$$\frac{dn_+}{dt} = Q - \alpha n_e n_+ - \gamma n_+ n_- \tag{123}$$

$$\frac{dn_-}{dt} = n_e \beta - \gamma n_+ n_- \tag{124}$$

From conservation of charge a fourth equation can be written,

$$n_+ = n_- + n_e \tag{125}$$

In Eqs. (122) and (123) Q is the secondary electron production rate, or ionization rate, which was discussed in Section III-1. Because of charge conservation, only two of the three rate equations need be solved. This is usually done numerically using a differencing scheme rather than obtaining a closed solution. Note that in obtaining the rate constants, α and γ, a lumped parameter approximation has been used. This approximation is necessary because of the lack of data concerning individual processes.

Having obtained the number densities through the solution of an of an appropriate combination of Eqs. (122) through (125), the mobility of the electrons and ions must next be found. Eq. (11) then yields the conductivity.

The determination of ionic mobilities is a difficult process involving a number of uncertainties. In SCX a single mobility, taken from DASA 1731, is used for both the positive and negative ions. The value used is

$$\mu_{ion} = 2.4E - 04 \text{ meter}^3/\text{volt-sec} \tag{126}$$

It is expected that the error in this quantity could be as great as 30%. However, the ion contribution to the conductivity is a late time effect, and the error will not affect early time predictions. Because codes such as SCX now run to 100 μsec, more work in this area is needed.

The electron mobility is a function of both the water vapor content in the atmosphere and the electric field. The electron mobility used in SCX was obtained by curve fitting results presented by C. Baum (Ref. 9). The water content is an input parameter and the fits give the mobility as a function of total the electric field for this content. Figure 7, taken from the paper by Baum, shows the electron mobility curves which were curve fit for use in SCX.

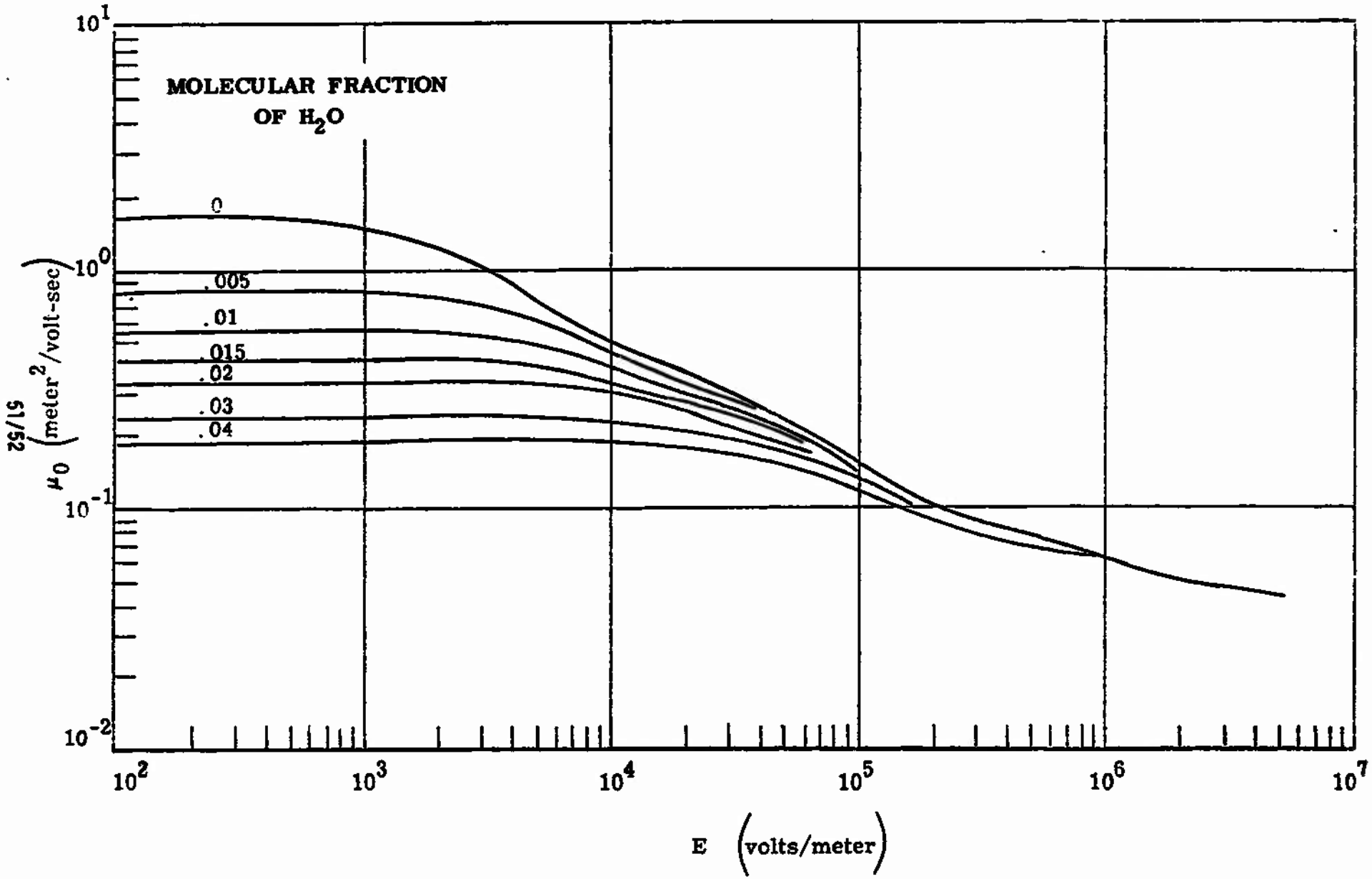

Figure 7. Electron mobility as a function of total electric field and water vapor content.

APPENDIX I
OUTER BOUNDARY CONDITION

1. INTRODUCTION

Whenever Maxwell's equations are solved by a finite-difference method in the source region, the calculation must be truncated at some surface surrounding the sources because of computer-memory and computation-time limitations. When one employs a central difference scheme in such a solution, he lacks sufficient conditions at the outer boundary to close the equations. The needed condition can be described physically as the statement that all the sources of fields are inside the boundary; mathematically this can be stated by requiring the fields to be represented by the outward-moving wave terms of a multipole expansion. From a practical (numerical) point of view the need is for field values at grid points on the outside boundary where a differencing of Maxwell's equations cannot supply them (since values at points outside the boundary would be required to calculate a central difference).

In the previous versions of the SC code, the assumption is made that at the outer calculational boundary the field is radiation field; i. e., the field has attained the asymptotic behavior that it must approach as $r \to \infty$. This assumption works well if the boundary is placed at a great enough distance that the field is indeed largely radiation. For large yields this is impractical and in all cases it saves computer storage and computation time to use a rigorous boundary condition since the difference equation solution can be truncated at a smaller range.

In the following, the mathematical analysis of the method is presented, then some numerical techniques to implement the scheme are given. Finally, the results of a sample calculation are presented.

2. ANALYSIS

The method can be described as two basic steps (taken at each retarded time):

1. Using the values of E_θ at the next-to-last range grid points, the outgoing-wave multipole expansion coefficients are found.
2. Using the expansion coefficients found in (1), the values of (rB_ϕ) at the last (outside boundary) range grid points are found. This is sufficient to close the SCX difference equations on the outside boundary.

To implement this scheme mathematically, one writes the general form for azimuthally-symmetric, electric-multipole, outgoing waves (Ref. 1):

$$E_r = -\sum_{\ell=1}^{\infty} \frac{\sqrt{\ell(\ell+1)}}{r} \Xi_\ell(r)\, a_\ell(t^*)\, \bar{P}_\ell(\cos\theta) \qquad (127)$$

$$E_\theta = \sum_{\ell=1}^{\infty} \Lambda_\ell(r)\, a_\ell(t^*)\, \bar{P}_\ell^1(\cos\theta) \tag{128}$$

$$cB_\phi = \sum_{\ell=1}^{\infty} \frac{1}{c} \frac{\partial}{\partial t^*} \Xi_\ell(r)\, a_\ell(t^*)\, \bar{P}_\ell^1(\cos\theta) \tag{129}$$

where only odd values of ℓ are needed in the summations for the assumed symmetry (the analysis will include both even and odd terms for the sake of generality). The functions $\bar{P}_\ell$ are normalized Legendre polynomials and $\bar{P}_\ell^1$ are the normalized associated Legendre polynomials of the first kind; t^* is retarded time defined as $t^* = t - r/c$; Λ_ℓ and Ξ_ℓ are differential operators given by

$$\Xi_\ell(r) = \sum_{j=0}^{\ell} \frac{\mu_{\ell j}}{r^{j+1} c^{\ell-j}} \frac{\partial^{\ell-j}}{\partial t^{*\,\ell-j}} \tag{130}$$

$$\Lambda_\ell(r) = \sum_{j=0}^{\ell+1} \frac{\nu_{\ell j}}{r^{j+1} c^{\ell+1-j}} \frac{\partial^{\ell+1-j}}{\partial t^{*\,\ell+1-j}} \tag{131}$$

$$\mu_{\ell j} = \frac{\prod_{k=0}^{j} (\ell+k)(\ell-k+1)}{\ell(\ell+1)2^j j!}, \quad j=0,\ 1,\ \ldots,\ \ell \tag{132}$$

$$\nu_{\ell j} = \mu_{\ell j} \frac{\ell(\ell+1) + j(j-1)}{\ell(\ell+1) - j(j-1)}, \quad j=0,\ 1,\ \ldots,\ \ell,\ \nu_{\ell,\ell+1} = \nu_{\ell\ell} \tag{133}$$

The field component E_θ is given at $r = R$ (R = next-to-the-last range) by

$$E_\theta (R, \vartheta, t^*) = \sum_{\ell=1}^{\infty} A_\ell(t^*) \bar{P}_\ell^1(\cos\theta) \tag{134}$$

Upon equating the coefficients of Eqs. (128) and (134), one can express the unknown coefficients $a_\ell(t^*)$ in terms of the known coefficients $A_\ell(t^*)$

$$\Lambda_\ell(R)\, a_\ell(t^*) = A_\ell(t^*) \tag{135}$$

It is convenient to express the above coefficients in terms of a dimensionless time variable $\tau = ct^*/R$. The operator $\Lambda_\ell(R)$ now becomes

$$\Lambda_\ell(R) = \frac{1}{R^{\ell+2}} \sum_{j=0}^{\ell+1} \nu_{\ell j} \frac{\partial^{\ell+1-j}}{\partial \tau^{\ell+1-j}} \tag{136}$$

Redefine the coefficients

$$b_\ell(\tau) = a_\ell\left(\frac{\tau R}{c}\right) R^{-(\ell+2)} \tag{137}$$

$$B_\ell(\tau) = \Lambda_\ell\left(\frac{\tau R}{c}\right) \tag{138}$$

Equation (135), expressed in terms of τ, becomes

$$R^{\ell+2}\, \Lambda_\ell(R)\, b_\ell(\tau) = B_\ell(\tau) \tag{139}$$

The application to the SCX code proceeds in the following steps:

A. For each retarded time, the coefficients $A_\ell(t^*)$ in Eq. (134) must be determined with r = R corresponding to the "next-to-the-last" value of r where E_θ is known. This is accomplished by the usual integration, i. e. ,

$$A_\ell(t^*) = 2\int_0^{\pi/2} E_\theta(R,\theta,t^*)\,\tilde{P}_\ell^1(\cos\theta)\sin\theta\,d\theta,\ \ell \text{ odd} \qquad (140)$$

B. The differential equation (135) must then be solved. Note:

1. $A_\ell(t^*)$ (obtained above) is the forcing function.
2. Not only $a_\ell(t^*)$, but its first $(\ell+1)$ derivatives will be needed for evaluating field components at other radii.
3. The equation and solution are simplified by changing to a dimensionless time variable $\tau = ct^*/R$, hence $\Delta\tau = c\Delta t^*/R$.

Thus, new variables are defined by Eqs. (137) and (138). The differential equation (135) (also 139) can be written

$$\sum_{j=0}^{\ell+1} \nu_{\ell j}\, b_\ell^{(\ell+1-j)}(\tau) = B_\ell(\tau) \qquad (141)$$

where $b_\ell^{(n)}(\tau) = \dfrac{d^n b_\ell(\tau)}{d\tau^n}$, $n = 1, 2, \ldots, \ell+1$

Suppose $b_\ell^{(n)}(\tau)$ is known for a given τ and it is desired to find $b_\ell^{(n)}(\tau+\Delta\tau)$. Using a Taylor expansion truncated after the $(\ell+1)^{th}$ order to represent $b_\ell(\tau)$ for the domain $[\tau,\tau+\Delta\tau]$ one obtains

$$b_\ell^{(n)}(\tau+\Delta\tau) = \sum_{j=0}^{\ell-n+1} \frac{b_\ell^{(j+n)}(\tau)}{j!}\Delta\tau^j,\ n=1,\ldots,\ell \qquad (142)$$

Substituting the $b_\ell^{(n)}(\tau+\Delta\tau)$, $n=1,\ldots,\ell$ into Eq. (141) (with τ set to $\tau+\Delta\tau$), one can solve for $b_\ell^{(\ell+1)}(\tau+\Delta\tau)$, i.e.,

$$b_\ell^{(\ell+1)}(\tau+\Delta\tau) = B_\ell(\tau+\Delta\tau) - \sum_{j=1}^{\ell+1} \nu_{\ell j}\, b_\ell^{(\ell+1-j)}(\tau+\Delta\tau) \tag{143}$$

(Note that $\nu_{\ell 0} = 1$)

Substituting back to find the field components for any radius, one obtains

$$a_\ell(t^*) = R^{\ell+2} b_\ell(ct^*/R)$$

$$\frac{d^n a_\ell(t^*)}{dt^{*n}} = R^{\ell+2}\left(\frac{c}{R}\right)^n b_\ell^{(n)}(ct^*/R)$$

$$\frac{d^n a_\ell(t^*)}{dt^{*n}} = R^{\ell+2-n} c^n b_\ell^{(n)}(\tau) \tag{144}$$

$$\Xi_\ell(r) a_\ell(t^*) = \sum_{j=0}^{\ell} \frac{\mu_{\ell j} R^{j+2} b_\ell^{(\ell-j)}(\tau)}{r^{j+1}} \tag{145}$$

$$\Lambda_\ell(r)\, a_\ell(t^*) = \sum_{j=0}^{\ell+1} \nu_{\ell j}\left(\frac{R}{r}\right)^{j+1} b_\ell^{(\ell+1-j)}(\tau) \tag{146}$$

$$E_r = -\sum_{\ell=1}^{\infty}\left[\sqrt{\ell(\ell+1)}\sum_{j=0}^{\ell} \mu_{\ell j}\left(\frac{R}{r}\right)^{j+2} b_\ell^{(\ell-j)}(\tau)\right] \bar{P}_\ell(\cos\theta) \tag{147}$$

$$E_\theta = \sum_{\ell=1}^{\infty}\left[\sum_{j=0}^{\ell+1} \nu_{\ell j}\left(\frac{R}{r}\right)^{j+1} b_\ell^{(\ell+1-j)}(\tau)\right]\bar{P}_\ell^1(\cos\theta) \qquad (148)$$

$$cB_\phi = \sum_{\ell=1}^{\infty}\left[\sum_{j=0}^{\ell} \mu_{\ell j}\left(\frac{R}{r}\right)^{j+1} b_\ell^{(\ell+1-j)}(\tau)\right]\bar{P}_\ell^1(\cos\theta) \qquad (149)$$

At each time step the $b_\ell^{(n)}(\tau)$ should be written on a tape for future field evaluation using Eqs. (147), (148), and (149). Note that $b_\ell^{(\ell+1)}$ represents the radiation (r^{-1}) term, $b_\ell^{(\ell)}$ represents r^{-2} term, etc. For extrapolation, one could include only b_ℓ terms found to be important and greatly reduce the storage requirements though probably including all significant effects. The proper selection of terms should be determined by trial and error.

C. The value of (rB_ϕ) is needed in SCX for r equal to the last range grid value, i.e., $r = R + \Delta r$. Hence,

$$(rB_\phi)_{r=R+\Delta r} = (rB_\phi)_{r=R} + \Delta r\,\partial(rB_\phi)/\partial r \qquad (150)$$

The quantity $\Delta r\,\partial(rB_\phi)/\partial r$ is calculated by multiplying both sides of Eq. (149) by r/c, then taking the partial derivative with respect to r to obtain

$$\Delta r\frac{\partial(rB_\phi)}{\partial r} = -\frac{\Delta r}{c}\sum_{\ell=1}^{\infty}\left[\sum_{j=1}^{\ell} \mu_{\ell j}\, j\left(\frac{R}{r}\right)^{j+1} b_\ell^{(\ell+1-j)}(\tau)\right]\bar{P}_\ell^1(\cos\theta) \qquad (151)$$

Notice that the radiation (j = 0) term does not contribute in Eq. (151) (since $r \cdot (1/r) = 1$ and $\partial(1)/\partial r = 0$). This underlines the fact that both incoming and outgoing waves have 1/r terms. Hence, enforcing 1/r (or "radiation") behavior at the outer boundary is not equivalent or similar to enforcing the outward-moving wave condition.

3. NUMERICAL TECHNIQUES

In this section various numerical procedures for implementing the analysis of the last section are discussed. In particular, the method of numerical integration used in Eq. (140) is given; the method used for calculating Legendre functions is given; stability problem arising in calculating the $b_\ell^{(n)}$'s (Eqs. 142 and 143) is discussed; and a criteria for truncating the multipole expansion is given.

A. Numerical Integration with Kernel P_n^1. The problem addressed is that of numerically performing the integration shown in Eq. (140). It is assumed that $E(\theta) = E_\theta(R, \theta, t)$ can be adequately represented (as a function of θ) between grid points by straight lines on the E - x plane, where $x = \cos\theta$. Analytic expressions for the indefinite integrals $\int P_\ell^1(\cos\theta)\sin\theta\, d\theta$ and $\int \cos\theta\, P_\ell^1(\cos\theta)\sin\theta\, d\theta$ are derived and the integral (140) is expressed as a sum of these applied between grid points.

Let $E_i = E(\theta_i)$ be the data set given, where $E_1 = E(0) = 0$, and $E_N = E(\theta_N) = E(\pi/2)$. The θ_i are assumed to be ordered. Between the two grid points θ_i and θ_{i+1} it is assumed that

$$E(\theta) = g\cos\theta + h \tag{152a}$$

where g and h are the constants

$$g = (E_i - E_{i+1})/(\cos\theta_i - \cos\theta_{i+1}) \tag{152b}$$

$$h = E_i - g\cos\theta_i \tag{152c}$$

Thus,

$$\int_{\theta_i}^{\theta_{i+1}} E(\theta)\,\bar{P}_\ell^1(\cos\theta)\sin\theta\,d\theta$$

$$= \int_{\theta_i}^{\theta_{i+1}} (g\cos\theta + h)\,\bar{P}_\ell^1(\cos\theta)\sin\theta\,d\theta$$

$$\int_{\theta_i}^{\theta_{i+1}} E(\theta)\,\bar{P}_\ell^1(\cos\theta)\sin\theta\,d\theta$$

$$= g\left[\bar{I}_1(\theta_{i+1}) - \bar{I}_1(\theta_i)\right] + h\left[\bar{I}_2(\theta_{i+1}) - \bar{I}_2(\theta_i)\right] \tag{153}$$

where $\bar{I}_1$ and $\bar{I}_2$ are the indefinite integrals

$$\bar{I}_1(\theta) = \int \cos\theta\,\bar{P}_\ell^1(\cos\theta)\sin\theta\,d\theta \tag{154}$$

and

$$\bar{I}_2(\theta) = \int \bar{P}_\ell^1(\cos\theta)\sin\theta\,d\theta \tag{155}$$

Let

$$I_1(\theta) = \int \cos\theta\,P_\ell^1(\cos\theta)\sin\theta\,d\theta \tag{156}$$

and

$$I_2(\theta) = \int P_\ell^1(\cos\theta)\sin\theta\,d\theta \tag{157}$$

then

$$\bar{I}_1(\theta) = -\sqrt{\frac{2n+1}{2n(n+1)}}\ I_1(\theta) \tag{158}$$

and

$$\bar{I}_2(\theta) = -\sqrt{\frac{2n+1}{2n(n+1)}}\ I_2(\theta) \tag{159}$$

From Jahnke and Emde (Ref. 10) one obtains (for n odd):

$$P_n(\cos\theta) = 2\cdot\frac{1\cdot 3\cdot 5\cdots(2n-1)}{2^n n!}\left[\cos n\theta + \frac{1}{1}\frac{n}{2n-1}\cos(n-2)\theta\right.$$

$$+\frac{1\cdot 3}{1\cdot 2}\frac{n(n-1)}{(2n-1)(2n-3)}\cos(n-4)\theta + \cdots \tag{160}$$

$$\left.+\frac{1\cdot 3\cdots(n-2)}{\frac{n-1}{2}\ !}\cdot\frac{n(n-1)\cdots\frac{n+3}{2}}{(2n-1)(2n-3)\cdots(n+2)}\cos\theta\right]$$

Equation (160) can be written

$$P_n(\cos\theta) = 2\sum_{j=0}^{\frac{n-1}{2}} a_{n-j}a_j\cos(n-2j)\theta \tag{161}$$

where

$$a_o = 1\ , \tag{162a}$$

$$a_i = \frac{1\cdot 3\cdot 5\cdots(2i-1)}{2^i i!}\ ,\ i = 1, 2, \ldots, n_{max} \tag{162b}$$

The associated Legendre function P_n^1 can be written

$$P_n^1(\cos\theta) = -\frac{dP_n(\cos\theta)}{d\theta}$$

$$P_n^1(\cos\theta) = 2\sum_{j=0}^{\frac{n-1}{2}} a_{n-j}\, a_j\, (n-2j)\sin(n-2j)\theta \tag{163}$$

Hence, the integrals I_1 and I_2 can be written as sums of terms of the form

$$T_1(\theta) = \int \cos\theta\ \sin(n-2j)\theta\ \sin\theta\ d\theta \tag{164}$$

and

$$T_2(\theta) = \int \sin(n-2j)\theta\ \sin\theta\ d\theta \tag{165}$$

Using trigonometric identities to combine the terms in the integrands and integrating, one obtains

$$T_1(\theta) = \frac{1}{4}\left[\frac{\sin(n-2j-2)\theta}{n-2j-2} - \frac{\sin(n-2j+2)\theta}{n-2j+2}\right] \tag{166}$$

and

$$T_2(\theta) = \frac{1}{2}\left[\frac{\sin(n-2j-1)\theta}{n-2j-1} - \frac{\sin(n-2j+1)\theta}{n-2j+1}\right] \tag{167}$$

Hence,

$$I_1(\theta) = \frac{1}{2}\sum_{j=0}^{\frac{n-1}{2}} a_{n-j} a_j (n-2j)\left[\frac{\sin(n-2j-2)\theta}{n-2j-2} - \frac{\sin(n-2j+2)\theta}{n-2j+2}\right] \tag{168}$$

In writing I_2, one should notice that for $j = \frac{n-1}{2}$, both numerator and denominator of the first term on the right-hand side of Eq. (167) vanishes; the limit value θ should be substituted for $\frac{\sin(n-2j-1)\theta}{n-2j-1}$ in this case. Thus,

$$I_2(\theta) = a_{\frac{n+1}{2}} a_{\frac{n-1}{2}} \left[\theta - \frac{1}{2}\sin 2\theta\right] + \sum_{j=0}^{\frac{n-3}{2}} a_{n-j} a_j (n-2j)$$

$$\times \left[\frac{\sin(n-2j-1)\theta}{n-2j-1} - \frac{\sin(n-2j+1)\theta}{n-2j+1}\right] \qquad (169)$$

Note that $j = \frac{n-1}{2}$ represents an unusual case in Eq. (168) that should be treated separately; that is $(n-2j-2) = -1$ in this case. If it is desired to use $(n-2j-2)$ as an index, then indeed it must be treated separately; one writes

$$I_1(\theta) = \frac{1}{2} a_{\frac{n+1}{2}} a_{\frac{n-1}{2}} \left(\sin\theta - \frac{\sin 3\theta}{3}\right) + \frac{1}{2} \sum_{j=0}^{\frac{n-3}{2}} a_{n-j} a_j (n-2j)$$

$$\times \left[\frac{\sin(n-2j-2)\theta}{n-2j-2} - \frac{\sin(n-2j+2)\theta}{n-2j+2}\right]$$

The quantities $\frac{\sin i\theta}{i}$, $i = 1, 2, \ldots, (n_{max}+2)$ are computed and stored for each data point (in the code) to avoid redundant computations.

B. Calculation of the Legendre Function. The form of the Legendre function requiring the fewest operations to compute is the Gauss normalized Legendre function denoted $P^{n,m}(\cos\theta)$. It is defined such that the coefficient of the highest order term is one; hence, the recursion formula has fewer arithmetic operations than for other normalizations. The recursion formula is:

$$P^{0,0}(\cos\theta) = 1 \tag{170a}$$

$$P^{n,n}(\cos\theta) = \sin\theta\, P^{n-1,n-1}(\cos\theta) \tag{170b}$$

$$P^{n,m}(\cos\theta) = \cos\theta\, P^{n-1,m}(\cos\theta) - K_{n,m} P^{n-2,m}(\cos\theta), \quad n > m \tag{170c}$$

where $K_{n,m} = \dfrac{(n-1)^2 - m^2}{(2n-1)(2n-3)}$

Note:

1) The constants $K_{n,m}$ should be computed once and stored; they should not be re-computed every time the recursion formula is used for a different value of θ.

2) Equation (170c) for $n = m + 1$ is a special case, i.e., $K_{m+1,m} = 0$ and $P^{m-1,m} = 0$

Since the Gauss-normalized functions are defined such that the highest order term has coefficient equal to one, it is easy to find the factor that transforms them to the Legendre functions as defined by Abromowitz and Stegun (Ref. 11) (A&S) or Jahnke and Emde (Ref. 10) (J&E); one must merely determine the coefficient of the highest order term. The coefficient can be deduced from A&D Eqs. 8.5.5 and 8.5.3 or taken directly from J&E p. 110, Eq. 1. The coefficient is

$$c(n,m) = \frac{(2n)!}{2^n \cdot n!\,(n-m)!}$$

$$c(n,m) = \frac{1 \cdot 3 \cdot 5 \cdots (2n-1)}{(n-m)!} \tag{171}$$

Thus

$$P_n^m(\cos\theta) = c(n,m)\, P^{n,m}(\cos\theta)$$

where the left-hand side is the associated Legendre function as it is usually defined (J&E or A&S).

The normalized functions are given by (A&S, p. 332)

$$\bar{P}_n^m = (-1)^m \sqrt{\frac{(2n+1)(n-m)!}{2(n+m)!}}\; P_n^m \tag{172}$$

Thus

$$\bar{P}_n^m = (-1)^m \sqrt{\frac{2n+1}{2(n+m)!\,(n-m)!}}\; \left[1 \cdot 3 \cdot 5 \cdots (2n-1)\right] P^{n,m} \tag{173}$$

C. Stability Criteria. In solving the differential Eq. (141) by differencing using Eqs. (142) and (143), one can encounter an instability if $\Delta\tau$ is too large. One can see this by writing Eq. (143) including only the j=1 term:

$$b_\ell^{(\ell+1)}(\tau+\Delta\tau) = B_\ell(\tau+\Delta\tau) - \nu_{\ell 1}\, b_\ell^{(\ell)}(\tau+\Delta\tau) \tag{174}$$

but

$$b_\ell^{(\ell)}(\tau+\Delta\tau) = b_\ell^{(\ell)}(\tau) + \Delta\tau\, b_\ell^{(\ell+1)}(\tau) \tag{175}$$

from Eq. (142). Substituting Eq. (175) into Eq. (174) one obtains

$$b_\ell^{(\ell+1)}(\tau+\Delta\tau) = B_\ell(\tau+\Delta\tau) - \nu_{\ell 1} b_\ell^{(\ell)}(\tau) - \nu_{\ell 1}\, \Delta\tau\, b_\ell^{(\ell+1)}(\tau) \tag{176}$$

Hence, if $\nu_{\ell 1}\Delta\tau > 1$, the updated value of $b_\ell^{(\ell+1)}$ will be changed by an amount greater than its previous value and an instability can result. For stability, one requires $\nu_{\ell 1}\Delta\tau < 1$, or

$$\frac{1}{2}\,\ell(\ell+1)\Delta\tau < 1 \tag{177}$$

Solving Eq. (177) for ℓ, one obtains

$$\ell < \sqrt{\frac{1}{4} + \frac{2}{\Delta\tau}} - \frac{1}{2} \tag{178}$$

Whenever $\Delta\tau$ is changed, it is necessary to adjust the maximum value of ℓ so that inequality 178 is satisfied.

D. Convergence Criteria. At early times near the source region of a ground burst, high field values occur only near the ground. Such a nonuniform field distribution results in a very slow convergence of the multipole expansion. After a short time the fields spread to a much more uniform configuration and the expansion is much more quickly convergent. After 7 μsec (for a sample calculation) only about eight terms are needed (odd orders through fifteen). Hence, the calculation is begun with a large number of terms; these terms are retained until the peak is passed, then (at each time) the two highest order terms (A_ℓ's) are compared with the dipole term. If <u>both</u> satisfy

$$\left|A_\ell(\tau)\right| < 10^{-3}\left|A_1(\tau)\right| \tag{179}$$

then the highest order term is dropped. Two terms are checked so that a truncation is not made on the basis of a zero crossing of one term. This is continued until a specified minimum number of terms remain.

4. RESULTS SAMPLE CALCULATION

In applying time-domain multipole theory to supply a proper boundary condition to the outer boundary of SC calculations, certain things have been learned about the properties of the fields at the outer boundary and the effects of the boundary condition on SC calculations. These are briefly discussed in the following paragraphs and are illustrated in the accompanying graphs.

A. Convergence Properties. Because of rapid field variation as a function of θ near the equator, the expansion is very slowly convergent at early times. The convergence improves rapidly (for the test problem) until about 7 μsec. This is illustrated in Figures 8, 9, and 10 where the magnitude of the multipole coefficients is plotted as a function of order at various times from 35 shakes to 40 μsec at 3090 meters range. Fewer orders are calculated at late times than at early times in accordance with two criteria: stability criteria, i.e., Eq. (177); and, convergence criteria, i.e., drop the last term when the two highest order terms are both smaller than 10^{-3} times the dipole term.

B. Radiation Field vs Near Field. At very early times the field is essentially all radiation field; this is because only high frequency (or very short wavelengths) are important at early times. As time advances the field energy moves to the near-field terms; the characteristic time for this process is $2R/c\ell(\ell+1)$ where R is the radial coordinate, c is the velocity of light and ℓ is the order of the multipole. Hence, the field

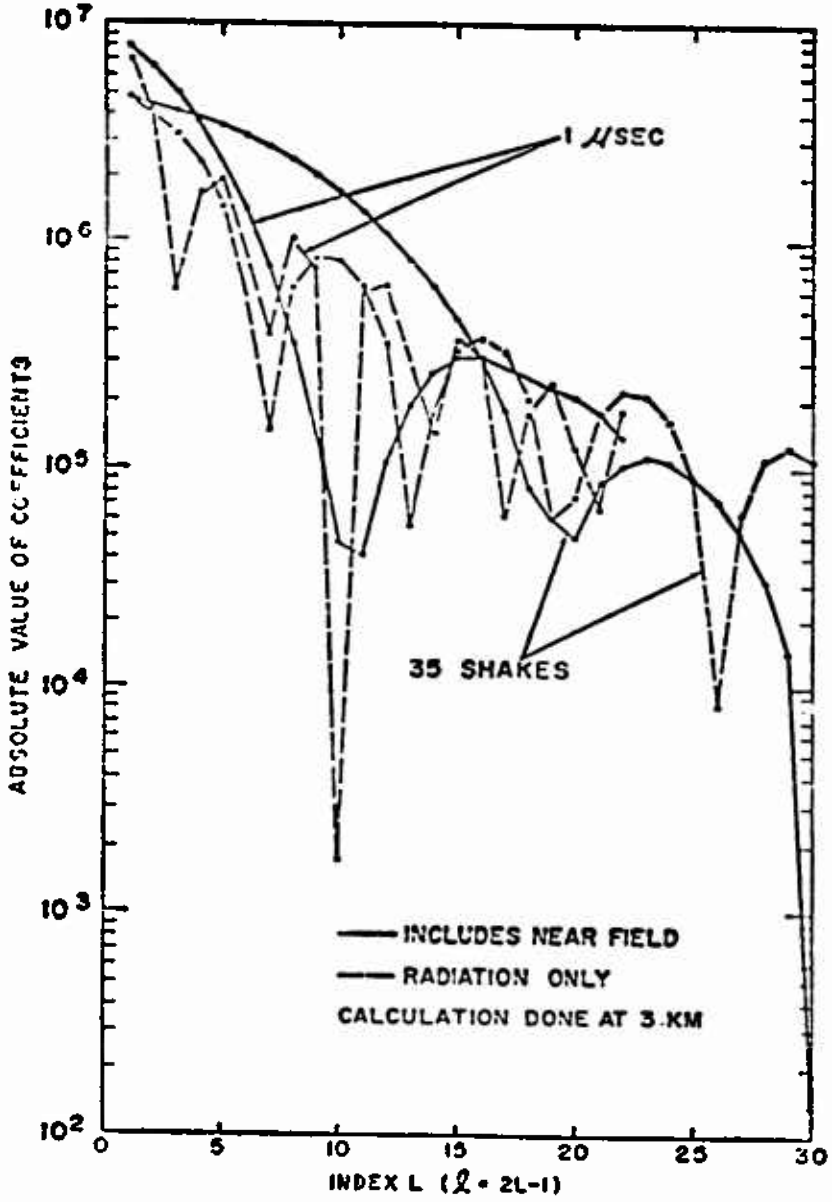

Figure 8. Magnitude of Multipole Coefficients at 35 Shakes and 1 μsec.

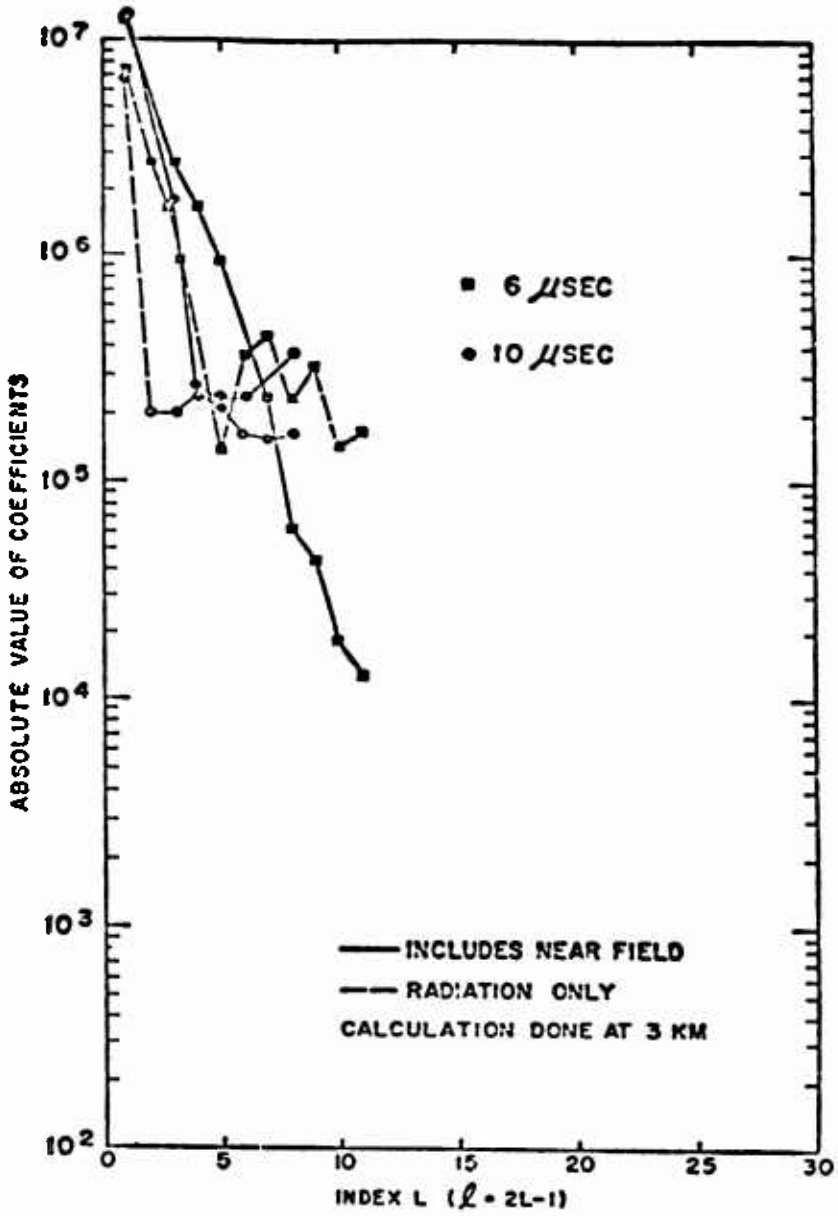

Figure 9. Magnitude of Multipole Coefficients at 8 μsec and 10 μsec.

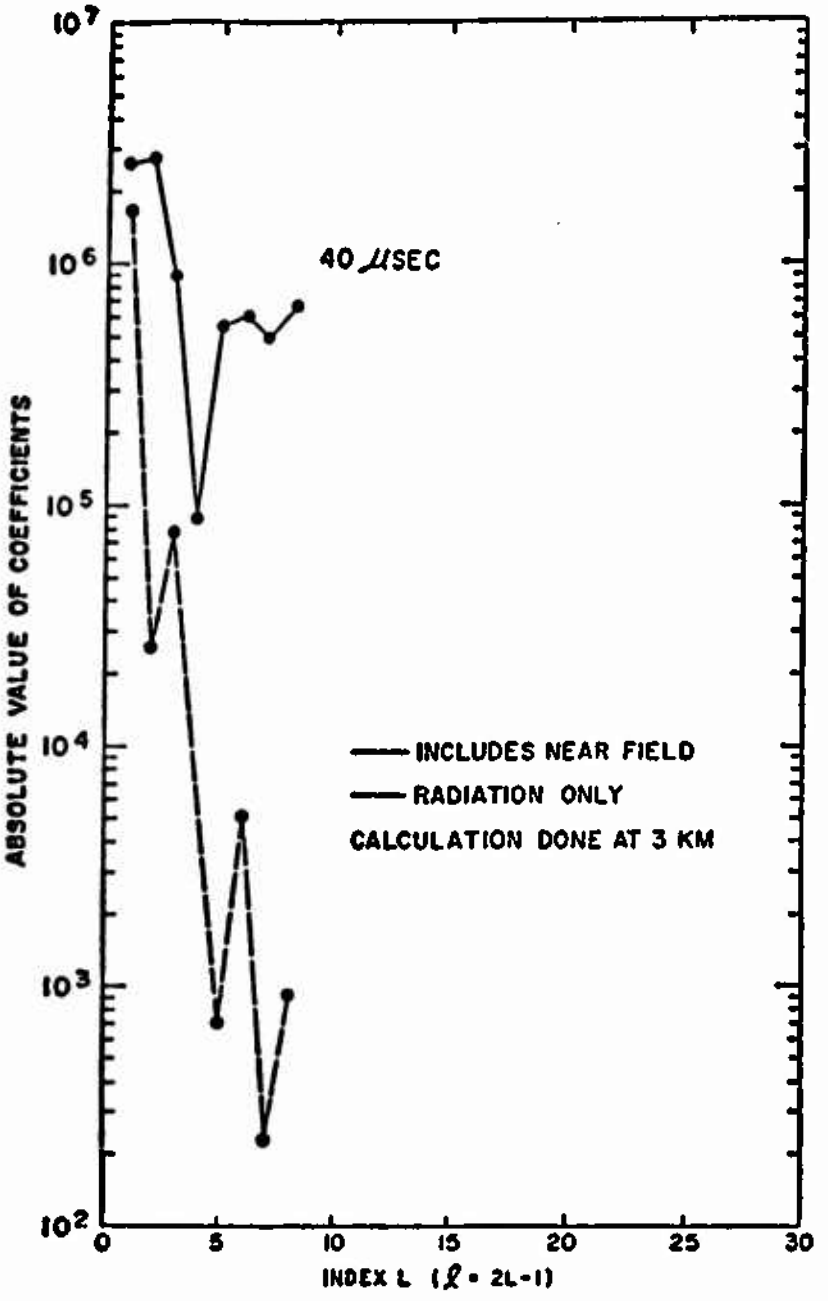

Figure 10. Magnitude of Multipole Coefficients at 40 μsec.

energy moves to the near-field terms very rapidly for high-order multipoles. A radiation field will be sustained only if high-frequency components are present; i. e., the fields change appreciably in the characteristic time just given. By 40 μsec at 3000 meters range (see Figure 10), the fields are almost entirely near field.

The convergence and near- vs far-field effects are illustrated in another way in Figure 11 which is a time history of E_θ (at 3 km) along with the total dipole and octopole contributions and their respective radiation terms. Notice that E_θ is approximated more and more closely by the first two terms as time progresses. Note also the relative rate at which the radiation terms diverge from the total contributions of the dipole and octopole terms. The characteristic times for these terms are 10 and 1.7 μsec respectively.

C. Comparison Calculations. The results of three SC runs are included in this report. The runs are:

1) SC-111 run to 3090 meters with the new boundary condition and source tape SS-15.
2) SC-112 run to 3090 meters with the old (radiation) boundary condition and source tape SS-15. This run is identical in all respects to SC-111 except for the boundary condition.
3) SC-102 run to 5090 meters with the old (radiation) boundary condition and source tape SS-34.

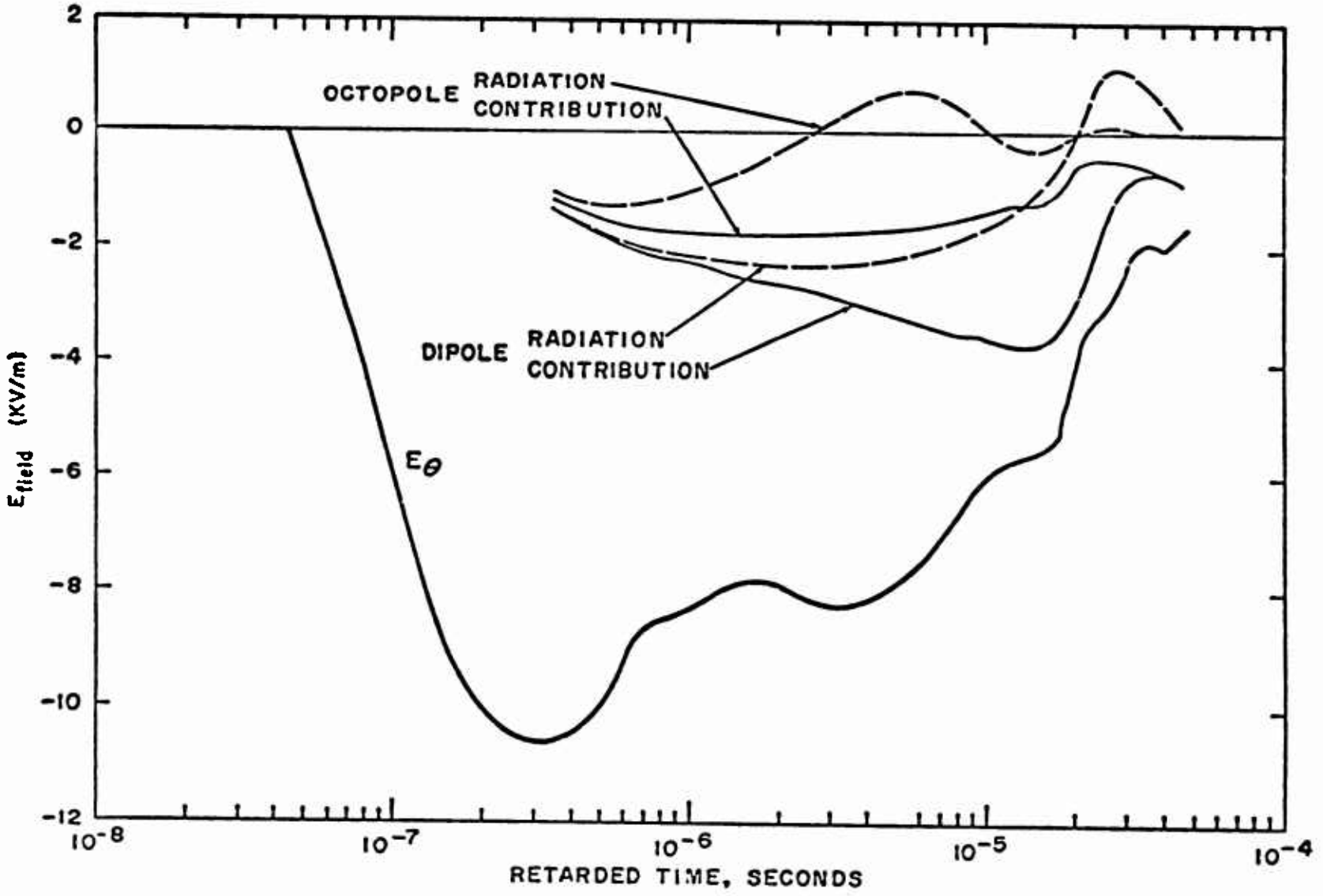

Figure 11. The Dipole and Octopole Contributions to E_θ.

Note that two source runs were used for the SC runs in this report. A 3090 meter run (SS-15) was used for SC-111 and SC-112. A newer version of the source code was used for a 5090 meter run (SS-34) for SC-102. This newer version used slightly modified functional forms for the dose rate and radial current after neutron arrival from those reported by Wood (Ref. 12), involving a better range curve fit to the parameters A3, B3, B4 and B5. Overlays of the radial current of these two SS runs at ranges of 2000 m and 3000 m are included in Figures 12 and 13 to show the minor differences involved. No difference in the ionization rate of the two runs is observable graphically.

Figures 14 through 17 illustrate the effect of the proper boundary condition on SC results. Figures 14 and 15 are graphs of E_θ and B_ϕ respectively at a range of 2000 meters. They show the large effect at 2000 meters of the boundary condition imposed at 3090 meters, the smaller effect of the boundary condition at 5090 meters, and the fact that a proper boundary condition at 3090 meters yields an improvement similar to that of moving the improperly-treated boundary out 2000 meters from 3090 meters to 5090 meters. Curve C falls away from A and B at about 2 - 3 μsec because its source term (SS-34) falls below SS-15 in that region. Figures 16 and 17 yield a similar result at 3000 meters range except that Curves A and C do not agree as closely as at 2000 meters. This suggests

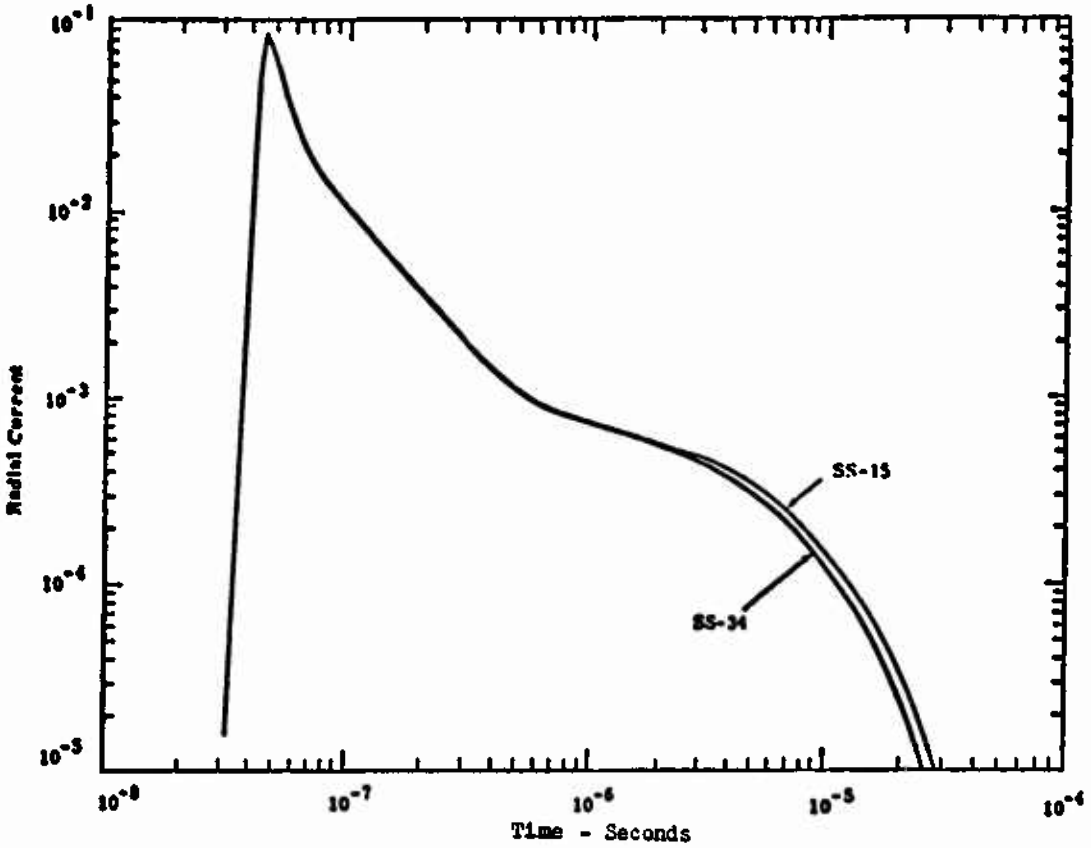

Figure 12. Source Current at 2 Km.

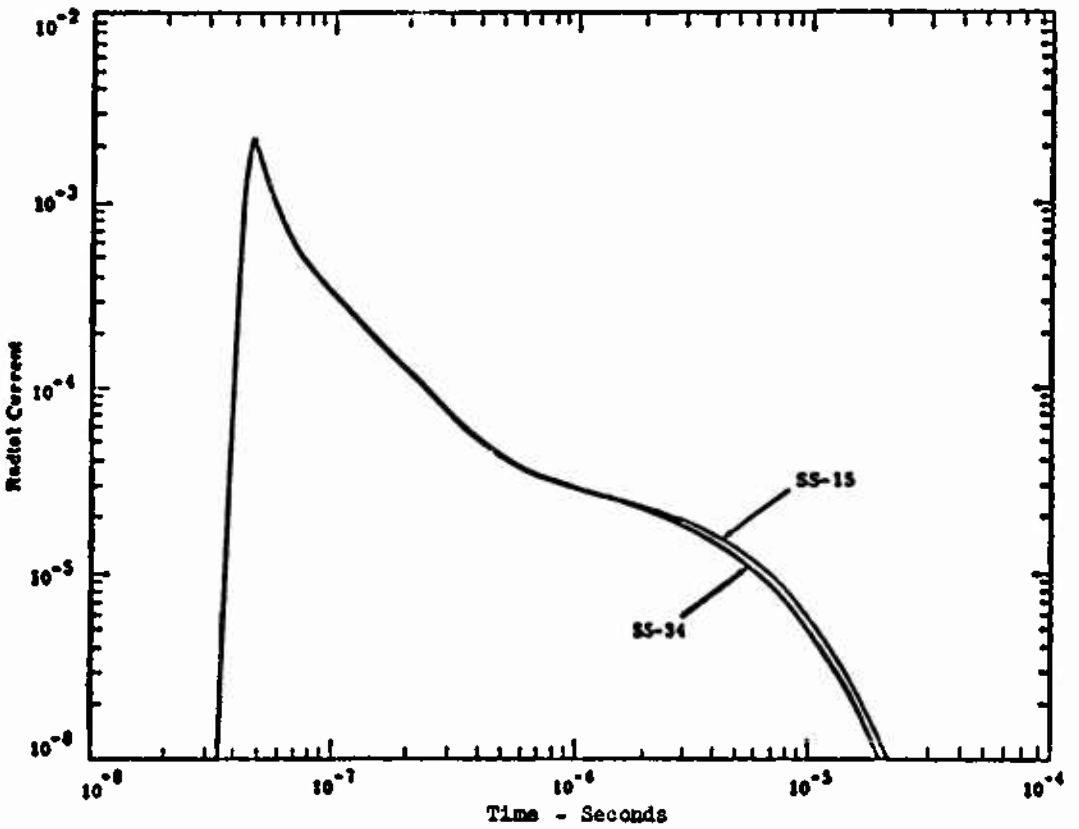

Figure 13. Source Current at 3 Km.

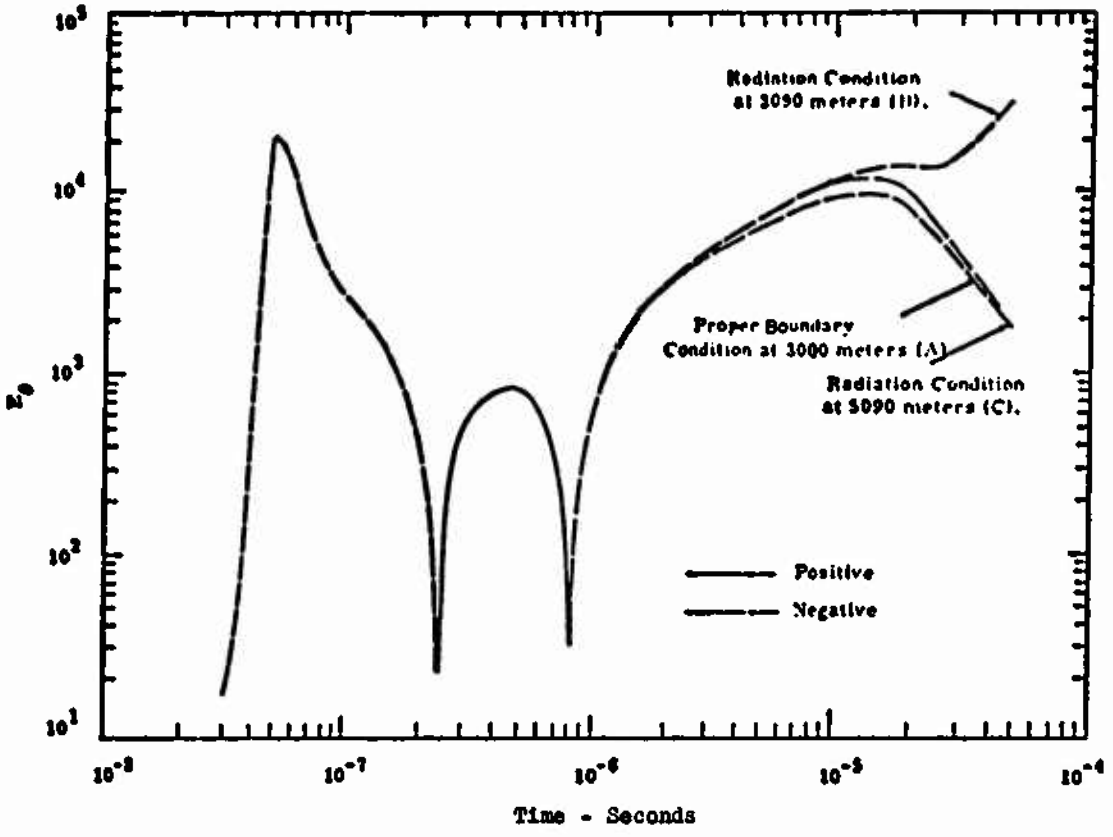

Figure 14. E_θ at 2000 Meter Range.

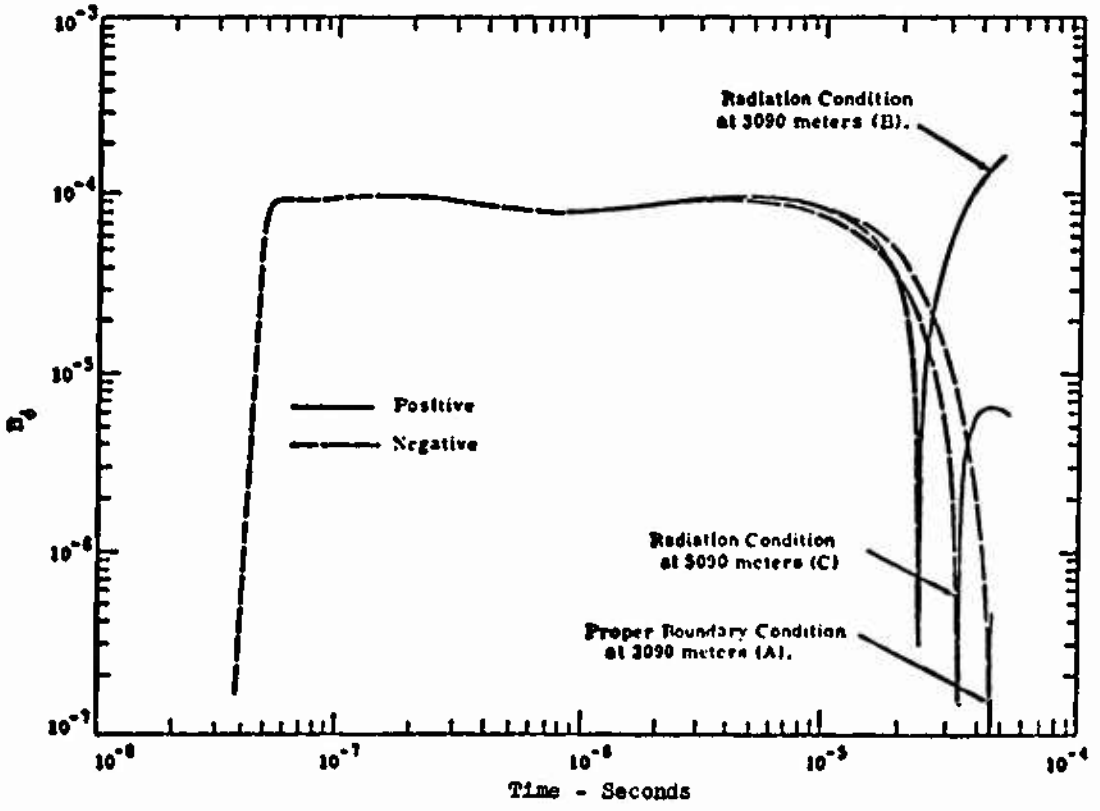

Figure 15. R_ϕ at 2000 Meter Range.

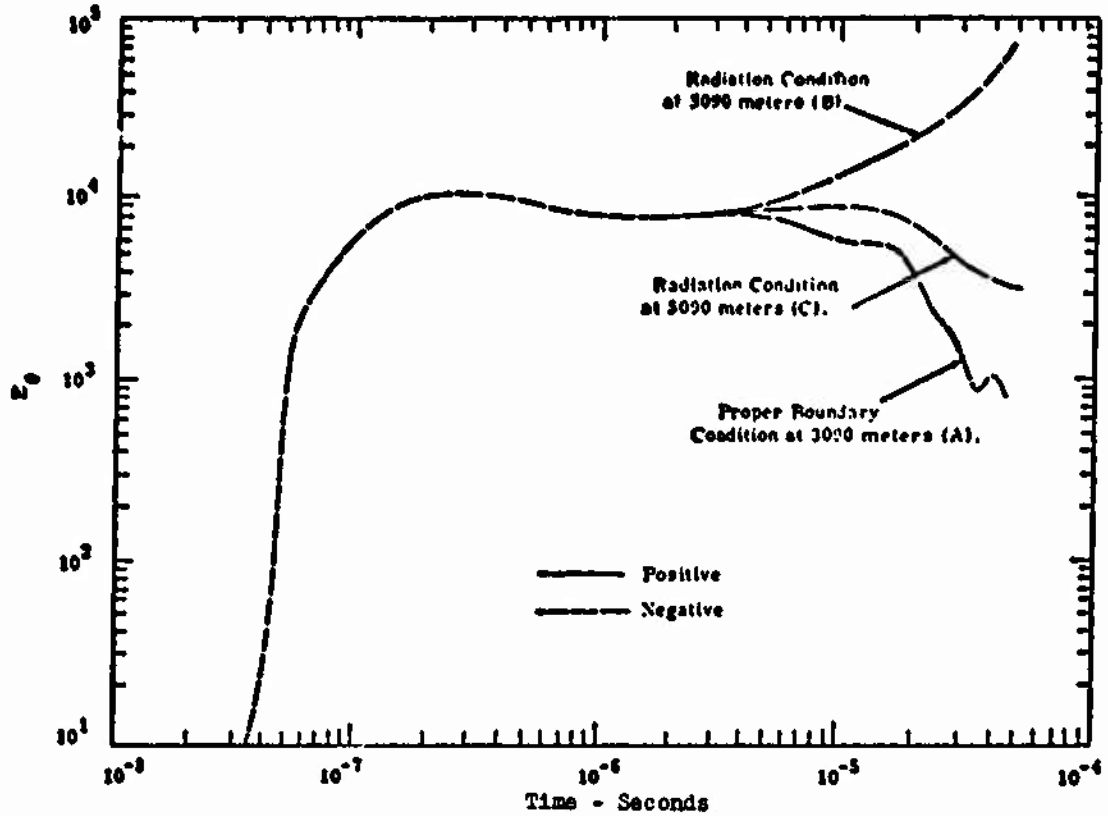

Figure 16. E_θ at 3000 Meter Range

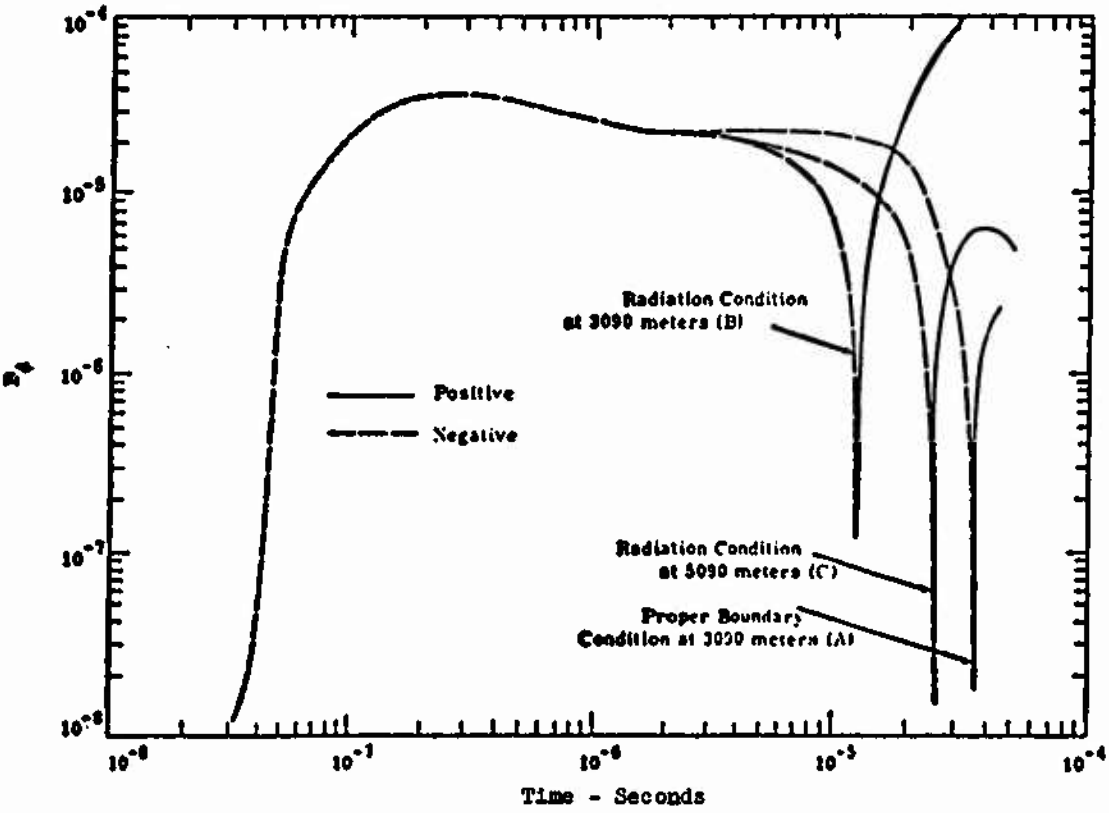

Figure 17. B_ϕ at 2000 Meter Range.

that the radiation condition enforced at 5090 meters for Curve C is affecting the field at 3000 meters in a manner similar to the way the radiation condition at 3090 meters affected the fields at 2000 meters (Curve B, Figures 14 and 15). If the boundary used for Curve C (Figures 16 and 17) was moved out farther, that curve would probably move toward convergence with Curve A except for the small effect of the source difference.

Note that run B is identical in every way except for the boundary condition to run A. Run B (SC-112) yielded results identical to SC-83 and appears to be an identical rerun. Though the SC code was modified extensively after SC-73 was run, the graphical results of run B have the same general behavior as SC-73 and lie within a few linewidths of the SC-73 graphs.

The cases reported here are an extreme example as the 3090 meter boundary for SC-111 and SC-112 is probably very near the edge of the source region. For lower yield devices or a larger radius for the outer boundary, the improvement with a proper boundary condition will be smaller but still significant. By using the expansion, however, these results show that we can truncate the calculation much farther in than before and still get good results. Furthermore, obtaining good results with the radiation condition will require differencing to larger radii for later-time calculations.

APPENDIX II
SCX-LEMP 1 COMPARISONS

1. INTRODUCTION

The LEMP 1 code was developed independently from SCX by C. Longmire and J. Longley (Ref. 13). This code performs the same calculation as SCX using slightly different numerical methods and different source methods. As a check on both codes a limited comparison of results has been made and is presented here.

The sources described for SCX in the main text were implemented around January of 1973. Prior to this the source terms did not include transverse currents, angular dependence or effects of neutron inelastic scattering. As a result, EMP predictions using SCX prior to this time are quite different in some respects than the predictions presently being obtained. To illustrate this difference, comparisons of new and old SCX results are also presented.

2. RESULTS

Two sets of comparisons are presented. The first set are time histories at 500 meters of SCX, LEMP, and SC results. SC refers to the SCX code prior to the implementation of the more sophisticated sources. The second set are time histories at 2000 meters of LEMP and SCX.

In examining the SCX-LEMP overlays one must keep in mind that the transverse currents represent different effects in the two codes. Transverse currents are obtained in SCX due to the air-ground

assymetry and the ground capture of neutrons. These currents have a negative sign. Transverse currents in LEMP are obtained through the self-consistent effect and are positive. Both sources of transverse current should be included in a complete treatment. Presently this is not done in either code. Because of the different types of transverse currents, the transverse electric field predicted by the two codes is quite different when the region of interest is well within the source region. In this region local effects dominate and this difference is well illustrated in the 500 meter overlays. At far ranges, where local effects are less important, the influence of the transverse current diminishes and the comparison is more favorable.

In general, the comparisons are quite good, considering the differences in sources. They indicate that SCX and LEMP EMP predictions are consistent with each other. In the figures on pages 79 through 90, hash marks indicate negative values.

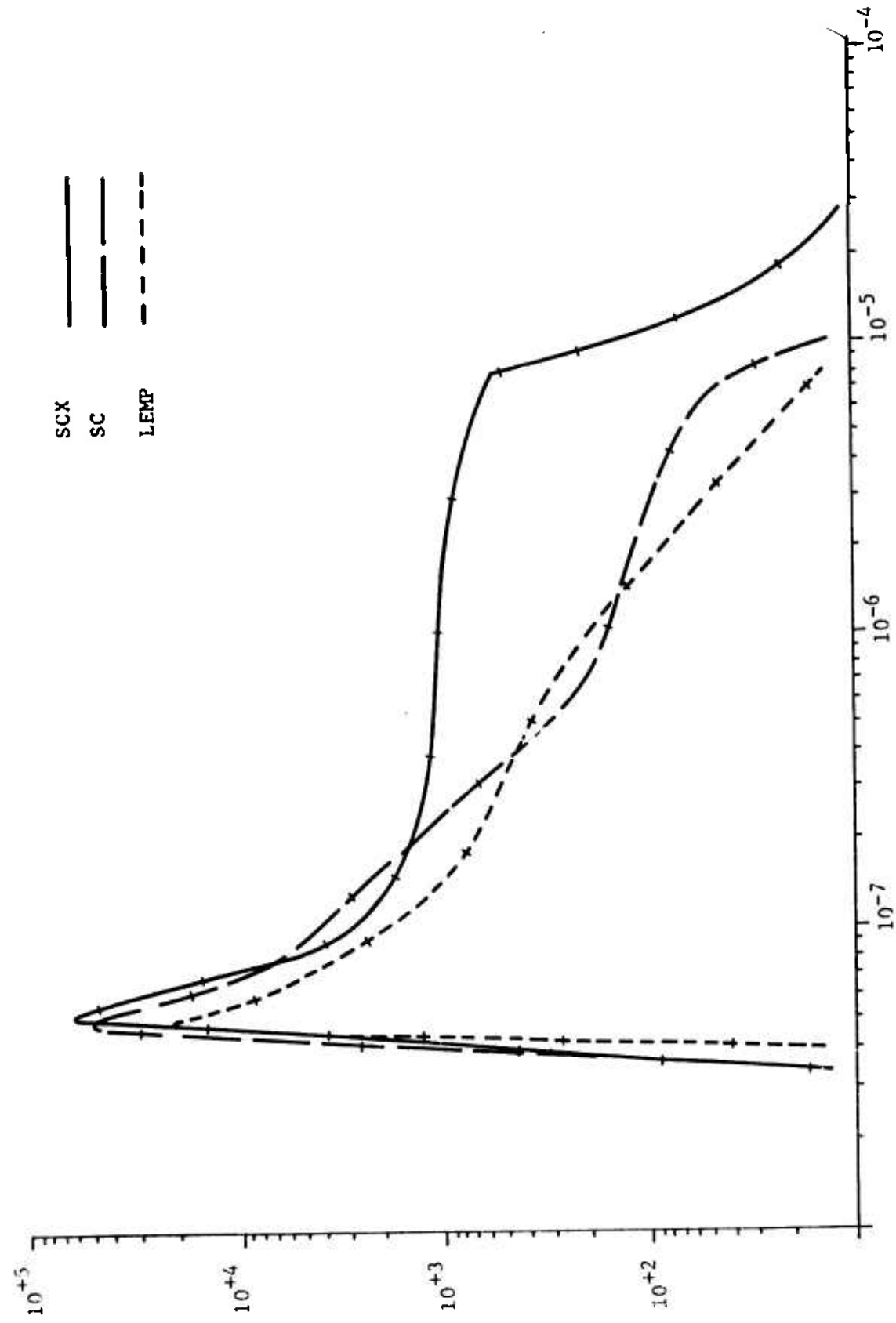

Figure 18. Radial current at 500 meters.

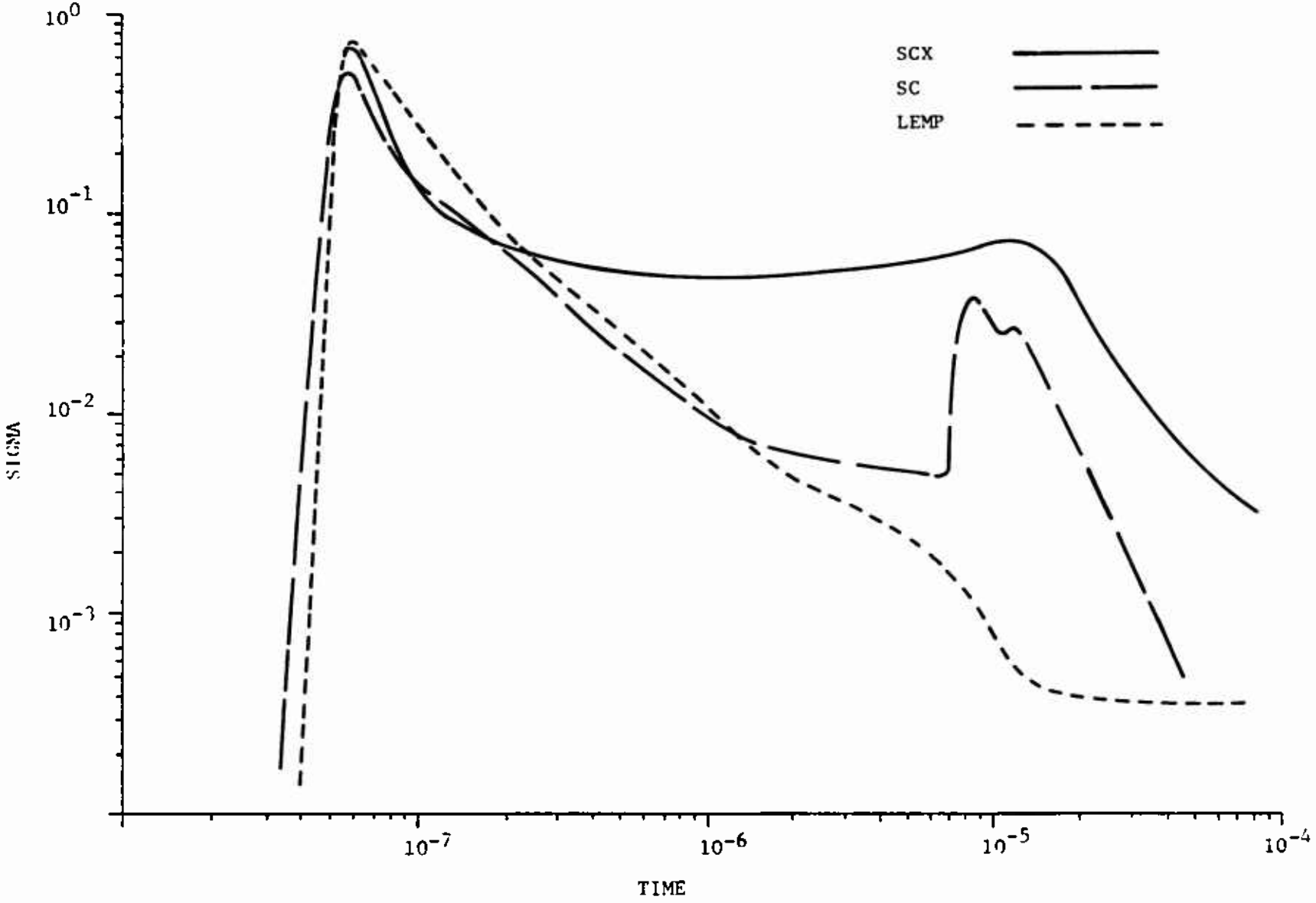

Figure 19. Conductivity at 500 meters.

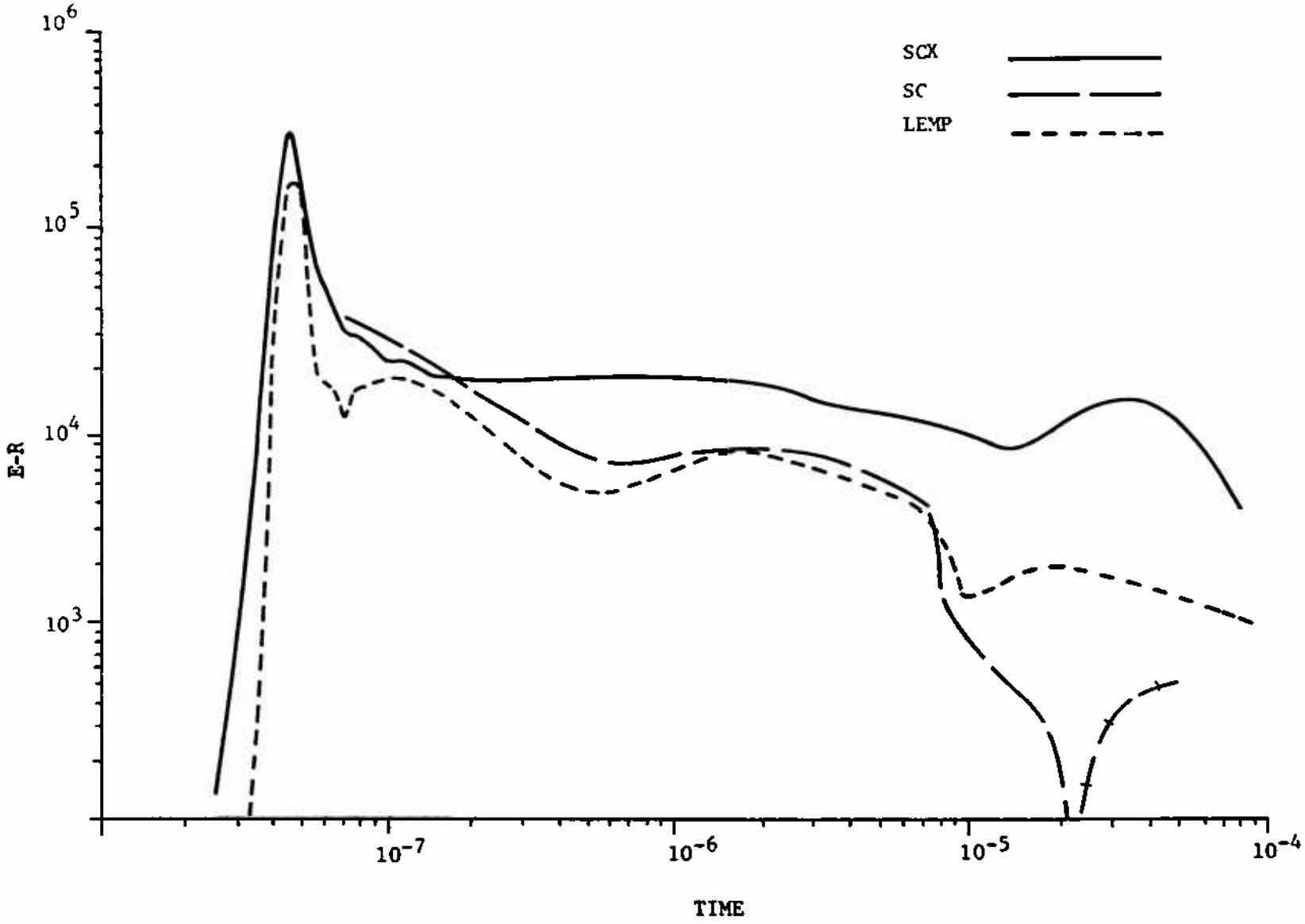

Figure 20. Radial E field at 500 meters.

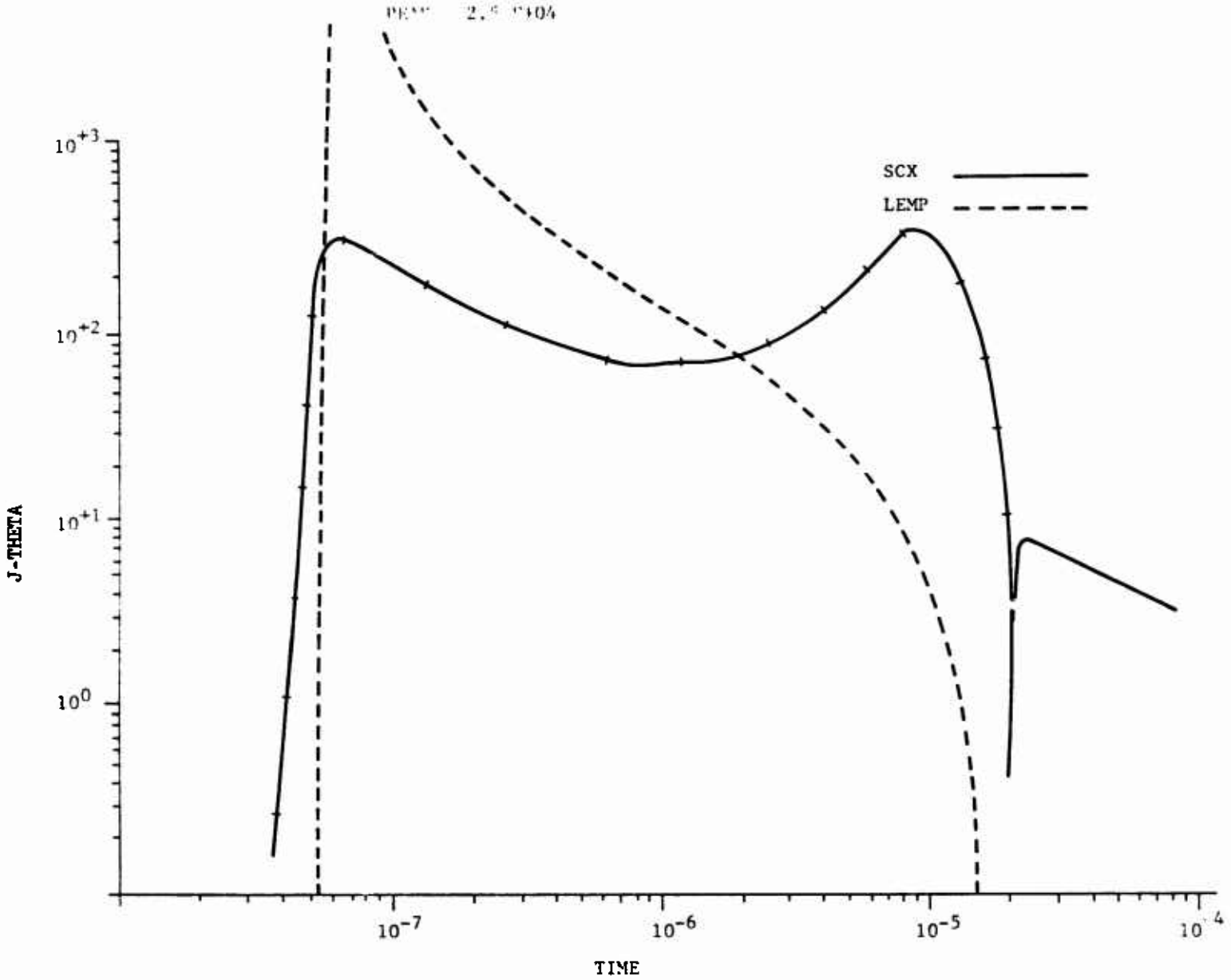

Figure 21. Transverse current at 500 meters.

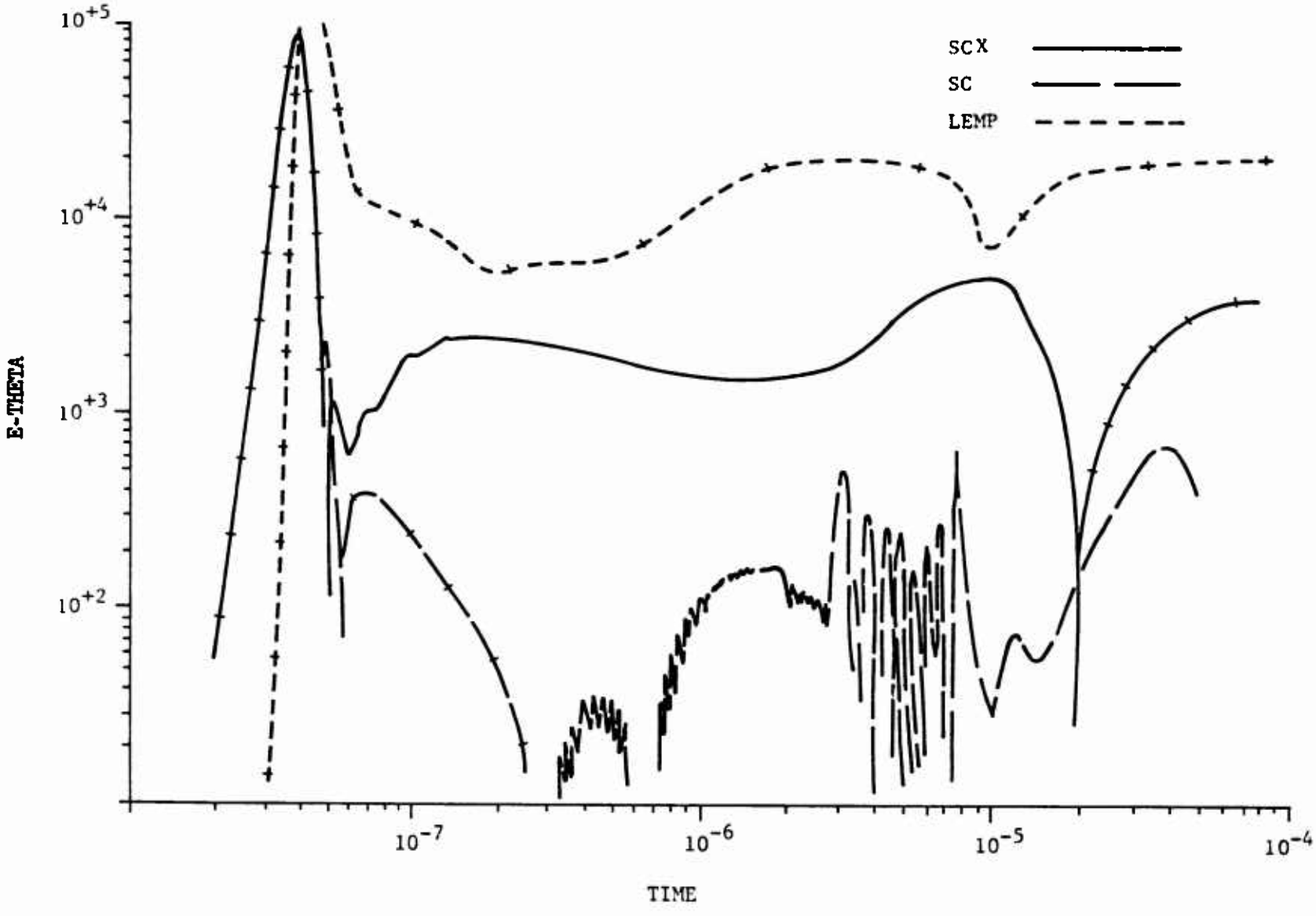

Figure 22. Transverse E field at 500 meters.

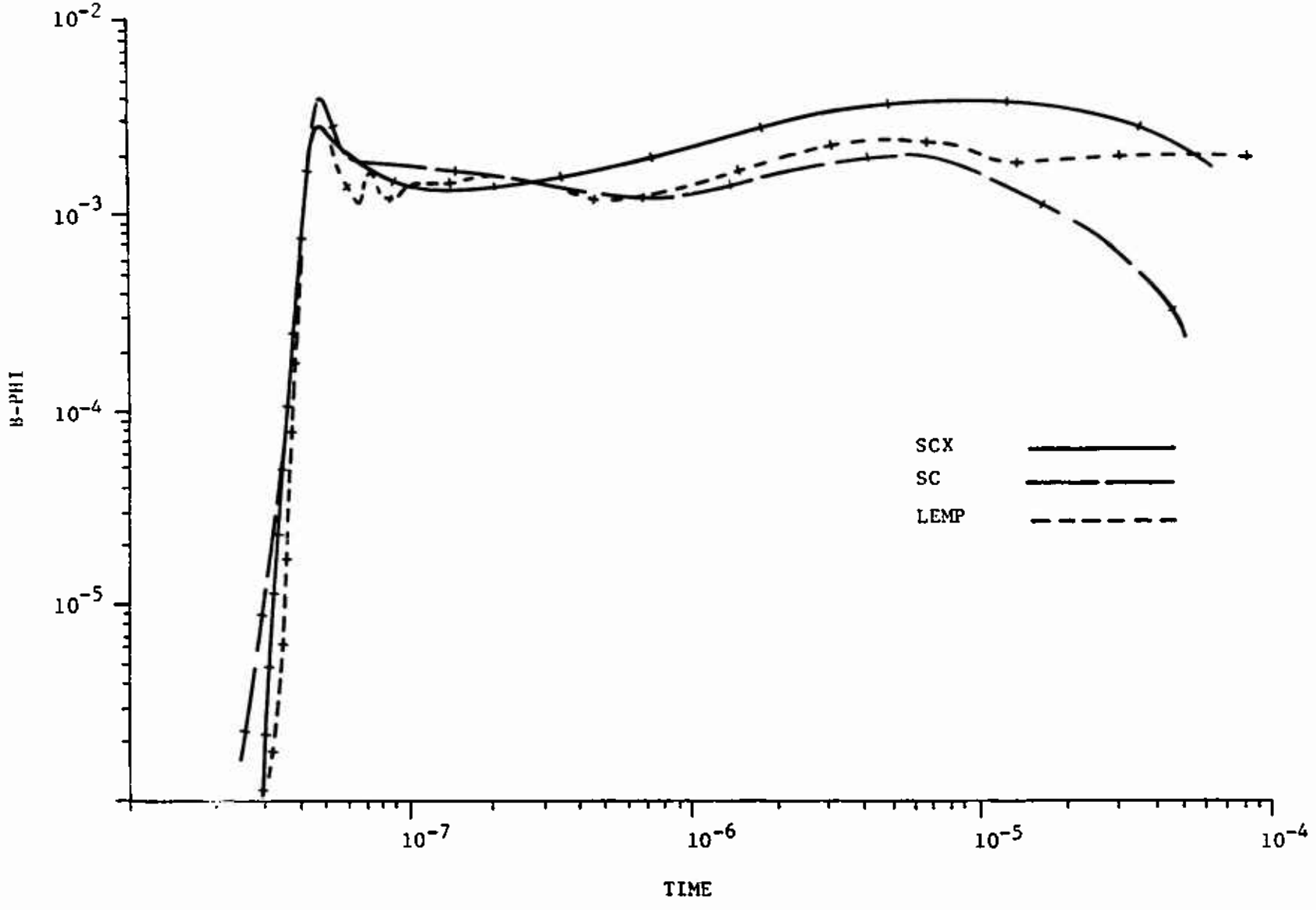

Figure 23. B field at 500 meters.

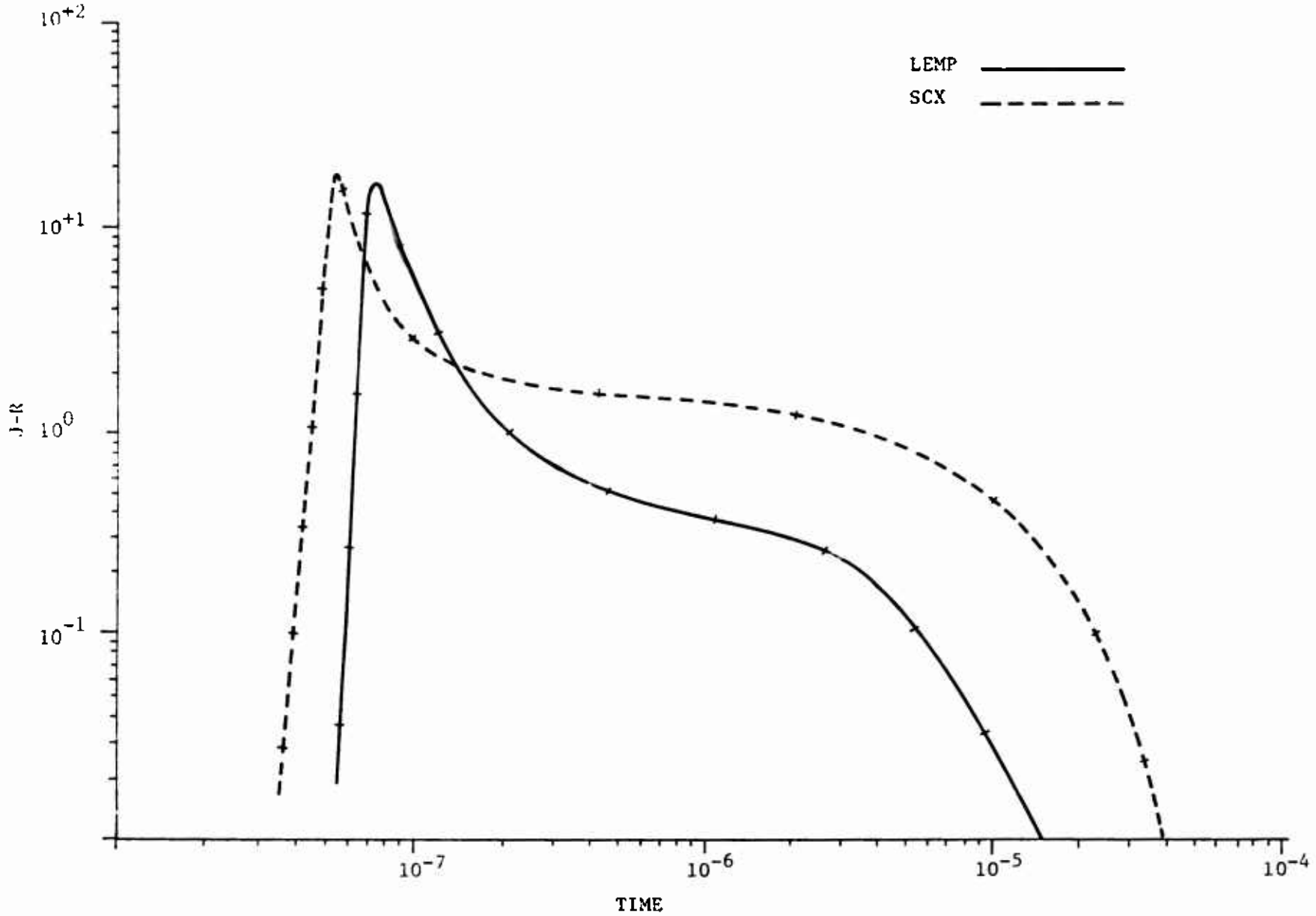

Figure 24. Radial current at 2 km.

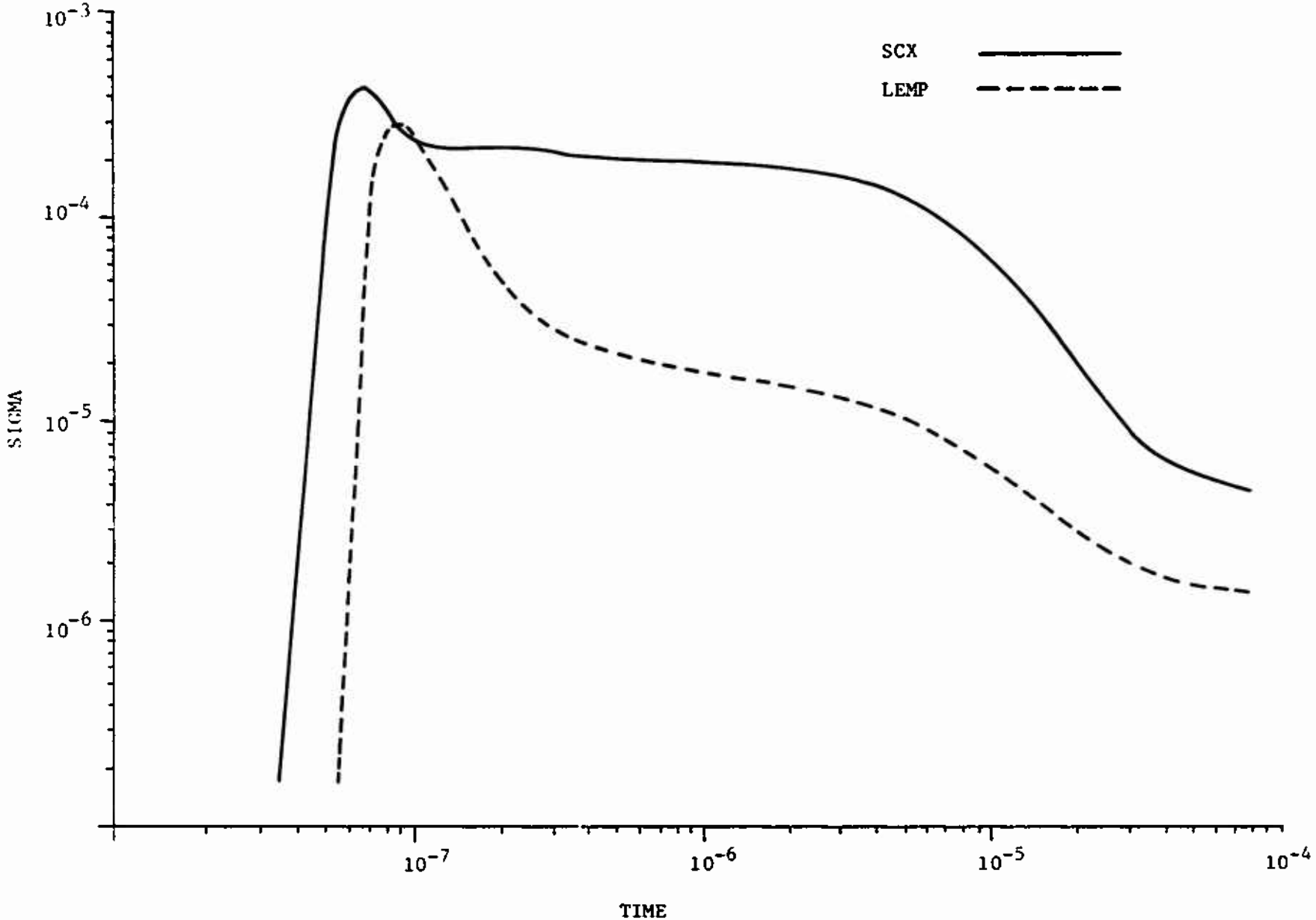

Figure 25. Conductivity at 2 km.

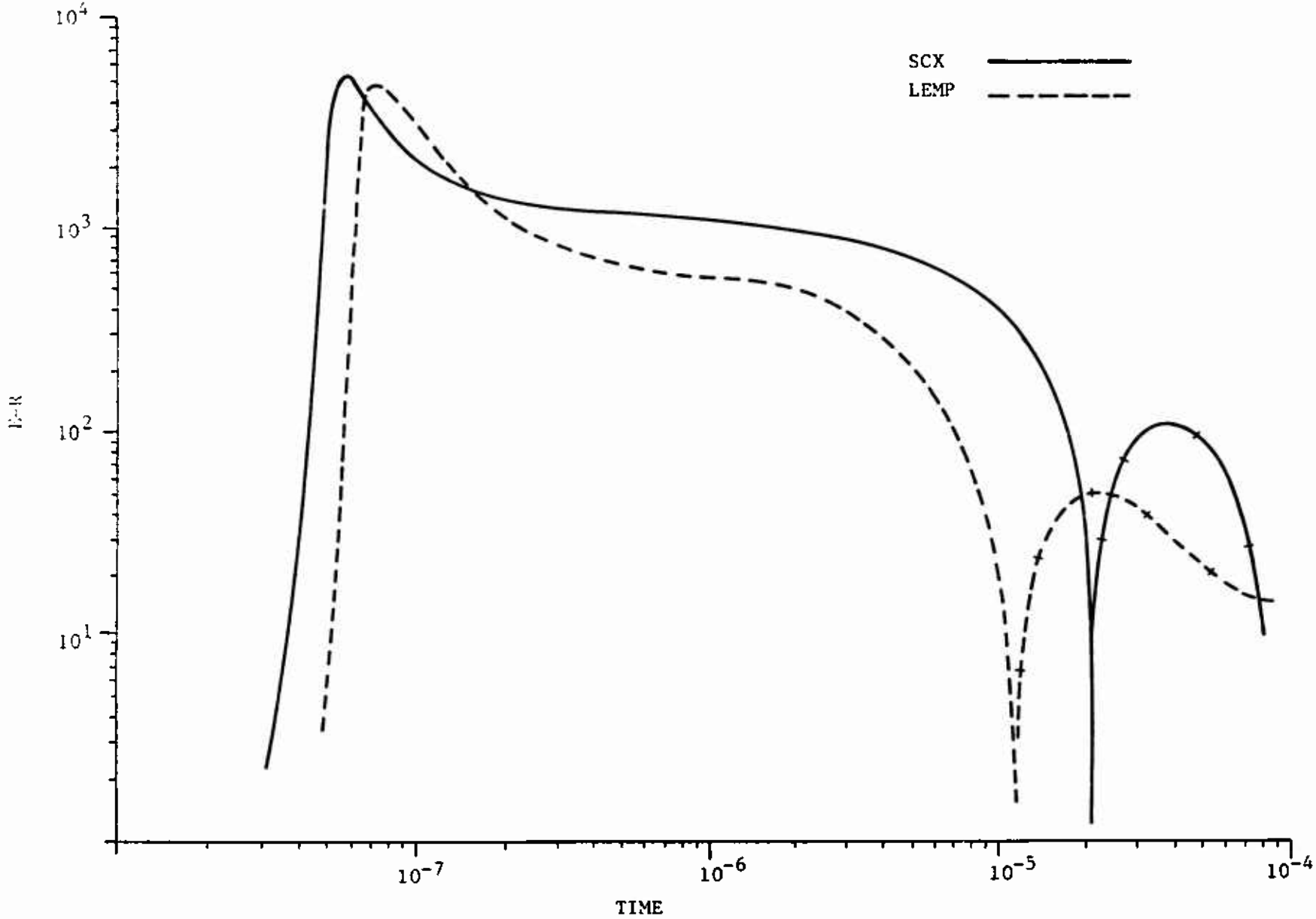

Figure 26. Radial E field at 2 km.

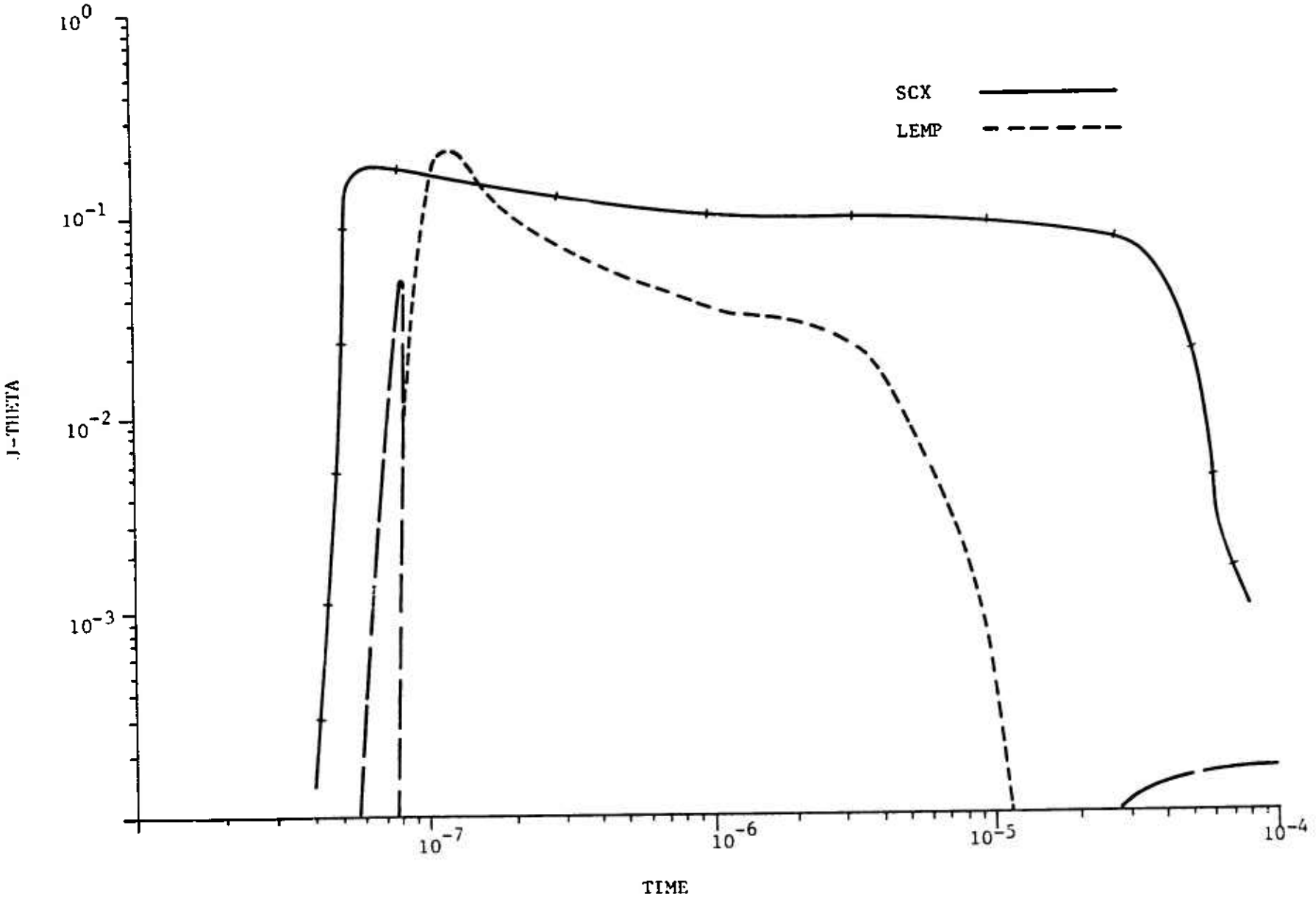

Figure 27. Transverse current at 2 km.

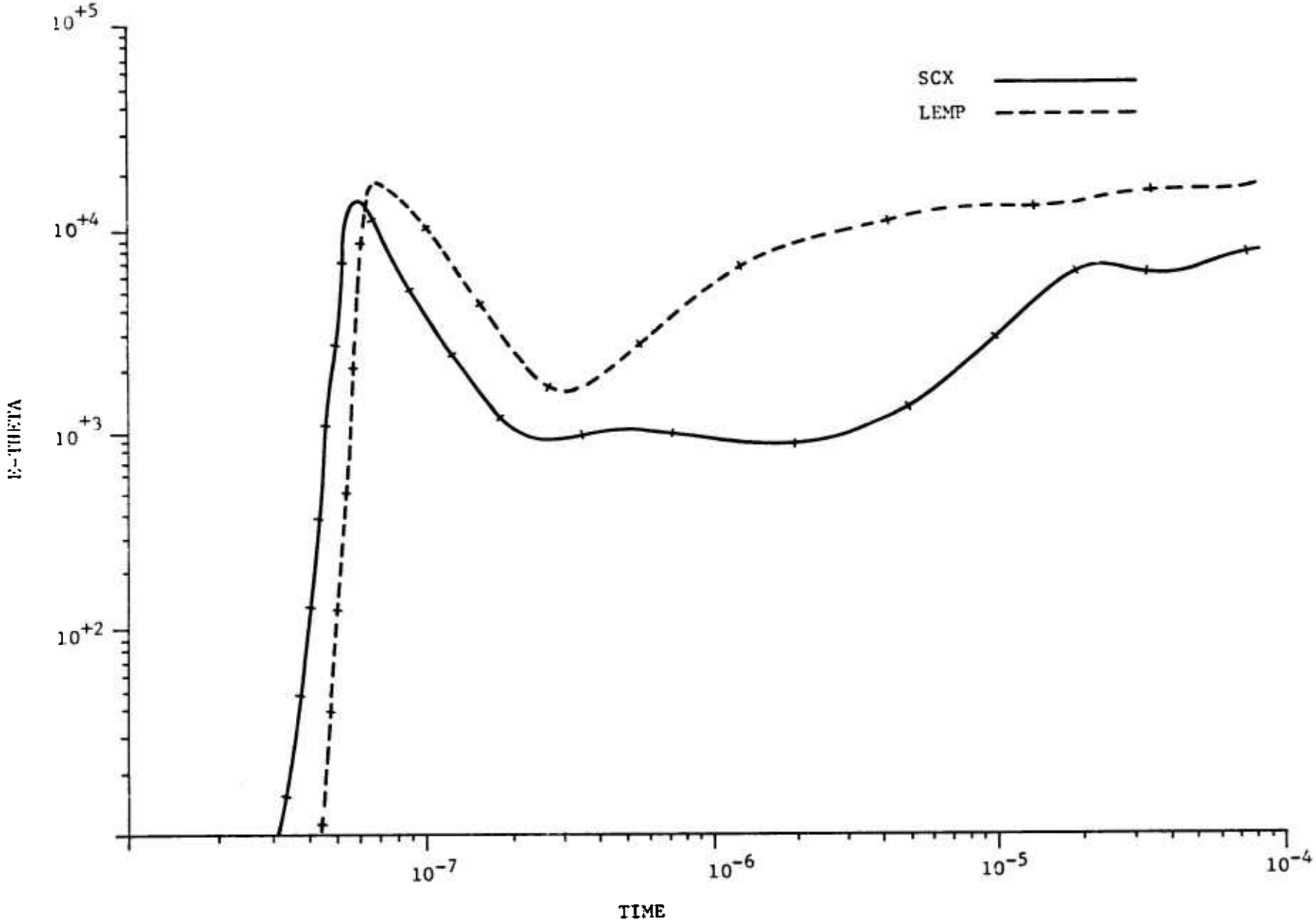

Figure 28. Transverse E field at 2 km.

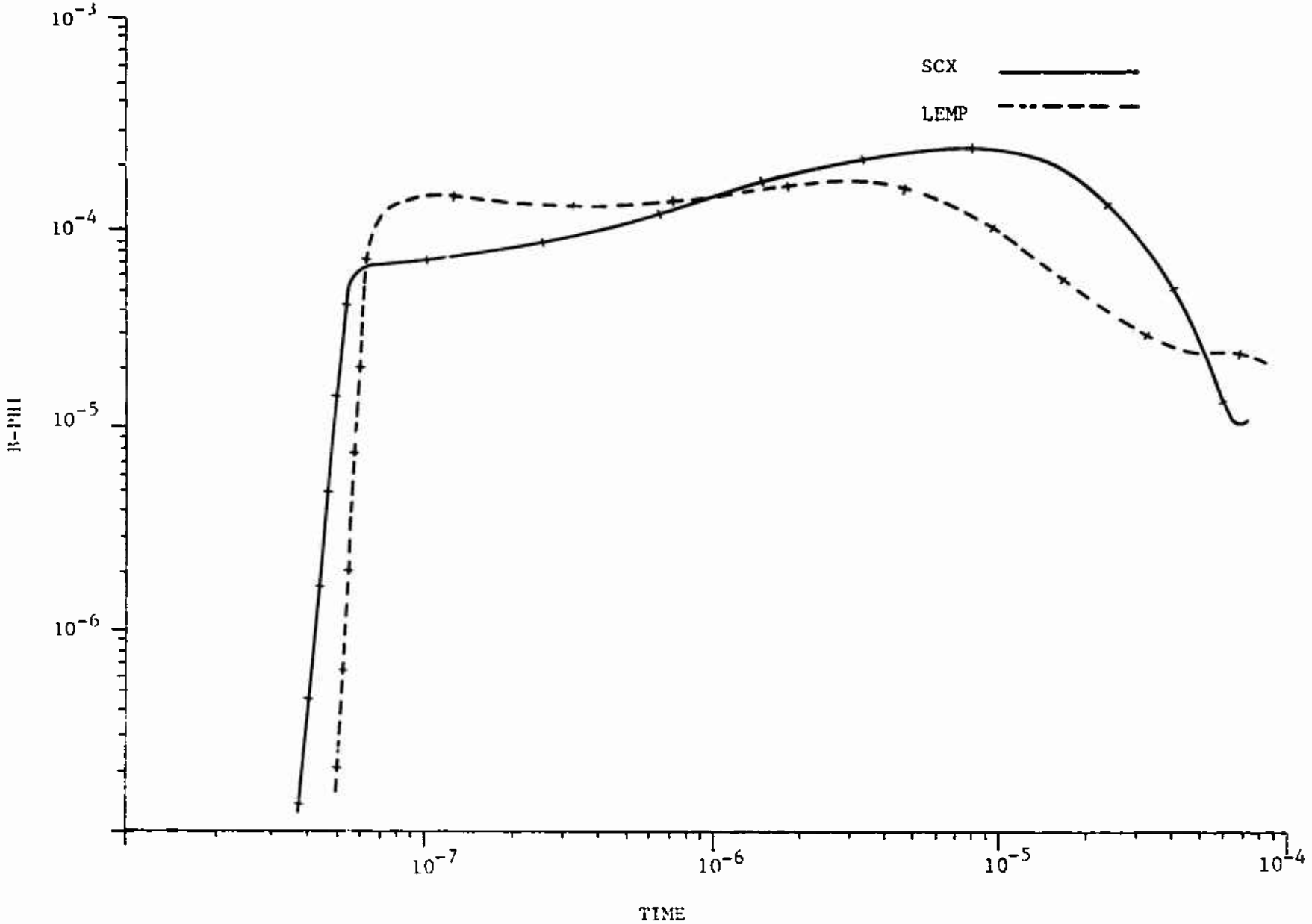

Figure 29. B field at 2 km.

APPENDIX III
INSTRUCTIONS FOR RUNNING SCX

1. INTRODUCTION

This appendix is written to provide potential users of the SCX code with a guide to the running and debugging of the code. The theory upon which the code is based is fully documented in the main text and should be consulted by those using SCX.

The SCX code is composed of one driving routine and 22 subroutines. Many of the subroutines are standard packages dealing with graphics. The standard packages will not be discussed in great detail for two reasons. First, they require no external input and are not essential in the calculations carried out by the code. Second, many of these packages are peculiar to the operating system used at the Air Force Weapons Laboratory and will have to be replaced by other graphics packages if SCX is run with a different system.

The subroutines essential to the calculation in SCX will be discussed in detail. The function of each of these routines, and also possible problem areas, will be included in the discussion. Happily, the number of routines which fall in this category is relatively small; only 5 subroutines and the driving program are involved.

External input to the code consists of data cards which deal with parameters in the field calculation and a set of block datum cards for the neutron source calculation. Input to the code is discussed in detail in Section III. This section also contains a typical SCX data setup for reference. A variable list for SCX is given in Section IV.

2. CALCULATIONAL ROUTINES

This group is composed of six subroutines and the driving program, SCX. The Subroutines are in order called

1. SCIN
2. NSOURCE
3. SIGMA
4. SBETA
5. FIELDS3
6. SCOUT

In the discussion that follows each of these subroutines will be discussed in the order that it is called from SCX. Thus, the entire discussion will represent a flow chart for the operation of the code.

A SCX rub begins in the driving program, which has the following program header.

```
PROGRAM SCX (INPUT, OUTPUT, FILMPL. FILMPR
TAPE1, TAPE5, TAPE6 = FILMPR)
```

The files listed above will be discussed as they are used.

a. Call SCIN

SCIN is the input routine for the code and is called only once for each SCX run. The subroutine performs several functions:

1. Zero blank common and extended core arrays.
2. Read first record from TAPE1.
3. Read card input.
4. Set up the calculational grid for the problem.
5. Fill grid dependent arrays.
6. Print input information, such as space grid being used, air chemistry parameters, and time grid used.

This subroutine is standard and should require no changes. If problems develop in this subroutine when SCX is being run, they will generally be the result of improper formatting on the input data cards. Since the first record of TAPE1 is read in SCIN, problems will occur if this record is not written properly.

RETURN

SCX next initiates the time step loop. Time steps ($\Delta\tau$) are variable throughout the time history of the calculation, and variables depending on this step are computed at the beginning of this loop. At each calculational time the gamma sources for all ranges and angles are set or read from TAPE1. For calculational times of 80 shakes or less they are read from TAPE1; at times greater than this they are set to zero.

Problems in this section of the code are usually a result of bad data from input cards or bad data in the block data subroutine.

The block data subroutine should never require altering; but if it has been incorrectly modified, problems will occur first in this section of the code. Since the time arrays are being used in this section, they should also be checked in debugging.

b. Call NSOURCE (RI, CON(J), TAUM, TAUM1, SSS, RAD)

NSOURCE calculates the neutron contribution to the sources. The calling parameters are

RI = range

CON(J) = $\cos \theta_j$

TAUM = τ_k microsec

TAUM1 = $\tau_k - \Delta\tau_k$ microsec

RAD = relative air density

SSS is a three-word array which returns to SCX the ionization rate, radial current, and transverse current, respectively. NSOURCE is called once for each angle-range combination at the present calculational time. The subroutine is standard and should not be modified. Note that while the current values returned by NSOURCE are for a single time, TAUM, the ionization rate returned is the sum of the rates at TAUM and TAUM1.

When called with a negative range NSOURCE reads a block of data for curve fitting. This negative call is performed in SCIN and occurs once for every SCX run. Also, the subroutine will return

zero values when called with times less than 3 shakes. This is done to eliminate early time problems in the neutron curve fits.

RETURN

c. Call SIGMA

SIGMA calculates the conductivity at the present calculational time for all angles and ranges. The calculation is based on a differences scheme for the air chemistry equations. These equations are discussed in the main text. The difference scheme calculates conductivities on half angles and an interpolation scheme is used to obtain full angle conductivities.

Two field dependent parameters, electron attachment and electron mobility, are needed to obtain the conductivity. Since the present time electric field is not available, the field at the last time is used. The electron attachment is calculated in subroutine SBETA. This subroutine is called from SIGMA and is the only calculational routine not called from SCX. Electron mobility is calculated directly in SIGMA.

Several areas of code problems may be traced to the SIGMA subroutine. SIGMA should be suspect whenever the fields become unusually large. If it becomes obvious that conductivity problems exist, the interpolation scheme for full angles should be checked first. Next, the various number densities being calculated should be examined.

The code logic requires conductivity values at the present and last calculational time. These values are transferred in and out of extended core storage in SIGMA, SCX, and FIELDS3. The transfer logic should be examined for possible problems when the conductivity shows unusual oscillations. Array overflows will also turn up as problems in SIGMA, and this possibility should be considered.

RETURN

d. Call FIELDS3

This subroutine contains the algorithm used in SCX for solving Maxwell's equations. The subroutine may be divided into three parts. The first part calculates constants dealing with the air portion of the grid. The next calculates similar constants for the ground grid. The last section obtains the field values. B_φ is obtained first, then E_r, and finally E_θ. The above calculations are performed for all angles at each of the range steps at the present calculational time.

The air equations in FIELDS3 are complete and should not be modified. The ground equations in the code assume zero current in this portion of the grid. If ground currents are added to the code, the following changes must be made (to ground constants)

$$A3(j)_g = A3(j)_g - \frac{\mu_g \delta\tau}{2} \left(J^{k-1}_{\rho ij} + J^{k}_{\rho ij}\right) \qquad (180)$$

$$A6(j)_g = A6(j)_g - \frac{\mu_g \delta\tau}{2}\left(J^{k-1}_{zij} + J^{k}_{zij}\right) \qquad (181)$$

where $\delta\tau$ is the present time step, i is the range index, j the depth index, and k the time index.

Program problems will normally not be directly associated with this subroutine but will originate elsewhere. For example, large field values are generally a result of problems in subroutine SIGMA. If it has been definitely established that the problems originate in FIELDS3; sections dealing with angle regridding should be examined first. These sections are labeled in Appendix A. Next, any constants involving source terms (current or conductivity) should be checked. Problems which occur at far ranges are generally due to the outer boundary condition, and this should be examined. SCX performs a range regrid, doubling the range step, at late times. A flag, ITS, is printed out next to the time grid printout which indicates the status of the range regrid. When ITS is one, no regrid has been performed; ITS of two indicates one regrid, and ITS of four two regrids. If code problems develop near these regrid times they are likely to be associated with the regrid. All logic involving range parameters should then be examined.

RETURN

e. Call SCOUT

All code output, with the exception of the initial four pages of printed output, is taken care of in this subroutine. Output is in two forms, printed and tape. The output tape is TAPE5. This tape becomes the input tape for the SD18 program which provides time history plots.

Printed output is recorded both on paper and 16 mm microfilm. To obtain the microfilm copy output is written on TAPE6, a scratch tape, which has been equivalenced to FILMPR.

SCOUT also calls and initiates the various plotting routines which give range and contour plots.

RETURN

The SCX code partouts and performs a checkpoint dump every half hour. After returning from SCOUT the time since the last checkpoint dump is computed, and a decision to continue or partout is made. After this the calculational time is advanced by $\Delta\tau$ and the cycle begins again.

3. CODE INPUT

In this section the inputs required to run the SCX code will be discussed in detail. The input is in two forms, tape and punched cards. TAPE1 is the gamma source tape and is generated using a separate code called GSOR. This code will be discussed in Section III.A below. Punched card input to SCX deals with the air chemistry, weapon size, spatial grid, and the neutron sources. Each of these inputs will be discussed in III.B. A sample input deck is also given in this section.

a. Gamma Source Input (TAPE1)

The currents and ionization rate due to gamma output of the device are calculated in a code called GSOR. The calculation is based on curve fit results obtained by G. Knutson. Since these curve fits are to delta function responses, a time history and energy spectrum is folded in by the GSOR code. Also, the time bin and range bin structure to be used in SCX is set in GSOR. This information is then transmitted to SCX through TAPE1.

GSOR is contained on an update tape. Two sets of cards are required to run the code. The first set deals with the variable common. This common block is given below.

```
C
C     *** GSOR VARIABLE COMMON NDR=290 ***
      TYPE ECS DFR(84,290)
      COMMON FJH(290),QH(290), FJP(290), FJN(290), FJI(290),QP(290)
      COMMON QN(290),QI(290), FIXJ(290), FIXQ(290), DECJ(290), DECQ(290)
      COMMON R(290),Q1(290),R2(290),DF(14,6)
      COMMON FJPTH(290),DUM(290), FIXJT(290), DECJTH(290). ARET(290,9,8)
      *** END OF GSOR VARIABLE COMMON ***
```

In the above, NDR is the number of range steps being run in the problem. Thus, a new variable common block must be inserted for each NDR value. The second set of cards in the data set, and this will be different for each problem run. The information and format of each data card is discussed below. Following this discussion a sample data deck is presented.

(1) TAPE1 Request (20X, A10, 30X, A10)

Two words are read from this card, ILIBD and IDONNO. The first is the tape library location of the GSOR output tape being used. IDONNO is the GSOR run number; i.e., GSOR-00.

(2) Comment (8A10)

This card contains a one-line comment concerning the present GSOR run.

(3) Grid and Time Information (2E10.3, I5, E10.3)

The following are read from this card: RSTART, DR, NDR, TEXIT. RSTART is the starting range value, DR the range step size,

and NDR the number of range steps. TEXIT is the maximum time to which the gamma sources are to be calculated.

(4) Time Grid (E10.3, I10, 51X, A3)

This is a block of cards up to a maximum of 10. Each card contains two words, DTS and NDTS. DTS is a time step and NDTS is the number of steps of this size to be used. The last card in this set is indicated by the word END, punched in columns 78, 79, and 80.

(5) Relative Air Pressure, Temperature (2E10.3)

RAP, the relative air pressure, and RAT, the relative air temperature, are contained on this card.

(6) Source Information (2E10.3I10, E10.3, I10, 2E10.3, I10)

This card contains information concerning the particular weapon being considered. The following parameters are defined in order of their occurence on the card:

CASEP, a gamma attenuation factor for the weapon case material. Usually set to 1.

DTDR, the time step to be used in the convolution routine.

NMAX, total number of time steps used in the convolution.

TRIP, maximum calculational time for performing convolution. Time histories for times greater than TRIP are obtained through curve fits.

NCAL, weapon parameter.

GCAL, weapon parameter.

SIZ, weapon parameter.

IFUN, flag equal to 1, 2, 3, or 4. Depending on the IFUN value, the time history folded on the gamma output is obtained from one of the following:

IFUN = 1, 2, double exponential;

IFUN = 3, two double exponentials;

IFUN = 4, digitized time history.

In the normal running mode IFUN is input as 1. The following cards are explained assuming this value for IFUN.

(7) Double Exponential Parameters (3E10.3)

Three parameters characterizing the double exponential time history are given: ALPHA, BETA, and TPEAK. ALPHA is the rise rate, BETA the fall rate, and TPEAK is the time of maximum output.

(8) Energy Spectrum (3E10.3, 47X, A3)

This is a block of cards defining the gamma output energy spectrum. The maximum length is ten cards and the read is terminated by putting END in columns 78, 79, and 80 of the last card. Each card contains GRPLO, GRPHI, the upper and lower bound of the energy bin, and FRAC, the fraction of the total contained in this bin.

This ends the data deck for GSOR. In card form a data deck appears as shown below.

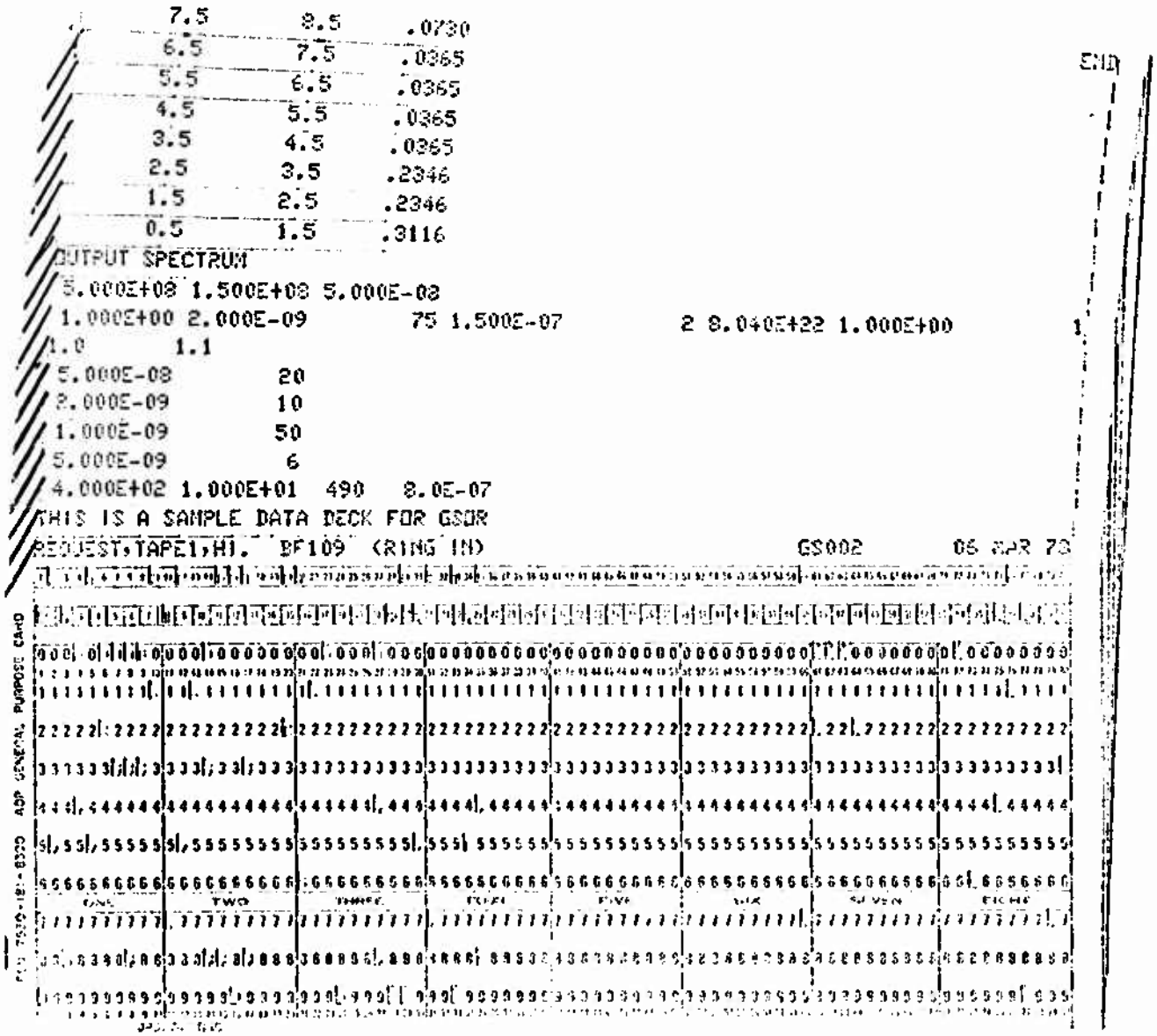

b. Input to SCX

The SCX code is set up to run under the update system presently (1973) in use at AFWL. The current production version of the code is on AFWL TAPE(AH015). To run the code three sets of input are required. The first involves the gamma sources and was discussed in Section III.A. These sources are input through TAPE1. The next set of input cards involve the variable common block and will change from run to run. The common block is 25 cards long, including comments and the necessary update control cards. The necessary cards are shown below.

```
      *IDENT LONG
      *DELETE BLNK.      BLNK.
C     ***SCX VARIABLE   COMMON NDR= 110  NTA= 29  NT= 53***
      TYPE ECS D       ( 53, 110), EH  ( 53, 110), RB      ( 53, 110)
      TYPE ECS S       ( 29, 110), S1  ( 29, 110), RHOEH   ( 29, 110)
      TYPE ECS RHOIH   ( 29, 110), SH  ( 29, 110), SH1     ( 29, 110)
      TYPE ECS FJR(29,110), FJR1(29,110), FJTH(29,110), FJTH1(29,110)
      TYPE ECS QH(29,110)
      COMMON  BMO    ( 53), BMP    ( 53), BOM  ( 53), BOO  ( 53)
      COMMON  DMO    ( 53), DMP    ( 53), DOM  ( 53), DOO  ( 53)
      COMMON  EMO    ( 53), EMP    ( 53), EOM  ( 53), EOO  ( 53)
      COMMON  TMA    ( 29), TMB    ( 29), TMC  ( 29), TMD  ( 29)
      COMMON  TME    ( 29), TMF    ( 29), A21  ( 53), A22  ( 53)
      COMMON TMG(29), TMH(29), TMI(29), TMJ(29)
      COMMON  ANG    ( 53), ANGH   ( 53), A5   ( 53), A8   ( 53)
      COMMON  DANG   ( 53), DANGH  ( 53), R    ( 110), R2   ( 110)
      COMMON  V      ( 29), W      ( 29), RR   ( 110)
      COMMON  TEMP   ( 53, 110), MCB  ( 53,   5), MCE  ( 53,   5)
      COMMON CT(29), IFLAG(53), SN(29)
      COMMON A1(53), A3(53), A4(53), A6(53)
      COMMON A81(53), CR(110), CTH(110), QR(110)
      COMMON A7(53), A9(53), A10(53), A11(53), A12(53), A13(53), A14(53)
      COMMON  E      ( 53), F      ( 53)
      DIMENSION TEM  ( 29, 110)
      COMMON/EC/D,  EH, RB, RHOEH, RHOIH, S, SH, SH1, S1, FJR, FJTH, FJR1,
        FJTH1, QH
      ***END OF SCX VARIABLE COMMON AND EXTENDED CORE STORAGE***
```

Usually the only change in this block will deal with NDR, the number of range steps. If this is the case, the number of change cards required is reduced to 16.

The data deck for SCX consists of eight or more cards, none of which are optional. The variables and input formats are given below, and a sample data deck follows.

(1) TAPE5 Request (20X, A10, 33X, I3)

This card provides the two variables ILIBS and IJOBNO which are used in labeling the printed output. The remaining fields need not be included, but their use is traditional. If the card is punched in the indicated format, it may also be used in the control card deck.

(2) Comment Card (8A10)

This card provides the one-dimensional array KOMENT which is used to identify printed output. The positioning of the comments is not important, but the form as shown has become traditional. Any comment may be used to identify the output, but care should be taken to avoid classified titles.

(3) Air Chemistry Card (E10.3, A10, 3E10.3, I110, E10.3, 2I5)

This card provides the air chemistry and output parameters: SALFA, IBETA, SGAM, SMUNG, SMUPG, NP, SIZ, NCON, and NSP.

SALFA is the electron-ion attachment coefficient.

IBETA is a Hollerith variable which indicates that the electron attachment coefficient is calculated as an internal function. The variable is not used, but the form shown has become traditional.

SGAM is the ion-ion attachment coefficient.

SMUNG and SMUPG are the negative and positive ion mobilities, respectively, at STP conditions.

NP is an integer variable which specifies the frequency with which printed output is produced. An NP of 5 indicates that printed output is to be produced every 5 time steps.

SIZ is a scaling factor which changes the gamma yield of the source run.

NCON is an integer variable which specifies the frequency with which contour plots are produced. An NCON of 5 indicates that contour plots are to be made every 5 times that printed output is produced. If NP is as above, contour plots are produced every 25 time steps.

NSP is an integer variable which specifies the frequency with which profile plots are produced. An NSP of 5 indicates that profile plots are produced every 5 times that printed output is produced. If NP is as above, profile plots will be made every 25 time steps.

If neither contour plots and/or profile plots are desired, the corresponding variable may be set to zero, or left blank.

(4) Physical Parameter Card (3E10.3)

This card provides the physical parameters: H20, SIGMAG, and EPGF.

H20 is the water fraction used in the mobility calculations.

SIGMAG is the ground conductivity.

EPGF is the relative dielectric constant for the ground.

(5) Air Grid Parameters Card (3I5, 55X, E10.3)

This card provides the parameters for the air grid: NA1, NA2, NA3, and ANGSTR.

NA1 specifies the number of angle bins which the air region is to be divided. In the example in the appendix we wish to divide the air region into 9 bins.

NA2 specifies the number of times the last group of bins are to be divided in half. In the appendix we wish to divide the last group of bins in half ten times so that the final bin size will be $0^{o}.005$.

NA3 specifies the number of bins which are included in the last group.

ANGSTR specifies the grid angle for the top of the air region. In the appendix we have specified that the top of the air region will be at 81^{o}. For most problems the top of the air region will be set at 0^{o} and the variable may be omitted.

The total number of air grids may be calculated by the formula NT2 = NA1 + NA2 x NA3. This is one of the numbers which should

be input into the SCCOM code and is one of the numbers used as a dimension in the SCX common block.

(6) Ground Grid Parameter Card (3I5, 55X, E10.3)

This card provides the parameters for the ground grid: NG1, NG2, NG3, and GDZ. These variables act similarly to the corresponding variables in the air.

NG1 specifies the number of bins of the original size to be used.

NG2 specifies the number of times that a group of bins is to be doubled in size.

NG3 specifies the number of bins which are to be included in each group of bins which is doubled.

GDZ specifies the original bin size. For most problems the variable may be left blank, and the SCX code will calculate a bin size based on the skin depth at a frequency of 10^8 Hz.

The total number of ground bins may be calculated by the formula NTX = NG1 + NG2 x NG3. This number is not needed by SCCOM but is used to calculate NT by the formula NT = NT2 + NTX.

(7) Observer Table Cards (A3)

The first card specifies the choice of observer option. The parameter read is IBO and may be any of the four following options: **3HSTA, 3HADD, 3HSPE, and 3HMAT, which stand for the options: standard observer table, additional observers, special observer table, and matrix observer table, respectively.**

The standard observer table provides a set of 80 observers at various locations within the grid. Since the observers are chosen by the code, they do not usually correspond with locations of interest and so this option is seldom used. However, no other data cards are required with this option.

(a) Additional observers (I10, E10.3, I110, 47X, A3)

The additional observer option allows for more observers than those provided by the standard option. The first 80 observers are the same as those chosen by the standard option. Twenty additional observers may be read in the above format. The first variable is the observer number. The second variable is the range for this observer. The third variable is the j value associated with the desired angle. The fourth variable is a flag which will terminate reading of additional observers. It is triggered by IEND = 3HEND. Since this option also uses the code to select observer locations, it too is seldom used.

(b) Special observer table (E10.3, I10, 57X, A3)

The special observer table is the most commonly used option. It allows for the specification of all the observers in the above format. The first variable is the range of this observer. The second variable is the j value associated with the desired angle. The third variable is a flag which will terminate reading of special observers. It is triggered by IEND = 3HEND.

(c) Matrix observer table (16F5.0,1615)

The matrix observer table is the easiest option to use which also allows observers to be placed where they are needed. The first card provides up to 16 ranges where observers are desired. The second card provides up to 16 j values where observers are desired. The code will place observers at every grid point which is at a specified range and a specified j value. If observers are desired at unique positions, the special observer option should be used. The code will check to see that no more than 100 observers are requested. If less than 16 ranges or j values are desired, the remaining fields of the data card may be left blank. The code uses only the requested values to generate observer locations.

(8) Neutron Source Parameters (2X, 2E10.3)

This card contains the weapon yield, y, and the neutron efficiency, EE, for the device being considered. A sample data deck is shown on the following page.

SAMPLE DATA DECK

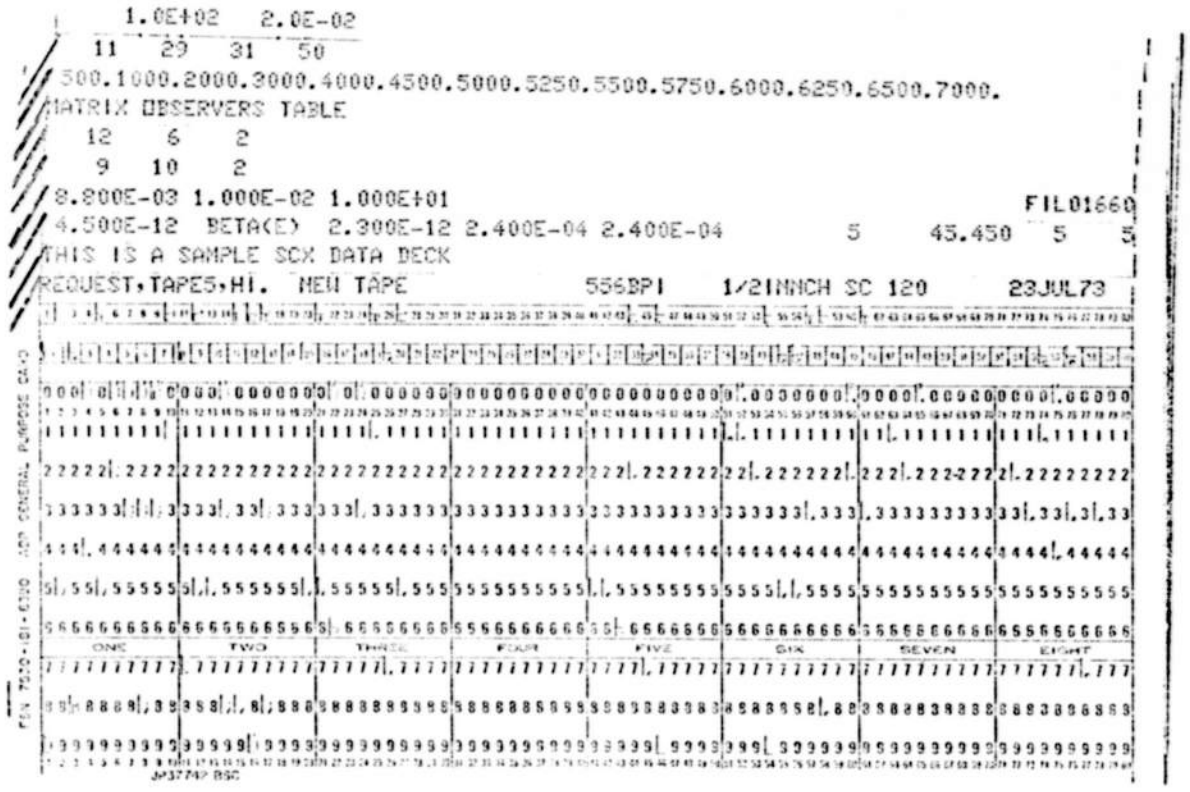

4. RESTART AND SCX OUTPUT

SCX allows for automatic restarting under the CHECKPOINT restart capabilities of the CDC 6600 SCOPE operating system. Under the SCOPE system the details of the restart are handled by the software package with little action required by the programmer.

A CHECKPOINT dump is instituted by the FORTRAN statement CALL CHECKPTR (FILES) in the main SCX. At the present time FILES is a zeroed variable. The use of a non-zero FILES variable will allow for selective dumping of files. For further details see the CHECKPOINT RESTART documentation in the SCOPE Reference Manual.

To reduce the amount of data stored on the CHECKPOINT tape, the files OUTPUT and FILMPL are PARTOUT'ed before every CHECKPOINT dump. Then, the CHECKPOINT tape will contain the contents of central memory and extended core, plus the positions of the files TAPE1 and TAPE5. Even with this reduction in data which has to be stored, it will still be possible to only store a few CHECKPOINT dumps on each CHECKPOINT tape. The exact number will depend upon the amount of storage associated with the SCX run.

CHECKPOINT dumps are currently taken every half hour. If dumps are desired at different time intervals, then change statement SCX in the update deck. In addition, a CHECKPOINT dump can be forced by

setting sense switch 6. The proper technique for terminating a SCX run is to have the operator set sense switch 6, then drop it after the CHECKPOINT dump is completed. The SCX run may then be restarted at a later date.

The actual restart is accomplished by using the RESTART package of the SCOPE operating system. For complete details see the CHECK-POINT RESTART documentation in the SCOPE System Manual.

It is possible to restart with a control card deck of only four cards. However, it has been found advantageous to use a larger deck with appropriate comments. A sample RESTART control card deck is given below. It will be noted that there are no REQUEST tape cards included in the control card deck. None are needed since RESTART will place its own tape requests. However, since RESTART does not contain any tape identification information, it is a good idea to include the tape identification comment cards for the operator's use.

Restart Control Card Deck

```
SAISCOO, P2, T7777, CM260000, EC740.
TASK (SMITH, CHARGE NO., ELE, 3414)
COMMENT. This is SCX-00
RESTART, TAPER, 3.
7
 8
  9
```

SCX produces two forms of output: printed output and graphical output.

The printed output consists of four parts: the update correction card listing, the memory map, two copies of the input parameters, and selected printout for the observers. A copy of the compiler output may also be included. The update correction card listing is detached from the body of the listing and filed with the correction card listings from other SCX runs. The memory map (and compiler output, if included) is discarded. One copy of the input parameters is filed with copies of the input parameters from other SCX runs. The second copy of the input parameters is kept with the main body of the listing and kept until the paper listing is no longer needed.

At the conclusion of the SCX run, the OUTPUT file is rewound and copied to the FILMPR file, providing a microfilm copy of the paper output. The microfilm copy is kept on permanent retention in the AFWL EMP microfilm library. With the addition of PARTOUT before CHECKPOINT dumping, it is recommended to move the microfilm copying inside the SCX program.

The main portion of the printed output is selected printout for all of the requested observers. The controlling parameter is the variable NP on the third data card. An NP of 5 indicates that printed output is to be produced every five time steps. The output is arranged in groups of all the ranges requested at a given angle or depth. All of the observers requested will be included in the printed output.

The graphical output consists of three parts: contour plots at a given retarded time, profile plots at a given retarded time, and maximum contour plots. These plots are recorded on the FILMPL file and the microfilm produced is kept on permanent retention in the AFWL EMP microfilm library.

Profile plots are of seven varieties: four are plots of B phi, E radial, E theta, and the theta directional derivative of E radial versus the coangle in the air; the remaining three are plots of B phi, E radial and E z versus depth in the ground. The controlling parameter is the variable NSP on the third data card. An NSP of 5 indicates that profile plots are produced every five times that printed output is produced. If NP is set to 5, then profile plots would be produced every 25 time steps. If NSP is set to zero or left blank, no profile plots will be produced.

Contour plots are of five varieties: E radial, E theta, B phi, E total, and vector plots of E total. The E radial, B phi, E total, and vector E total plots are whole grid plots; the E radial, E theta, B phi, and E total plots are also produced in a blown-up version which includes the region from 20 meters in the air to 20 meters in the ground. The controlling parameter is the variable NCON on the third data card. A NCON of 5 indicates that contour plots are produced every five times that printed output is produced. If NP is set to 5, then contour plots would be produced every 25 time steps. If NCON is set to zero or left blank, no contour plots will be produced.

The maximum contour plots represent the furthest extent that a field of given magnitude will reach. Maximum contour plots are produced at the end of the SCX run and consist of four plots: a whole-grid and a blown-up plot of B phi and a whole-grid and a blown-up plot of E total. There is no controlling parameter for these plots; they will automatically be produced.

APPENDIX IV

ALP	SCOUT	Hollerith variable for outputting, is set either to RHO or R depending if ground or air values used.
AMU	SCX, SCIN	Magnetic permeability of free space ($4\pi \times 10^{-7}$).
AN	CIRCLE	Angle used in generation of circles for contour grid.
ANG	PICTURE, SCIN, SCOUT	Array containing grid angles in the air and grid depths (negative) in the ground. Angles are in degrees, depths in meters.
ANGDIFF	SCIN	The difference in degrees of ANG(NTA) and ANGSTR.
ANGH	SCECS, SCIN, SCOUT	Array containing half angles for the air and half depths for the ground. Angles are in degrees, depths in meter
ANGND	SCOUT	Angle at which range profiles are to be taken.
ANGNT	SETUP	Set either to -20 or -100 (ANG(NT)) for contour plot depths depending on scale of plot.
ANGSTR	SCIN	Angle at top of grid.
A1	FIELDS3	Array containing $A1_j$ values for present range and time.
A1J	FIELDS3	$1/\left(1 + \frac{\Delta t}{2\epsilon}\right)\sigma_{ij}^{hk}$
A1JM	FIELDS3	$A1_{j-1}$
A1JP	FIELDS 3	$A1_{j+1}$
A10J	FIELDS 3	$(A8_j A4_j - A5_j A7_j)A22_j A1_j$

A10JM	FIELDS3	$A10_{j-1}$
A11J	FIELDS3	$A7_j - A4_j - (A8_jA4_j - A5_jA7_j)$
A11JM	FIELDS3	$A11_{j-1}$
A12J	FIELDS3	$(A8_jA4_j - A5_jA7_j)A21_{j+1}A1_{j+1}$
A12JM	FIELDS3	$A12_{j-1}$
A13J	FIELDS3	$A6_jA7_j - A4_jA9_j + (A8_jA4_j - A5_jA7_j) \times (A3_jA1_j - A3_{j+1}A1_{j+1})$
A13JM	FIELDS3	$A13_{j-1}$
A21	FIELDS3, SCX	$\left[\left[\frac{1}{c^2} - \frac{1}{cg^2}\right]^{1/2} - c^2\Delta t\right]/2$
A21J	FIELDS3	$\frac{\Delta t}{2\Delta\theta_j}\frac{c^2}{r_i^2}\frac{\sin\theta_j}{\sin\theta_j^h}$
A21JM	FIELDS3	$A21_{j-1}$
A21JP	FIELDS3	$A21_{j+1}$
A22	FIELDS3, SCX	$c^2\Delta t/2 - \left[\frac{1}{cg^2} - \frac{1}{c^2}\right]^{1/2}/2$
A22J	FIELDS3, SCX	$\frac{\Delta t}{2\Delta\theta_j}\frac{c^2}{r_i^2}\frac{\sin\theta_{j-1}}{\sin\theta_j^h}$
A22JP	FIELDS3, SCX	$A22_{j+1}$

A3	FIELDS3	Array containing $A3_j$ values for present range and time.
A3J	FIELDS3	Constant containing k-1 field values.
A3JM	FIELDS3	$A3_{j-1}$
A3JP	FIELDS3	$A3_{j+1}$
A4	FIELDS3	Array containing A4J values for present range and time.
A4J	FIELDS3	$\frac{1}{c} + \frac{\mu\Delta r}{2}\,\sigma_{ij}^{k}$
A4JM	FIELDS3	$A4_{j-1}$
A5	FIELDS3, SCX	$\Delta r/\left[2\left(c\Delta\theta_{j+1}^{h}\right)\right]$ Array containing $A5_j$ values for present range and time.
A6	FIELDS3	Array containing A6J values for present range and time.
A6J	FIELDS3	Constant containing i-1 field values.
A6JM	FIELDS3	$A6_{j-1}$
A7J	FIELDS3	$-\left(\frac{1}{c} + \frac{c\mu\Delta t}{4}\,\sigma_{ij}^{k}\right)$
A7JM	FIELDS3	$A7_{j-1}$
A8	FIELDS3, SCX	$\Delta t/\left(4\Delta\theta_{j+1}^{h}\right)$
A81	FIELDS3, SCX	$\left(\frac{1}{c_g^2} - \frac{1}{c^2}\right)^{1/2}/2 + \Delta t/\left(2\Delta\theta_{j+1}^{h}\right)$ Used only in ground code.
A9J	FIELDS3	Constant containing k-1 field values interpolated in range.

A9JM	**FIELDS3**	$A9_{j-1}$
BE	SIGMA	Value of β, electron attachment rate, returned by SBETA routine.
BEE	SCOUT	Value of B field used for outputting.
BET	SCOUT	Hollerith variable in outputting, set either to Z or THETA depending on ground or air plots.
BMAX	PICTURE	Maximum value of B field attained at a given time.
BMO	FIELDS3, SCIN	B_{ij}^{k-1} in ground, rB_{i+1j}^{k-1} in air.
BMP	FIELDS3	B_{i+1j}^{k-1} in ground, rB_{i+1j}^{k-1} in air.
BMP	PICTURE, SETUP	$\cot(\theta) \cdot \frac{\Delta y}{\Delta x}$ scaling factor.
BOM	FIELDS3, SCOUT	B_{i-1j}^{k} in ground, rB_{i-1j}^{k} in air.
BOO	FIELDS3, SCOUT	B_{ij}^{k} in ground, rB_{ij}^{k} in air.
BUFFER	SCOUT	511 word array used for writing output tape.
C	SCX, SCIN	Vacuum speed of light [2.997925×10^8 m/sec].
CA	FIELDS3, SCX	$\Delta t/(2\epsilon)$
CAG	FIELDS3, SCX SCIN	$\left[\frac{1}{cg^2} - \frac{1}{c^2}\right]^{1/2}/2$
CC	FIELDS3, SCIN	$1/c$

CCG	SCX, SCIN	$\frac{1}{cg^2}$
CD	FIELDS3, SCX SCIN	$\mu\Delta r/2$
CDG	FIELDS3	$\frac{\Delta t}{\Delta r}/(r_i + r_{i-1})$
CF	FIELDS3, SCX	$\Delta t \mu c/4$
CFG	FIELDS3, SCX	$\Delta t/(2\Delta r)$
CG	SCIN	Speed of light in the ground.
CH	FIELDS3, SCX	$c\Delta t/(2\Delta r)$
CHG	FIELDS3	$\frac{\Delta t}{\Delta r}/(r_i + r_{i+1})$
CI	FIELDS3,	$1 - c\Delta t/(2\Delta r)$
CIG	FIELDS3	$\left(\frac{\Delta t}{r_{i-1}\Delta r}\right)/\left(r_i + r_{i-1}\right)$
CKG	SCX	$\sigma_g \mu \Delta t/2$
CLG	FIELDS3, SCX	$\sigma_g \mu \Delta t/2 + \frac{1}{cg^2}$
CMG	FIELDS3. SCX	$1./\left(\mu\sigma_g \Delta t/2 + \frac{1}{cg^2}\right)$
COEF	SCIN	4 word array containing parameters used to calculate skin depth.
COG	FIELDS3, SCX	$\frac{1}{cg^2} - \sigma_g \mu \Delta t/2$
CON(J)	SCX, NSOURCE	$\cos \theta_j$

CONB	SCOUT	5 word array containing contour values used in generating max BPHI contour plots
CONE	SCOUT	5 word array containing contour values used in generating max ETOT contour plots
CONI	PICTURE	Temporary contour value used in obtaining contour crossover points.
CONTR	PICTURE	5 word array containing contour values to be placed in CONI for contour plots.
CT	PICTURE, SCIN, SCOUT, SETUP	NTA word array containing cotangent values for air grid angles.
CO1	FIELDS3	$3A1_{NTA}$ used to match B field across interface.
CO2	FIELDS3	$-A1_{NTA-1}$ used to match B field across interface.
CO3	FIELDS3	$3/\mu\sigma_g\Delta t/2 + \frac{1}{cg}$ used to match B field across interface.
C10	FIELDS3	Coefficient used to match B field across interface, used constant values at NTA, NTA-1, and NTA-2.
C11	FIELDS3	Coefficient used to match B field across interface, uses constant values at NTA+1 and NTA+2.
C12	FIELDS3	Coefficient used to match B field across interface, uses constant values at NTA+1 and NTA+2.
C2	SCX, SCIN	c^2
C2G	SCIN	c_g^2

C9	FIELDS3	Coefficient used to match B field across interface, uses constant values at NTA, NTA-1, and NTA-2.
D	FIELDS3, SCIN, PICTURE, SCOUT,	NT by NDR word ECS array containing rE_θ values for the air and E_z values for the ground.
DAN	CIRCLE	Complex variable representing $\cos(1^o)$ used to generate circles for contour plots.
DANG	FIELDS3, SCX	NT word array containing $\Delta\theta$'s for the air and Δz's for the ground.
DANGH	SCX, SCIN	NT word array containing $\Delta\theta^h$'s for the air and Δz^h's for the ground.
DATE	HEDING	Hollerith variable containing the date, used to identify printed output.
DEA	SCIN	Constant containing size of first NA1 < bins.
DEE	SCOUT	Variable used in outputting, contains E_θ for air values and E_z for ground values.
DEN	FIELDS3	Miscellaneous constant used to replace repeated divisions by repeated multiplications.
DMAX	PICTURE	Maximum value of the transverse E field attained at a given time.
DMO	FIELDS3	$(E_\theta)^{k-1}_{i,j}$ or $(E_z)^{k-1}_{i,j}$
DMP	FIELDS3	$(E_\theta)^{k-1}_{i+1,j}$ or $(E_z)^{k-1}_{i+1,j}$
DNT	SCX, SCIN	Conversion factor from degrees to radians, equals $2\pi/360$.

DOM	FIELDS3, SCOUT	$(E_\theta)^k_{i-1,j}$ or $(E_z)^k_{i-1,j}$
DOO	FIELDS3, SCOUT,	$(E_\theta)^k_{i,j}$ or $(E_z)^k_{i,j}$
DR	FIELDS3, SCX SCIN	Current range increment, Δr.
DR2	SCX, SCIN	$\Delta r/2$
DT	SCX, SCIN	Current time increment, Δt.
DTHS	SCIN	20 word array containing the angle increments.
DTS	SCX, SCIN	10 word array containing the time increments.
DT2	FIELDS3, SCX	$\Delta t/2$
DT4	SCX	$\Delta t/4$
DZ	SCIN	20 word array containing Δz steps in ground.
DZZ	SCIN	Approximate skin depth.
E	FIELDS3, SCOUT	NT word array used in two term recursion formula for the B field.
EE	SCIN	Neutron efficiency.
EEE	SCOUT	Value of E radial field used for outputting.
EH	FIELDS3, SCX PICTURE, SCIN, SCOUT, SETUP, SIGMA	An NT by NDR word ECS array containing E_r field values for a given time.
EJMM	FIELDS3	E_{j-2} in air.
EJPP	FIELDS3	E_{j+2} in ground.

EMAX	**PICTURE**	**Maximum value of radial E field attained at a given time.**
EMO	FIELDS3	$(E_r)^{k-1}_{i,j}$ or $(E_\rho)^{k-1}_{i,j}$
EMP	FIELDS3	$(E_r)^{k-1}_{i+1,j}$ or $(E_\rho)^{k}_{i+1,j}$
EOM	FIELDS3, SCOUT	$(E_r)^{k}_{i-1,j}$ or $(E_\rho)^{k}_{i-1,j}$
EOO	FIELDS3, SCOUT,	$(E_r)^{k}_{i,j}$ or $(E_\rho)^{k}_{i,j}$
EP	SCECS, SCIN	ϵ, value of dielectric constant in air.
EPG	SCIN	ϵ_g
EPGF	SCIN	Relative dielectric constant for the ground.
ET	SIGMA	Total electric field at a given angle.
ETERM	FIELDS3	Statement function used in differencing.
ETMAX	PICTURE	Maximum value of total E field attained at a given time.
F	FIELDS3, SCIN, SCOUT	NT word array used in two term recursion formula for B.
FJH	FIELDS3	$\frac{\Delta t}{2\epsilon}\left(J_r^k + J_r^{k-1}\right)$
FJMM	FIELDS3	F_{j-2} in air.
FJPP	FIELDS3	F_{j+2} in ground.
FJR	SCOUT	Variable used in outputting, contains J_r in air and J_ρ in ground.

FJT	SCOUT	Variable used in outputting, contains J_r in air and J_ρ in ground.
FJT	SCOUT	Variable used in outputting, contains J_θ in air and J_z in ground.
FJTH	SCX, FIELDS2	$J^k_{\theta ij}$
FJTH1	SCX, FIELDS2	$J^{k-1}_{\theta ij}$
FR	FIELDS3, SCX SCOUT	J^k_r
FR1	FIELDS3, SCX	J^{k-1}_r
GDZ	SCIN	Original ground bin size.
GF	PICTURE, SCOUT	y scaling factor used for contour plots, GF = 8./(YMAX - ANGNT)
G10J	FIELDS3	$A8_j G5 \cdot A22_j CMG$
G10JP	FIELDS3	$G10_{j+1}$, different for regrid angles.
G11J	FIELDS3	$G5[1 + (A81_j A22_{j+1} CMG + A8_j A21_j CMG) - G4_j G7_j]$
G11JP	FIELDS3	$G11_{j+1}$, different for regrid angles.
G12J	FIELDS3	$G5A81_j A21_{j+1} CMG$
G12JP	FIELDS3	$G12_{j+1}$, different for regrid angles.
G13J	FIELDS3	$G5[G9J - CMG(A81_j \cdot G3_{j+1} + A8_j G3_j) - G6_j G7]$

G13JP	FIELDS3	$G13_{j+1}$, different for regrid angles.
G3J	FIELDS3	Ground constant depending on k-1 values of B_φ and E_ρ.
G3JP	FIELDS3	$G3_{j+1}$
G4	FIELDS3	$\frac{1}{c} - \frac{r_i \Delta t}{\Delta r}/(r_i + r_{i-1})$
G5	FIELDS3	$\sigma_g \mu \Delta t/2 + \frac{1}{cg^2}$
G6J	FIELDS3	Ground constant depending on values of B_φ and E_z.
G7	FIELDS3	$\frac{1}{c} - \frac{\Delta t}{2\Delta \rho}$
G9J	FIELDS3	Ground constant depending on values of B_φ, E_z, and E_ρ.
G9JP	FIELDS3	$G9_{j+1}$
H	TABLIN	x value of the table for which y value is to be returned.
HMX	SETUP	x value used in drawing tic marks on contour plots.
HMY	SETUP	y value used in drawing tic marks on contour plots.
HOB	SCIN	Not used--a dummy variable containing height of burst written onto tape by SS.
HX	SETUP	Maximum x value used in generating 30° and 60° lines and tic marks for contour plots.

HY	SETUP	Maximum y value used in generating 30^{o} and 60^{o} lines and tic marks for contour plots.
H20	SCIN	Water fraction used in the mobility calculations.
IBO	SCIN	Integer variable read to select observer table option.
IBUF	SCOUT	Index used in putting field values into BUFFER array for tape outputting.
IDATE	HEDING	Current date used for outputting.
IDNO	SCX	Used for labeling partouts, = 10. ISCNO plus a running index.
IDONNO	SCIN	Dummy variable, not used.
IFORM	PICTURE	Plot identification name.
IOBNO	SCIN, SCOUT	Observer number.
IOBSV	SCIN, SCOUT	Range of observer.
IOB100	SCIN, SCOUT	Observer number 100.
IPAGE	HEDING, SCIN	Page number of output.
IREG	SCIN	20 word array containing IST for each time bin, used on output to indicate when range regridding took place.
ISCNO	HEDING, NOTER, SCX, SCIN. SETUP	Integer constant containing SC run number
ISSNO	HEDING, SCIN	Integer constant containing SS run number.
IST	FIELDS3, SCX PICTURE, SCIN, SCOUT, SIGMA	Index variable used for range regridding.
ITHETA	SCIN, SCOUT	Index storing observer angle.

ITIME	HEDING	Current Mountain Standard Time used for outputting.
KOMENT	HEDING, SCIN	8 word Hollerith array used for placing an appropriate comment on output.
LIBSC	HEDING, SCIN	SC tape number.
LIBSS	HEDING, SCIN	SS tape number.
LYMIN	PICTURE, SCOUT SETUP	Logical variable used to control type of contour plot produced.
MANG	SCIN	Angle index number.
MCB	SCOUT	NT by 5 word array containing range values at which BPHI MAX contour values are plotted.
MCE	SCOUT	NT by 5 word array containing range values at which ETOT MAX contour values are plotted.
NAPR	SCIN	Print variable containing NA1, NA2, and NA3.
NA1	SCIN	Number of angle bins which the air region is to be divided.
NA2	SCIN	Number of times the last group of bins is to be divided in half.
NA3	SCIN	Number of bins which are included in the last group.
NCO	SCOUT	Counting index to determine when contour plots are to be produced.
NCON	SCIN, SCOUT	Integer variable which specifies the frequency with which contour plots are produced.

NCTR	PICTURE	**Variable used to determine which exponent values are to be used in contour plots.**
ND	SCOUT	Set equal to NTA.
NDR	FIELDS3, SCX PICTURE, SCIN, SCOUT, SIGMA	Number of range steps.
NDRM1	FIELDS3, SCX PICTURE, SCIN, SCOUT	NDR-1
NDRM2	FIELDS3, SCX SCIN	NDR-2
NDT	SCX	Number of time steps of current Δt size.
NDTHS	SCIN	Array containing number of steps for each $\Delta\theta$.
NDTS	SCX, SCIN	Number of time steps using current value of Δt.
NDZ	SCIN	20 word array containing number of steps to be taken of size Δz.
NGPR	SCIN	Integer variable containing NG1, NG2, NG3 used for output.
NG1	SCIN	Number of ground bins of the original size to be used.
NG2	SCIN	Number of times the ground group of bins is to be doubled in size.
NG3	SCIN	**Number of ground bins which are to be included in each group of bins that is doubled.**
NJ	SCIN	**Integer variable containing angle index for observer.**

NPO	SCOUT	Counting index to determine when printout is to be produced.
NRA	SCIN, SCOUT	Index determining range used in field vs. angle profile plots.
NS	SCX	Index over time grid.
NSHA	SCIN	Number of shadow array points.
NSP	SCIN, SCOUT	Integer variable which specifies the frequency with which profile plots are produced.
NSS	SCOUT	Counting index to determine when profile plots are to be produced.
NT	FIELDS3, SCX PICTURE, SCIN, SCOUT, SIGMA	Maximum number of angle and z values combined.
NTA	FIELDS3, SCX PICTURE, SCIN, SCOUT, SIGMA, SETUP	Maximum number of grid angles in air.
NTAM	FIELDS3, SCX PICTURE, SCIN, SCOUT, SIGMA	NTA-1
NTAM2	FIELDS3, SCIN	NTA-2
NTAP	FIELDS3, SCIN, PICTURE, SIGMA, SCOUT	NTA+1
NTAP2	FIELDS3, SCIN	NTA+2
NTG	FIELDS3, SCIN, SCOUT	Maximum number of z values.
NTGP	SCIN, SCOUT	NTG+1
NTH	SCIN	NA2+1

NTM1	FIELDS3, SCIN, PICTURE, SCOUT	NT-1
NTOT	PICTURE, SCIN, SCOUT	Number of octal words in a NT x NDR word array.
NTOT2	SCX, SCIN	Number of octal words in a NTA x NDR word array.
NTS	SCX. SCIN	Number of time bins.
NTU	SXC, SCIN	Index containing largest size of angle, time or Δz arrays, used in outputting these arrays.
NTY	SCIN	Total number of time steps.
NW	SCOUT	Number of field points to be graphed.
NZ	SCIN	NG2+1
ORD	CIRCLE, SCOUT, PICTURE, SETUP	Air-ground interface y value on plots.
PRT	SCOUT	8 or 9 word array used for filling BUFFER array.
Q	SCOUT	Value of ionization rate, used in outputting.
QR	SCX SIGMA	Q_r^k
R	FIELDS3, SCIN, PICTURE, SCOUT, SETUP	NDR word array containg r_i
RAD	SCIN, SIGMA	Relative air density.
RADIUS	CIRCLE	Range at which r grid line is drawn.
RANGE	SCIN	Inputted observer range.
RAP	SCIN	Air density at point of observation.
RAT	SCIN	STP air density.

RB	SCX, SCIN SCOUT, FIELDS3, PICTURE, SETUP, SIGMA	An NT by NDR word ECS array containing rB_{φ} values for a given time.
RDEA	SCIN	$\Delta\theta$ · conversion factor from degrees to radians.
RHOEH	FIELDS3, SCX PICTURE, SCIN, SCOUT, SETUP, SIGMA	N_e^h = number density of electrons on half angles.
RHOIH	FIELDS3, SCX PICTURE, SCIN, SCOUT, SETUP, SIGMA	N_+^h = number density of positive ions on half angles.
RI	FIELDS3, NOTER, PICTURE, SCOUT	r_i
RIS	PICTURE	r_i · (x scaling factor)
RLAST	SCIN, SETUP	r(NDR)
RM	SCIN	Observer range for matrix observer option.
RMI	FIELDS3	r_{i-1}
RMMI	FIELDS3	r_{i-2}
RPI	FIELDS3	r_{j+1}
RR	FIELDS3, SCIN, PICTURE, SCOUT, SIGMA	NDR word array containing $1/r_i$ values.
RRAD	SCIN, SIGMA	1/RAD
RRI	FIELDS3, SCOUT, PICTURE, SIGMA	$1/r_i$

RRI2	**FIELDS3**	$1/r_i^2$
RS	CIRCLE	Range YSLPE
RSCL	SETUP	1000 meter range steps for CIRCLE.
RSTART	SCIN, SETUP	Beginning range value.
R2	SCIN, SCOUT	r^2
S	FIELDS3, SCX SCIN, SCOUT, SIGMA	ECS array containing σ_{ij}^k values.
SA	SCX, SIGMA	$2/\delta t$
SALFA	SCIN, SIGMA	Electron-ion attachment coefficient α.
SB	SIGMA	N_t^{k-1}
SC	SIGMA	N_e^{k-1}
SCALE	PICTURE, SCOUT, SETUP	x scaling factor used in graphs.
SD	SIGMA	$\alpha N_e^{k-1} + \gamma\left(N_t^{k-1} - N_e^{k-1}\right)$
SEE	SCOUT	Value of conductivity used in outputting.
SF	SIGMA	αN_t^k
SGAM	SCIN, SIGMA	Ion-ion attachment coefficient γ.
SH	FIELDS3, SCIN, SCOUT, SIGMA	ECS array containing σ_{ij}^{hk}
SHAD	SCIN	**Table of gamma output assymmetries of the weapon used.**
SHB	**FIELDS3, SCIN, SCOUT, SIGMA**	**NT word array containing values of SHAD at grid angles.**

SHE	**SCOUT**	**Value of conductivity on half angle used in outputting.**
SH1	SCX, SCIN SCOUT, FIELDS3, PICTURE, SETUP, SIGMA	**ECS array containing** σ_{ij}^{hk-1}
SIGMAG	SCX SCOUT	Ground conductivity σ_g.
SIM	PICTURE	Sumbol plotted at contour point in contour plots.
SKIN	SCIN	Factor used in calculating skin depth for frequency of 10^8 Hz.
SMUE	SIGMA	Electron mobility.
SMUN	SCIN, SIGMA	Negative ion mobility.
SMUNG	SCIN	Negative ion mobility at STP.
SMUP	SCIN, SIGMA	Positive ion mobility.
SMUPG	SCIN	Positive ion mobility at STP.
SMUW	SCIN, SIGMA	$\psi_\omega = H_2O/9 \times 10^{-3}$
SN	PICTURE, SCX SCIN, SCOUT, SETUP	NTA word array containing the sine of the air angle grids.
SNON	SCX	Neutron source turn on function.
SSS(3)	SCX	J_θ, J_r, and Q returned from NSOURCE.
STDRHO	**SCIN**	**Dummy variable, not used.**
SYM	**PICTURE**	**A 5 word array containing Hollerith symbols used in generating contour plots.**
SYME	**PICTURE**	**A 9 word array containing Hollerith Symbols used in B phi contour plots.**

S1	**FIELDS3, SCX PICTURE, SCIN, SCOUT, SETUP, SIGMA**	**ECS array containing** σ_{ij}^{k-1}
TABLE	**TABLIN**	Complex array containing 2D table values for interpolation.
TAU	NOTER, SCX SCIN, SCOUT, SETUP	Present value of time.
TAUM	SCX. NSOURCE	Present time in micro-sec.
TAUM1	SCX, NSOURCE	Last time in micro-sec.
TEM	FIELDS3, SCX PICTURE, SCIN, SCOUT, SETUP, SIGMA	An NTA by NDR word array used for working spaces.
TEMP	FIELDS3, SCX PICTURE, SCIN, SCOUT, SETUP, SIGMA, LOG, POWER	An NT by NDR word variable array containing field values for contour plot in question in PICTURE, SETUP and SCOUT, working array in other subroutines.
TMA	FIELDS3	σ_{ij}^{hk}
TMA	SIGMA	N_t
TMB	FIELDS3	σ_{ij}^{hk-1}
TMB	SIGMA	N_e
TMB	SCOUT	σ_{ij}^{hk}
TMC	FIELDS3	σ_{ij}^{k-1}
TMC	SIGMA	Q_r

TMC	SCOUT	σ_{ij}^{k}
TMD	FIELDS3	σ_{ij-1}^{k-1}
TMD	SIGMA	σ_{ij}^{hk-1}
TME	FIELDS3	σ_{ij}^{k}
TME	SIGMA	σ_{ij}^{hk}
TMF	FIELDS3	$\sigma_{i-1,j}^{k}$
TMF	SIGMA	σ_{ij}^{k}
TS	SCIN	Time used in range regridding.
TSHIFT	SCIN	Shift factor to start time at 0+TSHIFT
TTOT	SCIN	Total time, used in outputting.
T1	SCX	Current reading of accumulated CP time.
T2	SCX	Time readoff of input tape.
V	FIELDS3, SCX	$\left[\left(c^2\Delta t/2\right)/\Delta\theta_j\right]\cdot\left[\sin\left(\theta_j\right)/\sin\left(\theta_j^h\right)\right]$
VS	PICTURE	x value for ETOT vector plots.
VXX	PICTURE	x value for end of arrow for ETOT vector plots.
VY	PICTURE	y value for ETOT vector plots.
VYY	PICTURE	y values for end of arrow for ETOT vector plot.

W	FIELDS3, SCX	$\left[\left(c^2\Delta t/2\right)/\Delta\theta_{j+1}\right]\cdot\left[\sin\theta_j/\sin\theta^h_{j+1}\right]$
WA	SCX, SCIN	$c^2\Delta t/2$
WB	FIELDS3, SCX SIGMA	$\Delta t/\left(2\Delta\theta^h_{j+1}\right)$
WBM	FIELDS3	WB_{j-1}
WC	SIGMA	$\frac{1}{r_i}\cdot E^k_{\theta_{j-1}}$
XCTR	SCOUT	Exponent used in plotting ETOT MAX contour plots.
XPLOT	CIRCLE, PICTURE SCOUT	x values for contour plot points.
XS	SCX	Neutron source scaling factor.
XX30	SETUP	Minimum x value for generating 30^o and 60^o lines for contour plots.
Y	SCIN	Yield in kilotons.
YMAX	SETUP	Maximum vertical range value used in generating contour plots.
YPLOT	CIRCLE, SCOUT, PICTURE	y values for contour plot points.
YSLPE	CIRCLE, SETUP	y scaling factor/x scaling factor.
YY30	SETUP	Minimum y value for generating 30^o and 60^o lines for contour plots.
Z	TABLIN	TABLE(L) - TABLE (L-1)

REFERENCES

1. Granzow, K. D., "Transient Spherical Waves," EMP Theoretical Notes, Vol. II, No. 24 (1971).

2. Wood, J. N., Waller, G. W., "The Current Status of SC Development," Dikewood Corporation No. DC-TN-2099-4 (1969).

3. Richtmyer, (1957).

4. Peterson, D., "TIG2," The Dikewood Corporation, DC-TN-1214-2 (1970).

5. Knutson, G., Personal Communication (1972).

6. Stevens, C. A., Dietz, R. E., "Late Time EMP Sources Including Ground Contributions," AFWL-TR-71-8 (1970).

7. Sargis, D. A., Parkinson, E. R., Wood, J. N., Dietz, R. E., Stevens, C. A., "Late-Time Sources for Close-In EMP," Vol. I, SAI-72-556-LJ (1972).

8. Nielson, R., Bradbury, N., Phys. Rev. 51 (1937), p. 69.

9. Baum, C., "Electron Thermalization and Mobility in Air," EMP Theoretical Notes, Vol. I, No. 12 (1971).

10. Jahnke, E., and F. Emde, Tables of Functions (Dover Publications, N. Y., 1945), p. 107.

11. Abromowitz, M., and I. A. Stegun, Handbook of Mathematical Functions (Dover Publications, N. Y., 1965).

12. Wood, J. N., "The Implementation of Improved Neutron Sources in D and SS," DC-TN-2099-29, June 18, 1970.

13. Longmire, C. L., Longley, H. J., "Development and Testing of LEMP 1," Los Alamos Scientific Laboratory, LASL Report LA-4346, December 1969.